A UNIQUE MITOCHONDRIAL BIOENERGETIC PATHWAY UNDERLIES ACUTE MYELOID LEUKEMIA SURVIVAL AND CHEMORESISTANCE

by
James T. Hagen
December 2023

Director of Dissertation: Kelsey H. Fisher-Wellman

Department of Physiology

In his early research on cancer cell metabolism, Otto Warburg made the hypothesis that the respiration of cancer cells has become damaged. The insult to cancer cell respiration, Warburg proposed, was either 1) a decrease in oxygen consumption, or 2) with undiminished oxygen consumption, the coupling of respiration and ATP synthesis has become broken. Herein, using multiple models of acute myeloid leukemia (AML) (i.e., chemosensitive and chemoresistant), we present evidence that supports the early hypothesis of Otto Warburg. Specifically, we discovered that 1) AML mitochondria present with defects in respiration that are masked by increases in mitochondrial content and 2) under basal conditions, AML mitochondria consume, rather than synthesize, ATP. The ATP consumption of AML cells confers a survival advantage and poises AML cells to participate in a futile cycle that mimics an alternating current circuit model.

In chapter I, we provide a background on acute myeloid leukemia bioenergetics that establishes the groundwork for the research outlined in this dissertation. Specifically, our previous research discovered that relative to normal blood cells, AML cells are characterized by two important mitochondrial phenotypes: 1) AML cells present with deficiencies in oxidative phosphorylation (i.e., OxPhos) that are more pronounced in the context of chemoresistant disease; and, 2) AML import extramitochondrial ATP into the mitochondrial matrix space where it inhibits respiratory flux. In Chapter II, we discovered that, universally, the AML mitochondrion presents with 1) reductions in respiratory flux, driven by intrinsic lesions in the electron transport

system, that were associated with 2) a utilization of ATP synthase as an F_1-ATPase proton pump to sustain the mitochondrial membrane potential. Sustaining polarization across the inner mitochondrial membrane via F_1-ATPase activity conferred chemoresistance to AML. Importantly however, chemoresistant AML were re-sensitized to chemotherapy when F_1-ATPase mediated polarization was disrupted using mitochondrial-targeted lipophilic small molecules. In Chapter III, we discovered that reactivation of AML OxPhos induces BAX-independent cytotoxicity that, based on unpublished data in Chapter IV, appears to involve cytotoxic ROS production. Collectively, this dissertation proposes a unique model of AML mitochondrial bioenergetics where ATP consumption, rather than ATP synthesis, supports AML survival and confers resistance to chemotherapy. Furthermore, this dissertation presents a novel AML-specific mitochondrial pathway that can be selectively targeted by 1) disrupting F_1-ATPase mediated polarization of the mitochondrial membrane, or 2) reactivating AML OxPhos.

A UNIQUE MITOCHONDRIAL BIOENERGETIC PATHWAY UNDERLIES ACUTE MYELOID LEUKEMIA SURVIVAL AND CHEMORESISTANCE

A Dissertation

Presented to the Faculty of the Department of Physiology

Brody School of Medicine

East Carolina University

In Partial Fulfillment of the Requirements for the Degree

Doctor of Philosophy in Biomedical Sciences

By
James T. Hagen
December 2023

Dissertation Advisor
Kelsey H. Fisher-Wellman, PhD

Committee Members
Joseph M. McClung, PhD
Jessica M. Ellis, PhD
Myles C. Cabot, PhD

ACKNOWLEDGEMENTS

The completion of this dissertation was made possible only with the collaboration and support from many others. First, I would like to thank my mentor Dr. Kelsey Fisher-Wellman for his knowledge, expertise, and guidance throughout my graduate training. I fully believe that Dr. Fisher-Wellman is among the best mitochondrial bioenergetics researchers of our time, and I am excited to see what the future holds for his lab. With Dr. Fisher-Wellman's direction, I truly feel that this dissertation provides myself a sense of completion as I move on to the next chapter. As I take those next steps, Dr. Fisher-Wellman has taught me invaluable skillsets that will follow me throughout a future academic career. I would also like to express my gratitude for the collaborative efforts from my colleagues who have applied their own unique skillsets to assist the endeavors herein. I am incredibly appreciative for the oversight of my graduate training provided by my committee members (Dr. McClung, Dr. Ellis, and Dr. Cabot) as well as the rest of the faculty at ECDOI and the BSOM. With their help, my graduate training has been a highly enjoyable and rewarding process. Lastly, I would like to thank my family for their love and support that has indirectly contributed to my graduate training. Because my youngest daughters, Lydia and Luna, tend to use my lab notebook as a coloring book, I have learned the importance of quickly analyzing data. However, without the help of my son, Levi, I would not have taken as many intermittent breaks from writing to go outside, get some exercise, and play a little baseball.

TABLE OF CONTENTS

LIST OF FIGURES

LIST OF SYMBOLS AND ABBREVIATIONS

°C – degrees in Celsius

Δp – Protonmotive Force

$\Delta\Psi_m$ or Mitochondria$_{\Delta\Psi m}$ – Mitochondrial Membrane Potential

17-AAG - 17-N-allylamino-17-demethoxygeldanamycin

2-DG – 2-deoxyglucose

AC – Alternating Current

ACK – ammonium-chloride-potassium

ADP – Adenosine Diphosphate

AGC – Automatic gain control

AML – Acute Myeloid Leukemia

ANOVA – Analysis of Variance

ANT – Adenine Nucleotide Translocase

Ant or Ant A – Antimycin A

ATP – Adenosine Triphosphate

ATP/ADP – The ratio of ATP to ADP

ATP5IF1 – ATP synthase inhibitory factor 1

ATPase – Adenosine triphosphotase

BAI1 - 3,6-Dibromo-α-(1-piperazinylmethyl)-9*H*-carbazole-9-ethanol dihydrochloride

BAK – Bcl-2-antagonist/killer 1

BAM15 - N^5,N^6-bis(2-Fluorophenyl)-[1,2,5]oxadiazolo[3,4-*b*]pyrazine-5,6-diamine

BAX – Bcl-2 associated X

Bcl-2 – B-cell lymphoma 2

BMC – Bone marrow concentrate

BSA – Bovine Serum Albumin

$CaCl_2$ – Calcium chloride

CB-839 – Glutaminase inhibitor III, Telaglenastat

CI – Complex I

CII – Complex II

CIII – Complex III

CIV – Complex IV

CK Clamp – Creatine Kinase Clamp

CO2 – Carbon dioxide

CoA – Coenzyme A

CPT – Cell Preparation Tubes

CR or Cr – Creatine

CSA – Cyclosporin A

Cyt – Cytochrome C

d-TPP – Dodecyltriphenylphosphonium

DAPI - 4',6-diamidino-2-phenylindole

DDA – data dependent acquisition

DephOx – Dephosphorylative Oxidation

Digi – Digitonin

DMSO – Dimethyl Sulfoxide

DNA – Deoxyribonucleic acid

DTT – dithithreitol

EDTA - Ethylenediaminetetraacetic acid

EGTA - ethylene glycol-bis(β-aminoethyl ether)-N,N,N′,N′-tetraacetic acid

ETS – Electron Transport System

$FADH_2$ – Flavin Adenine Dinucleotide

FBS – Fetal Bovine Serum

FC or FCCP - Carbonyl cyanide-p-trifluoromethoxyphenylhydrazone

FDA – Food and Drug Administration

FDR – False Discovery Rate

Fractional OxPhos – Respiration stimulated by ATP synthesis divided by the maximal respiration

Glut or G – Glutamate

H_2O – Water

H_2O_2 – Hydrogen Peroxide

HEPES - 4-(2-hydroxyethyl)-1-piperazineethanesulfonic acid

$HL60_{Vclax}$ – Venetoclax resistant HL60 cells

HMB – Healthy Bone Marrow

HPLM – Human Plasma-Like Medium

IACS or IACS-10759 – IACS-10759 hydrochloride

IDH – Isocitrate dehydrogenase

IDH2 – Isocitrate dehydrogenase 2

IMDM – Iscove's Modified Dulbecco's Medium

JO_2 – Oxygen Consumption Rate

K'_{CK} – the equilibrium constant for the creatine kinase reaction

KCl – Potassium chloride

KD – knockdown

KH_2PO_4 – Monopotassium phosphate

Log_2FC – Log_2 Fold Change

Mal or M – Malate

MEF – Mitochondrial enrichment factor

MES - 4-Morpholineethanesulfonic acid

$MgCl_2$ – Magnesium chloride

$MgSO_4$ – Magnesium sulfate

MitoQ – Mitoquinone mesylate

$MOLM\text{-}13_{Vclax}$ – Venetoclax resistant MOLM-13 cells

$MOLM\text{-}13_{WT}$ – Wild type MOLM-13 cells

MOPS - 3-(N-morpholino)propanesulfonic acid

MPBMC – Mobilized Peripheral Blood Mononuclear Cells

MS/MS – Tandem mass spectrometry

MS1 – Mass spectrometry 1

MS2 – Mass spectrometry 2

mtDNA – Mitochondrial DNA

$MV411_{shCtrl}$ – Scramble lentiviral control MV4;11 cells

$MV411_{shIF1}$ – ATP5IF1 lentiviral knockdown MV4;11 cells

$MV411_{Vclax}$ – Venetoclax resistant MV4;11 cells

$MV411_{WT}$ – Wild type MV4;11 cells

NaCl – Sodium chloride

NAD+ - Nicotinamide Adenine Dinucleotide

NADH - Nicotinamide Adenine Dinucleotide + Hydrogen

O_2 – Oxygen

O2k – Oroboros Instruments Oxygraph-2K

OCI_{Rh0} – Respiration-deficient OCI-AML2 cells

OCI_{shBAX} – BAX lentiviral knockdown OCI-AML2 cells

$OCI_{shScramble}$ – Scramble lentiviral control OCI-AML2 cells

OCI_{Vclax} – Venetoclax resistant OCI-AML2 cells

OCI_{WT} – Wild type OCI-AML2 cells

Oct or O – Octanoyl Carnitine

Oligo – Oligomycin

OxPhos – Oxidative Phosphorylation

p^0 – Rho 0

PBMC – Peripheral Blood Mononuclear Cells

$PBMC_{Lymphoid}$ – Peripheral Blood Mononuclear Cells, Lymphoid Fraction

$PBMC_{Myeloid}$ – Peripheral Blood Mononuclear Cells, Myeloid Fraction

PBS – Phosphate-buffered saline

PCR pr PCr – Phosphocreatine

pH – potential of hydrogen

PI – Propidium iodide

PPP – Pentose Phosphate Pathway

PSM – Peptide Spectrum Match

Pyr or P – Pyruvate

Q – Ubiquinone

ROS – Reactive Oxygen Species

Rot – Rotenone

RPMI-1640 – Roswell Park Memorial Institute 1640 Medium

RSLC – Rapid separation liquid chromatography

SEM – standard error of the mean

shRNA – short hairpin ribonucleic acid

State IV – Non-Phosphorylating Respiration

Succ or S – Succinate

TCA – Tricarboxylic Acid

TMRM – Tetramethylrhodamine methyl ester, perchlorate

TRAP1 - tumor necrosis factor receptor-associated protein 1

Tris - tris(hydroxymethyl)aminomethane

UCP2 – Uncoupling protein 2

Vclax – Venetoclax

VDAC – Voltage-dependent anion channel

WT – Wild Type

x *g* – times gravity

ΔG_{ATP} – Gibb's free energy of ATP hydrolysis

Chapter 1: A unique model of mitochondrial bioenergetics underlies acute myeloid leukemia oxidative metabolism

BACKGROUND

Acute myeloid leukemia (AML) is among the deadliest and most aggressive forms of blood cancer[107,37,38]. Characterized by an abnormal clonal expansion of myeloid progenitor cells in the peripheral blood and bone marrow, AML is a rapidly advancing hematological malignancy that remains difficult to treat despite advancements in chemotherapeutics[50,124,125]. Some available treatments for AML include induction chemotherapy with cytarabine plus an anthracycline such as daunorubicin[104] (e.g., "7 + 3" chemotherapy induction), targeted therapies such as midostaurin[1] (i.e., a FLT3 inhibitor), and hypomethylating agents such as azacitidine[35]. Although these therapies may achieve complete remission in some patients, treatment failure remains to be a concern because of the propensity to develop chemoresistant disease[37,38]. Chemoresistance is caused by the ability of drug resistant AML subclones to evade current chemotherapeutics, clonally expand, and emerge to cause fatal relapse[136,36] – an abysmal outcome that occurs in over 70% of patients[37,38]. Improving patient outcomes, therefore, appears contingent upon three factors: 1) elucidating key mechanisms of chemoresistance, 2) identifying AML-selective drug targets and 3) developing novel chemotherapeutics that thwart chemoresistance in AML.

Prior research has established that mitochondrial metabolism is involved in AML disease progression[120,33,128,108,13]. From leukemogenesis[3] to relapsed/refractory AML[19,115], alterations in mitochondrial metabolism has been reported to be a factor that contributes to leukemic cell survival[12], proliferation[121], and resistance to current chemotherapeutics[41]. Some chemotherapeutics designed to disrupt the mitochondrial metabolism of AML, or mitochondrial-targeted therapies, have received FDA approval. Specifically, FDA approved mitochondrial-

targeted therapies include inhibitors of mutated variants of IDH (i.e., isocitrate dehydrogenase) such as ivosidenib[83] and enasidenib[40]. In addition to these mitochondrial-targeted therapies, the Bcl-2 (i.e., B-cell lymphoma 2) inhibitor venetoclax, a targeted therapy that mediates BAX/BAK-dependent apoptosis, is emerging to be a frontline chemotherapeutic[23]. Although mitochondrial respiration is impacted by venetoclax and IDH inhibitors, they are highly selective for the metabolic vulnerabilities of AML[20] over that of normal blood cells, thus contributing to their demonstrable safety and clinical efficacy. However, their clinical efficacy remains stifled by AML chemoresistance.

Chemoresistance is multifactorial[39,18,119], thus, many current approaches have sought to combine monotherapies to achieve synergistic efficacy, for example, by targeting mitochondrial metabolism in combination with other chemotherapeutics. One such combination includes that of IACS-010759 (i.e., a Complex I inhibitor) with venetoclax[74]. Although these strategies have shown promising efficacy in pre-clinical experiments, global inhibition of mitochondrial respiration by IACS-010759 is unable to discriminate cancer from non-cancer. This results in a lower therapeutic window, a reduced safety profile, and hinders the translation of pre-clinical efficacy to clinical efficacy[138]. To enhance these clinical benchmarks, it may be possible to discriminate cancer from non-cancer by synergistically disrupting AML mitochondrial metabolism using mitochondrial-targeted therapies. However, mitochondrial-targeted therapies should be carefully designed as to not disrupt the efficient energy transduction that supports vital organ physiology. To do this, it is critical to comprehensively characterize the mitochondrial phenotype of normal cells compared to that of AML when selecting mitochondrial drug targets.

Mitochondrial energy transduction

The electron transport system (ETS) consists of a series of membrane-bound respiratory complexes (Complex I-IV) that accept electrons from redox carriers (i.e. NADH and $FADH_2$)

derived from the oxidation of TCA cycle substrates by a network of dehydrogenases (e.g. pyruvate dehydrogenase). Ultimately, those electrons are transported along a series of redox centers within the respiratory network where redox potential energy at Complexes I, III and IV is harnessed to drive proton translocation across the inner membrane[87] (**Fig. 1A**). Proton pumping generates a driving force in the form of the mitochondrial membrane potential ($\Delta\Psi_m$). The $\Delta\Psi_m$ can then be utilized to drive various thermodynamically unfavorable processes (e.g. ATP synthesis, substrate transport, etc.) within the mitochondrion (**Fig. 1A**). However, the mitochondrion's ability to capture electrons, conserve energy during each successive electron transfer, and convert it into a more useable form (i.e. the $\Delta\Psi_m$), is dependent upon a multitude of factors (e.g. efficiency of the respiratory complexes, availability of carbon substrates, activity of the dehydrogenases, etc.) that may vary depending on the physiology of the cell. Importantly, cell physiology is supported by the mitochondrial phenotype that contributes to meeting cell-specific metabolic or ATP synthesis demands[82].

ATP synthesis during OxPhos is catalyzed by the F_1F_0-ATP synthase (used interchangeably with "ATP synthase"). The F_1F_0-ATP synthase is characterized by a fully reversible, mechanical rotary catalysis mechanism and consists of two functional domains: 1) the catalytic F_1 sector (i.e. the site of ATP hydrolysis or synthesis) situated in the mitochondrial matrix, and 2) the inner membrane-bound F_o motor (i.e. the site of proton pumping or conductance)[61]. These two domains are connected by a central "rotor" stalk, as well as a peripheral "stator" stalk that binds the non-rotating portions of the enzyme[61]. The F_1F_0-ATP synthase synthesizes ATP when the $\Delta\Psi_m$ is sufficient, based on thermodynamic principles, to drive rotation of the F_1 sector. Rotation of the F_1 sector, fueled by proton reentry into the mitochondrial matrix through the F_0 motor, creates a torque force that results in ATP synthesis (i.e., ATP synthase activity) by ATP synthase, thereby coupling ATP synthesis to the consumption of the $\Delta\Psi_m$[61]. When the $\Delta\Psi_m$ is insufficient to force rotation of the F_1-sector, a

counter-rotation of the F_1 sector can be driven by the free energy of ATP hydrolysis[129,22]. The hydrolysis of ATP by the F_1-ATPase fuels the pumping of protons through the F_0 motor and into the inner membrane space, thus sustaining polarization of the $\Delta\Psi_m$ (i.e., F_1-ATPase activity)[22]. Therefore, polarization of the $\Delta\Psi$ is a major determinant for the hydrolysis or synthesis of ATP by the F_1F_0-ATP synthase (**Fig. 1B**).

For ATP to exit the mitochondrial matrix, it must be exported by the adenine nucleotide translocase (ANT). The ANT protein is situated in the inner mitochondrial membrane where it functions as an antiporter, catalyzing the exchange of ATP for ADP across the inner mitochondrial membrane[85]. Across the inner membrane, the direction of this exchange is driven by the $\Delta\Psi_m$[72] (**Fig. 1C**). The reason for this being, at physiological pH, ATP carries a negative charge of ~3.5 while ADP carries a negative charge of ~2.5. Because of this charge difference between the two ions, the antiport of ATP and ADP by ANT results in an electrogenic exchange (i.e., a net flow of charge)[79]. Therefore, the export of matrix ATP in exchange for the import of cytosolic ADP results in a decrease of the $\Delta\Psi_m$. On the other hand, if the $\Delta\Psi$ is insufficient to drive ATP export from the mitochondrial matrix, ANT will import cytosolic ATP in exchange for the export of matrix ADP and thereby increase the $\Delta\Psi_m$.

Mitochondrial bioenergetics of acute myeloid leukemia

Compared to normal blood cells, AML cells are characterized by increases in mitochondrial content[118,92] and whole cell respiration[92] (i.e., basal respiration and maximal respiration). Our data in Chapter II demonstrates that when whole cell respiration is normalized to account for differences in mitochondrial content however, individual mitochondria within the AML cell, relative to that in normal blood cells, present with a reduction in maximal respiration. The reduced respiration of AML mitochondria appears to be driven by downregulation of the proton pumping respiratory complexes (i.e., Complexes I/III/IV) that is most pronounced in that

of the oxygen-consuming Complex IV. Therefore, Complex IV downregulation, is described in Chapter II as an intrinsic lesion of the AML electron transport system.

Intrinsic lesions in the AML electron transport system would be expected to reduce the ability of respiratory complexes to pump protons and generate a $\Delta\Psi_m$, the driving force for ATP synthesis. In agreement with this, OxPhos-stimulated respiratory flux is consistently reduced in AML models relative to normal blood cells[92]. Furthermore, unlike normal blood cells that use the energy available within the $\Delta\Psi_m$ to synthesize ATP, Chapter II and III show that AML hydrolyze ATP via the F_1-ATPase to contribute to polarization of the $\Delta\Psi_m$. Polarization of the $\Delta\Psi_m$ by the F_1-ATPase implies that either ATP synthesized in the mitochondrial matrix is recycled, or, extramitochondrial ATP first gains access to the AML mitochondrial matrix. Matrix ATP import occurs when the $\Delta\Psi_m$ is insufficient to drive the ANT-mediated export of matrix ATP. Importantly, our previous publication demonstrated that AML mitochondria consume extramitochondrial ATP where it becomes inhibitory to maximal respiratory flux from within the mitochondrial matrix[92]. Related to this, matrix ATP allosterically inhibits multiple TCA cycle enzymes including fumarase[99], isocitrate dehydrogenase[122], and citrate synthase[59] as well as Complex IV[10,11]. When these enzymes are inhibited by matrix ATP it would be expected to result in a loss of AML respiratory flux and a reduction of the $\Delta\Psi_m$. Consistent with this, it has been shown that allosteric regulation of Complex IV by ATP is a feature that keeps the $\Delta\Psi_m$ low and reduces respiration[10,11,62]. For respiratory flux in AML to be rescued in the presence of extramitochondrial ATP, therefore, ATP may need to be depleted from the matrix space. Matrix ATP depletion by two different mechanisms has been shown to restore AML respiration: 1) an inhibition of ANT-mediated matrix ATP import by carboxyatractyloside[92] (i.e., an inhibitor of ANT) (**Fig. 2A**) or, in Chapter II, 2) F_1-ATPase mediated hydrolysis of matrix ATP that can be inhibited with oligomycin (i.e., an inhibitor of ATP synthase) (**Fig. 2B**). Importantly, Chapter II shows that matrix ATP is hydrolyzed by the F_1-ATPase to sustain $\Delta\Psi_m$ polarization in living AML cells under

basal conditions despite the fact that AML present with increases in intact cell basal respiration relative to normal blood cells. These data suggest that proton pumping by the respiratory complexes occurs simultaneously with F_1-ATPase activity in AML. Collectively, these data inform a unique model of AML mitochondrial bioenergetics where the dephosphorylation of matrix ATP by the F_1-ATPase supports the oxidation of TCA cycle substrates – a phenomenon reflected in the novel term dephosphorylative oxidation (DephOx) (**Fig. 2C**).

The F_1-ATPase and AML chemoresistance

The F_1-ATPase mediated polarization of the $\Delta\Psi_m$ in AML is a conserved feature of respiratory incompetent cells that opposes depolarization of the $\Delta\Psi_m$[9]. Given that depolarization of the $\Delta\Psi_m$ is a known hallmark of apoptosis[68], F_1-ATPase activity may confer survival to cells under bioenergetic stress. Related to this, cell stress is a known effect of chemotherapeutics such as cytarabine[141] and daunorubicin[135] that are known to interfere with the electron transport system[4,56]. Because the electron transport system is affected by exposure to chemotherapeutics, chemoresistance in AML may be driven by adaptations that further enhance the utilization of F_1-ATPase activity to sustain polarization of the $\Delta\Psi_m$. Consistent with this, Chapter II and III demonstrate that $\Delta\Psi_m$ polarization by the F_1-ATPase is a universal phenotype of AML cells, however, this phenotype is much more pronounced in chemoresistant AML. Moreover, although some chemoresistant AML present with increases in mitochondrial content, Chapter II demonstrates that individual mitochondria within the chemoresistant AML cell present with even lower expression of Complexes I/III/IV relative to treatment naïve AML, and this occurs concomitantly with increased expression of Complex V and a lower expression of *ATP5IF1*, the physiological inhibitor of the F_1-ATPase. Importantly, increasing F_1-ATPase activity by knocking down *ATP5IF1* in treatment naive AML was found to confer chemoresistance in our unpublished data. Collectively, this research supports a model of AML chemoresistance where adaptations that enhance F_1-ATPase mediated polarization of the $\Delta\Psi_m$ allow AML cells to evade

apoptotic induction by chemotherapeutics, placing F_1-ATPase mediated polarization of the $\Delta\Psi_m$ at the nexus of AML chemoresistance.

Alternative fuel sources in AML

Chapters II and III show AML consume ATP to support F_1-ATPase mediated polarization of the $\Delta\Psi_m$. These findings suggest that AML may need to increase the utilization of other metabolic pathways to meet the energetic and metabolic demands that support AML physiology. Consistent with this, the physiology of AML cells is known to be supported by alterations in key bioenergetic pathways such as glycolysis[84,55] and glutaminolysis[46,78], both hallmarks of cancer cells often described as "metabolic reprogramming"[97,134]. Reprogramming of AML metabolism is understood to drive AML cell survival and proliferation by providing the metabolic precursors and cofactors needed to facilitate the biosynthesis of lipids, proteins, and nucleic acids[26,86]. The biosynthesis of these molecules are, ultimately, fueled by an increased consumption of upstream metabolic precursors such as glutamine and glucose[134,26,86]. How these two key nutrients fit into our proposed model of AML mitochondrial bioenergetics will be discussed in this section.

AML, like other cancers, is hallmarked by increased glucose consumption[67]. The consumption of glucose fuels important biosynthetic pathways such as the pentose phosphate pathway (PPP)[31], the hexosamine biosynthesis pathway[34], the serine synthesis pathway[6], and the glycine synthesis pathway[6]. In addition to fueling biosynthetic pathways, glycolysis, via substrate-level phosphorylation, is a source of non-mitochondrial ATP production[142]. Although ATP production is necessary for all life, mitochondrial ATP production is not necessary to support the energetic demands of proliferating cells such as AML cells[121]. Consistent with this, Chapter II and III demonstrated that AML contribute to polarization of the $\Delta\Psi_m$ by hydrolyzing ATP via the F_1-ATPase. These data suggest that AML may rely on some substrate-level

phosphorylation via glycolysis to sustain intracellular ATP content and contribute to polarization of the $\Delta\Psi_m$. Given that depolarization of the $\Delta\Psi_m$ is a hallmark of apoptosis[68], inhibition of glycolysis may perturb F_1-ATPase mediated polarization of the $\Delta\Psi_m$ in AML and result in apoptosis. In agreement with this, apoptosis has been demonstrated in various AML cell lines when the glycolytic pathway is inhibited[71].

In addition to their increased utilization of the glycolytic pathway, AML cells are also understood to be heavily reliant on glutamine[49]. Glutamine is known to be a source of nitrogen for the biosynthesis of amino acids and nucleotides[114], as well as an alternative carbon source for the biosynthesis of fatty acids[42]. The biosynthesis of fatty acids from glutamine occurs through a process known as reductive carboxylation[42]. During reductive carboxylation, glutamine-derived alpha-ketoglutarate is reductively carboxylated into citrate, which is then exported to support fatty acid synthesis[42,91]. Fatty acid synthesis has recently been shown to occur via reductive carboxylation in AML cells[140]. AML cells were found to upregulate IDH2 (isocitrate dehydrogenase 2) to catalyze the conversion of alpha-ketoglutarate to isocitrate during reductive carboxylation[140]. Reductive carboxylation is observed in cells with compromised respiratory function[91], as it requires a reductive (i.e. as opposed to oxidative) TCA cycle. Furthermore, the TCA cycle features the succinyl-CoA synthetase enzyme which can, via substrate-level phosphorylation, synthesize ATP[95]. Given that ATP is synthesized by succinyl-CoA synthetase in the mitochondrial matrix space, increased glutamine consumption by AML cells may also contribute to supporting F_1-ATPase mediated polarization of the $\Delta\Psi_m$ that sensitizes AML cells to inhibitors of glutamine metabolism. Consistent with this, CB839 is a glutaminase inhibitor that is cytotoxic to AML[58] and has previously been entered into clinical trials for the treatment of AML[133].

Central Hypothesis

The goal of this research was to 1) fully characterize the mitochondrial phenotypes of treatment naïve AML and chemoresistant AML, 2) establish a novel model of AML mitochondrial bioenergetics, 3) identify AML-selective drug targets that confer AML resistance to chemotherapy, and 4) target those protein mediators to, ultimately, thwart AML chemoresistance. We hypothesized that mitochondrial ATP consumption underlies AML survival and resistance to chemotherapy. In Chapter II, we demonstrate that AML cells sustain polarization of the $\Delta\Psi_m$ by hydrolyzing ATP via the F_1-ATPase. F_1-ATPase activity was discovered to oppose depolarization of the AML $\Delta\Psi_m$, a hallmark of apoptosis, in response to the chemotherapy. Relative to treatment naïve AML, however, chemoresistant AML were found to present with an increase in F_1-ATPase mediated polarization of the $\Delta\Psi_m$ that was also discovered to confer resistance to chemotherapy. Chemoresistance was then thwarted by leveraging mitochondrial-targeted lipophilic small-molecules that disrupt polarization by F_1-ATPase activity. In Chapter III, we demonstrate that AML OxPhos can be reactivated by BAI1, a small-molecule inhibitor of the BAX protein. Given that BAX mediates apoptosis by inducing damage to the outer mitochondrial membrane that results in the release of cytochrome C[53], we hypothesized that OxPhos deficiency in AML is driven by elevated BAX activity. However, when BAX protein expression was knocked down, we found that reactivation of AML OxPhos by BAI1 occurred in a BAX-independent manner and resulted in BAX-independent cell death. AML cell cytotoxicity following OxPhos reactivation, based on data in Chapter IV, appeared to be caused cytotoxic increases in ROS production due to a loss of ATP-dependent allosteric inhibition of the respiratory complexes. Collectively, our data inform a unique model of AML mitochondrial bioenergetics that can be preferentially targeted over that of normal blood cells in two different ways: 1) disrupting F_1-ATPase mediated polarization of the AML $\Delta\Psi_m$, and 2) reactivating AML OxPhos.

Figure 1. The electron transport system and OxPhos: (A) Schematic depicting the electron transport system and the proton circuit. (B) Schematic depicting the ATP synthase and F_1-ATPase activities of the F_1F_0-ATP synthase. (C) Schematic depicting adenylate exchange via the adenine nucleotide translocase (i.e., ANT).

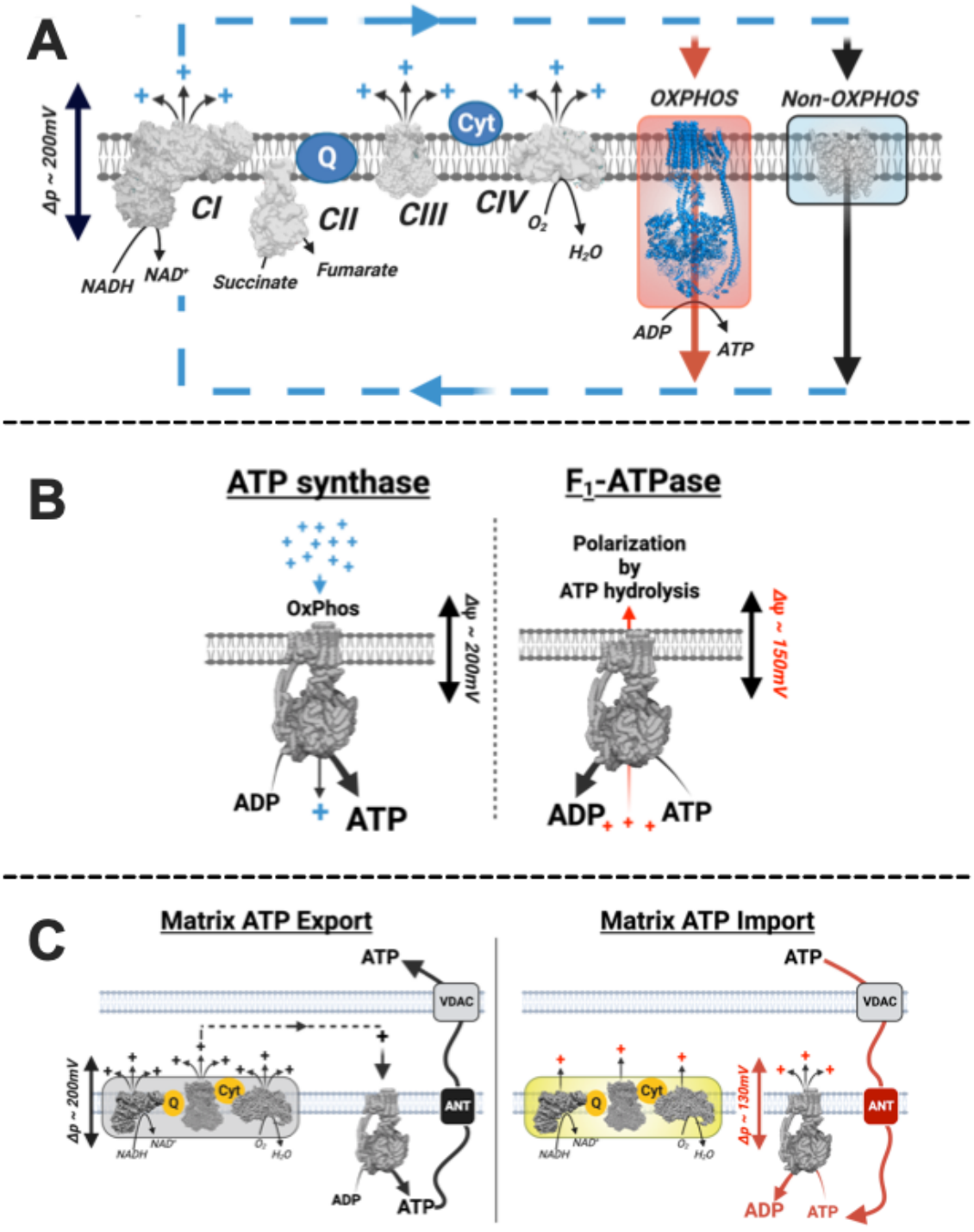

Figure 2. A unique model of AML mitochondrial bioenergetics: (A) Schematic depicting the import of ATP into the AML matrix space via ANT and inhibition by carboxyatractyloside. (B) Schematic depicting the hydrolysis of matrix ATP by the AML F_1-ATPase and inhibition by oligomycin. (C) Schematic depicting the proposed mechanism of dephosphorylative oxidation (i.e., DephOx) in AML.

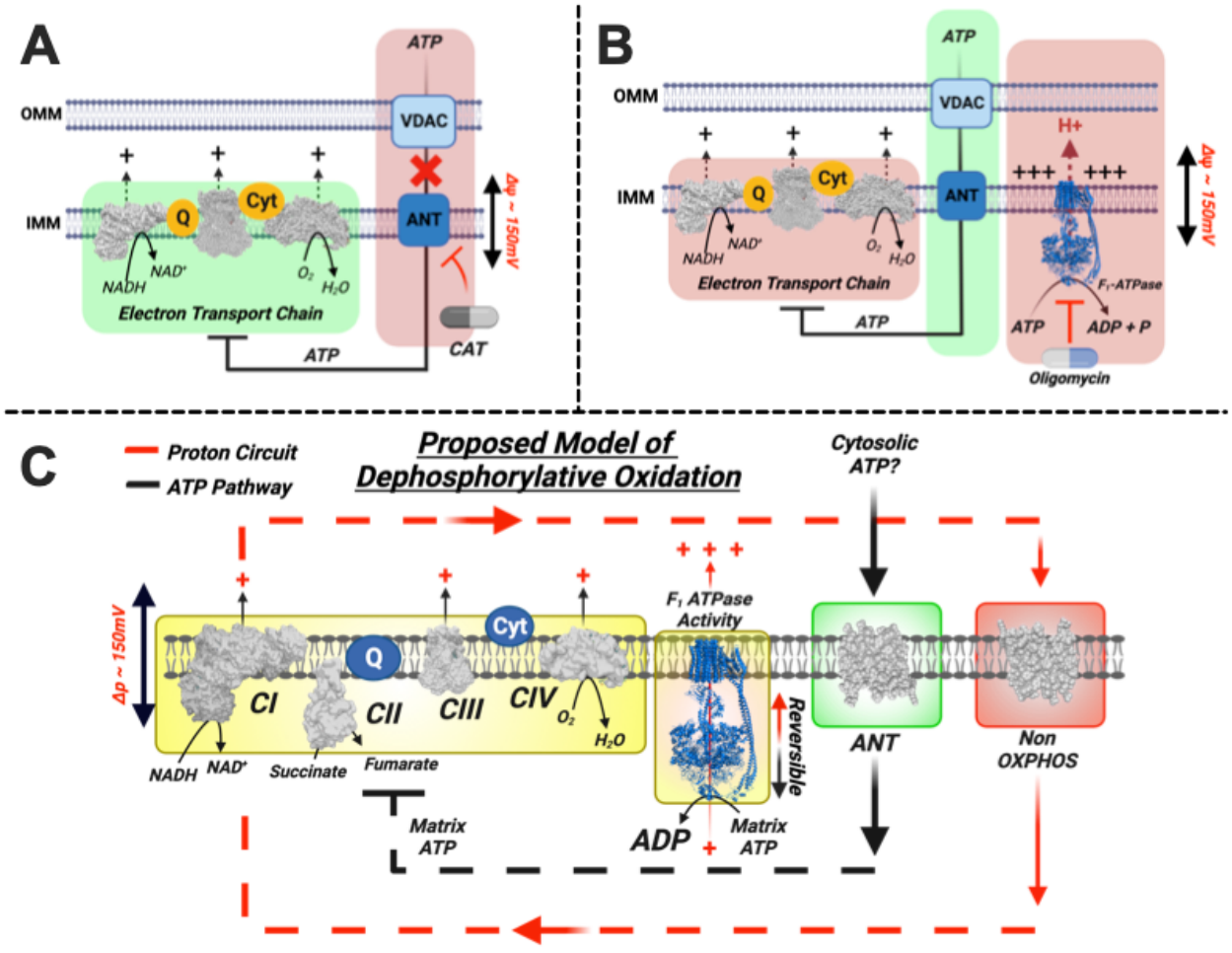

Chapter 2: ATP hydrolysis by the F_1-ATPase confers resistance to Bcl-2 inhibition in acute myeloid leukemia

ABSTRACT

Approximately three out of four patients diagnosed with acute myeloid leukemia (AML) will succumb to fatal relapse caused by the development of chemoresistant disease. Chemoresistant AML cells present with alterations in mitochondrial metabolism. For example, relative to chemosensitive AML, chemoresistant AML present with deficiencies in oxidative phosphorylation (OxPhos). While OxPhos deficiency is also a feature of chemosensitive AML, we discovered that AML cells polarize the mitochondrial membrane by hydrolyzing ATP via the F_1-ATPase. F_1-ATPase activity opposes depolarization of the mitochondrial membrane potential, a hallmark of apoptosis. Cell death was opposed by F_1-ATPase activity during AML cell respiratory inhibition. Given that respiratory impairments are known to occur in response to chemotherapy, we hypothesized that F_1-ATPase activity confers resistance to chemotherapy. Related to this, chemoresistant AML were discovered to downregulate *ATP5IF1*, the physiological inhibitor of the F_1-ATPase. Increased F_1-ATPase activity following *ATP5IF1* knockdown conferred resistance to chemotherapeutics. Chemotherapeutic exposure in combination with mitochondrial-targeted lipophilic small molecules that induced depolarization of the AML $\Delta\Psi_m$, however, resulted in synergistic cytotoxicity towards treatment naïve AML and resensitized chemoresistant AML to chemotherapy. Collectively, these data place polarization of the $\Delta\Psi_m$ via F_1-ATPase activity at the nexus of AML chemoresistance.

INTRODUCTION

Over 70% of patients suffering from acute myeloid leukemia (AML) will succumb to relapse[37,38]. Relapse in AML is caused by the inability of current treatments to eradicate drug

resistant subclones. Drug resistant subclones evade chemotherapy, fester below minimal residual disease cutoffs, and ultimately emerge to initiate fatal AML relapse. Therefore, improving AML patient outcomes depends on defining and, ultimately, thwarting the cellular mechanism(s) that drive chemotherapy resistance. Importantly, chemoresistance is often associated with alterations in mitochondrial metabolism[43,41,77]. In our hands, chemosensitive AML cells present with intrinsic limitations in oxidative phosphorylation (OxPhos)[92], relative to normal blood cells, and this becomes even more pronounced in chemoresistant AML[45]. How chemoresistant AML evade chemotherapeutics despite an OxPhos-deficient respiratory network appears to be counterintuitive - OxPhos deficiencies suggest that the proton-pumping respiratory complexes (i.e. CI/III/IV) are unable to sufficiently polarize the mitochondrial membrane potential ($\Delta\Psi_m$). However, depolarization of the $\Delta\Psi_m$ is a hallmark of apoptosis[80,48]. To evade apoptosis therefore, chemoresistant AML may sustain polarization via a non-canonical mitochondrial pathway.

Inducing apoptosis of chemoresistant AML appears to be contingent upon identifying mechanisms that sustain polarization of the $\Delta\Psi_m$ despite apparent limitations in the proton pumping respiratory complexes. Although the respiratory complexes can pump protons and sustain polarization of the $\Delta\Psi_m$, the $\Delta\Psi_m$ can also be sustained when ATP synthase reverts to an F_1-ATPase[139]. The F_1-ATPase hydrolyzes ATP to pump protons across the inner membrane (i.e., F_1-ATPase activity), thereby sustaining a voltage potential when respiratory function is limited[60]. Importantly, reductions in respiratory function are known to occur following early apoptotic induction, driven by permeabilization of the outer mitochondrial membrane and the subsequent release of cytochrome C[88]. Despite the release of cytochrome C however, F_1-ATPase activity can sustain the $\Delta\Psi_m$[103]. Given that depolarization of the $\Delta\Psi_m$ is implicated in apoptosis, it is not currently known if sustaining the $\Delta\Psi_m$ via F_1-ATPase activity allows AML to resist apoptosis in response to chemotherapeutics. To answer this, we leveraged the chemotherapeutic venetoclax. Venetoclax, an inhibitor of the anti-apoptotic Bcl-2 protein, mediates BAX/BAK dependent apoptosis[63]. In addition to mediating apoptosis, however, prior research has established that

venetoclax inhibits AML mitochondrial respiration[69]. Although mitochondrial respiration is inhibited by venetoclax, chemoresistant AML subclones evade apoptotic induction. Circumvention of apoptotic induction by chemoresistant AML therefore, hinders the eradication of chemoresistant AML blasts that, ultimately, result in fatal AML relapse. Herein, a novel mitochondrial phenotyping platform[44] was leveraged to systematically define the interplay between chemotherapy exposure, mitochondrial bioenergetics, and AML survival.

Across multiple AML models (i.e. both human[92] and mouse[21]) we consistently observe reductions in OxPhos flux, a phenotype that is even more pronounced in chemoresistant AML[45]. The current investigation sought to 1) elucidate the bioenergetic mechanisms that underlie reductions of AML OxPhos flux, 2) determine the link between reduced OxPhos flux and AML chemoresistance, and 3) leverage AML-specific vulnerabilities to thwart AML chemoresistance. Herein, the reduced OxPhos flux of AML cells was linked to intrinsic lesions in Complex IV. Complex IV lesions were masked by increased mitochondrial content in AML cells. When AML respiratory capacity was normalized to total mitochondrial protein, maximal respiration of individual mitochondria within the AML cell were lower relative to that of normal hematopoietic cells. Unlike normal hematopoietic cells that synthesize ATP, when we assessed the AML $\Delta\Psi_m$, it was discovered that ATP hydrolysis by the F_1-ATPase contributes to $\Delta\Psi_m$ polarization. Moreover, polarization of the AML $\Delta\Psi_m$ following venetoclax exposure was found to be restricted to that by F_1-ATPase activity. Given that F_1-ATPase activity opposes depolarization of the $\Delta\Psi_m$, a hallmark of apoptosis, we hypothesized that polarization mediated by the F_1-ATPase confers resistance to venetoclax. In support of this, chemoresistant AML were found to upregulate Complex V expression and downregulate *ATP5IF1* (i.e. the specific inhibitor of ATP hydrolysis by the F_1-ATPase[66,14]) expression, two adaptations expected to increase F_1-ATPase activity. Increasing F_1-ATPase activity in AML via knockdown of *ATP5IF1* conferred venetoclax chemoresistance. Given that the AML $\Delta\Psi_m$ may be actionable, we hypothesized that venetoclax would synergize with compounds that oppose F_1-ATPase mediated polarization. For this purpose, we leveraged

mitochondrial-targeted lipophilic small molecules dodecyltriphenylphosphonium (d-TPP) and MitoQ. These compounds depolarize the $\Delta\Psi_m$ by nature of their charge, independent of the source of polarization. Via this mechanism, depolarization of the AML $\Delta\Psi_m$ with either d-TPP or MitoQ, in combination with venetoclax, resulted in a loss of colony formation in treatment naïve AML. Importantly, this efficacy extended even to chemoresistant AML, where either d-TPP or MitoQ, in combination with venetoclax, restored drug sensitivity. Collectively, our findings highlight that targeting F_1-ATPase mediated polarization of the $\Delta\Psi_m$ is a novel strategy to thwart AML chemoresistance.

RESULTS

Intrinsic lesions in respiratory complex IV limit OxPhos flux in AML cells

Relative to normal myeloid progenitor cells, AML blasts are characterized by high mitochondrial content[92]. Despite having more mitochondria per cell, we previously demonstrated that less than half of the AML mitochondrial network is capable of coupling respiration to the synthesis of ATP – a phenomenon indicative of OxPhos limitations[92,45]. Across a panel of AML cells lines (both human[92,45] and mouse[21]), as well as AML patient samples, the ratio of maximal OxPhos flux to total respiratory capacity (ratio represented as 'Fractional OxPhos') is consistently below 0.5 (**Fig. 3A**) (**Supp. Fig 1A-H**). With Fractional OxPhos ratios of < 0.4, OxPhos limitations are even more pronounced in cells made resistant to chemotherapy[45] (**Fig. 3A**), suggesting that intrinsic limitations in OxPhos flux is a conserved bioenergetic feature of AML cells with potential implications for combating treatment resistance.

To explore the underlying mechanisms of OxPhos dysfunction in AML, we comprehensively evaluated both OxPhos complex expression, as well as OxPhos flux in distinct AML cell lines (e.g., MV4;11 and OCI-AML2) and compared the results to healthy myeloid progenitors isolated from bone marrow aspirate. As reported previously[92], mitochondrial protein abundance was higher in AML blasts, corresponding to a ~ 40% increase in mitochondrial content

(**Fig. 3B-C**). High mitochondrial content would be expected to lead to a corresponding increase in cellular respiratory capacity. However, protein normalized respiratory capacity was not elevated in AML blasts (**Fig. 3D**), indicating discordance between mitochondrial network size and respiratory kinetics – a feature diagnostic of respiratory complex lesions. To investigate the intrinsic composition of the respiratory system in AML, the expression of each respiratory complex and ATP synthase (i.e., the components of OxPhos) were normalized to mitochondrial content. Upon normalization to mitochondrial content, mean scaled abundance of several respiratory complexes were lower in AML cells (**Fig. 3E**) (**Supp. Fig. 1I-M**). Complex specific lesions were most pronounced for cytochrome oxidase (i.e., Complex IV), the terminal O_2 consuming enzyme in the electron transport system (ETS) (**Fig. 3E**). Consistent with impaired ETS function, cellular respiratory capacity per unit of mitochondrial protein was lower in AML cells (**Fig. 3F**). These data agree with recent findings in mouse AML cells where we observed AML-specific lesions in complexes III and IV sufficient to impair OxPhos flux[21]. Together, these data implicate low OxPhos functionality as a conserved bioenergetic feature of AML cells driven by intrinsic lesions in respiratory complex IV. Although complex IV lesions restrict respiration for a given AML mitochondrion, AML cells sustain baseline respiratory flux at levels comparable to or even higher than normal cells by expanding mitochondrial content (**Fig. 3G**).

Mitochondria in AML cells consume cellular ATP to sustain mitochondrial polarization

Despite stark deficiencies in OxPhos, AML cells have more mitochondria than normal cells and those mitochondria sustain a voltage potential across their inner membrane[92]. The $\Delta\Psi_m$ can be generated in two different ways: 1) via the proton-pumping respiratory complexes – complexes I/III/IV; or 2) matrix ATP uptake and subsequent hydrolysis by the F_1-ATPase[139]. Given that AML cells present with intrinsic lesions within the ETS that would be expected to reduce the ability of the respiratory complexes to pump protons, we hypothesized that AML mitochondria may polarize the inner membrane by hydrolyzing ATP via the F_1-ATPase. To test this, we assessed

mitochondrial polarization (using TMRM fluorescence) in individual AML cells in the absence and presence of the ATP synthase inhibitor oligomycin. Operating in non-quench mode, an increase in TMRM fluorescence with oligomycin was taken to indicate functional OxPhos, whereas a decrease in TMRM fluorescence with oligomycin was assumed to indicate that the $\Delta\Psi_m$ was being generated via F_1-ATPase activity (**Fig. 4A**). To first validate our assay, the $\Delta\Psi_m$ was assessed in respiration-incompetent p^0 OCI-AML2 ("OCI_{Rho0}") cells[52] that present with a lack of mitochondrial respiration and a hyper-reduced NADH pool. (**Supp. Fig. 2A-B**). Despite being depleted of mtDNA, p^0 cells are known to sustain the $\Delta\Psi_m$ by consuming cytosolic ATP[14]. Consistent with this, inhibition of ATP synthase with oligomycin triggered depolarization in OCI_{Rho0} cells (**Fig. 4B-C**). Importantly, in mononuclear cells isolated from healthy bone marrow, as well as PBMCs from healthy volunteers, the addition of oligomycin increased TMRM fluorescence, indicating functional OxPhos (**Fig. 4D-E**). However, the $\Delta\Psi_m$ was sustained in the presence of rotenone (i.e., a Complex I inhibitor) and antimycin A (i.e., an inhibitor of Complex III), indicating that normal blood cells, and importantly the myeloid population, are able to sustain polarization of the $\Delta\Psi_m$ by matrix ATP uptake when the ETS is compromised.

Having established the validity of our approach, we next assessed $\Delta\Psi_m$ in the absence or presence of oligomycin in AML cells. Across multiple AML cells lines (MV4;11, "$MV411_{WT}$" and OCI-AML2, "OCI_{WT}"), as well as AML patient samples, the addition of oligomycin lowered TMRM fluorescence (**Fig. 4F-G**). Remarkably, the magnitude of depolarization in AML cells upon ATP synthase inhibition was comparable to that seen in OCI_{Rho0} cells, suggesting that $\Delta\Psi_m$ is driven by F_1-ATPase activity in AML. Importantly, the AML $\Delta\Psi_m$ was also depolarized by oligomycin when OCI_{WT} cells were assayed in a medium formulated to mimic the physiological profile of human plasma (i.e. Human Plasma-Like Medium, or HPLM)) (**Fig. 4H**). However, a limitation to our approach is that changes in TMRM fluorescence of whole cells reflects the average TMRM signal of the entire mitochondrial population within a single cell. Given that single cells contain many individual mitochondria, a single AML cell may contain distinct subsets of mitochondria: 1) a

subset of “healthy” mitochondria that couple respiration to ATP synthesis and 2) a subset of “damaged” mitochondria that cannot respire, thereby consuming ATP to sustain polarization. To test this, we designed an assay that measures mitochondrial polarization (using TMRM fluorescence) of individual mitochondria within a mitochondrial population. To begin, mitochondrial populations isolated from either mouse heart or HL60 cells were energized with Complex I substrates (i.e., pyruvate and malate “P/M”) and an ATP/ADP ratio with a ΔG_{ATP} value of -61.5 kJ/mol using our creatine-kinase clamp. Oligomycin was then added to inhibit ATP synthase and FCCP (“FC”) was used as a negative control. As seen in normal healthy blood cells, oligomycin increased TMRM fluorescence in mouse heart, indicative of functional OxPhos (**Supp. Fig. 2C-D**). However, oligomycin lowered TMRM fluorescence in HL60 cells, indicative of F_1-ATPase activity (**Supp. Fig. 2C-D**). Importantly, the TMRM fluorescence signal of individual mitochondria within the mouse heart or HL60 mitochondrial population were plotted before (“Vehicle”) and after the addition of oligomycin (“Oligomycin”), revealing that oligomycin-induced changes in TMRM fluorescence of each mitochondrial population shifted homogenously (**Supp. Fig. 2E**). These data suggest that AML cells contain one mitochondrial population that consumes ATP to sustain polarization. Collectively, our data demonstrate that unlike normal blood cells with functional OxPhos, AML mitochondria consume ATP to sustain polarization of the $\Delta\Psi_m$ (**Fig. 4I**).

Inhibition of either glycolysis or glutaminolysis does not alter polarization sustained by F_1-ATPase activity

Given that AML hydrolyze ATP to sustain polarization of the $\Delta\Psi_m$, we hypothesized that this ATP may be derived from non-mitochondrial sources of ATP production. For example, non-mitochondrial ATP production can be generated via substrate-level phosphorylation during glycolysis[5] or glutaminolysis[27]. As proof of concept, the $\Delta\Psi_m$ of OCI_{Rho0} cells was measured in response to either rotenone and antimycin A, oligomycin, and 2-DG (i.e., an inhibitor of glycolysis), along with combinations thereof. In this assay, when rotenone and antimycin A inhibited the ETS,

the membrane potential was sustained, in part, by the matrix consumption of glycolytically derived ATP (**Supp. Fig. 2G**). In the presence of oligomycin, rotenone and antimycin A and 2-DG, the $\Delta\Psi_m$ of OCI_{Rho0} cells was almost completely depolarized (**Supp. Fig. 2C**). However, given that some polarization remained in the presence of 2-DG, antimycin A and oligomycin, some ATP may be generated by non-glycolytic sources (**Supp. Fig. 2C**). For example, reductive carboxylation can produce ATP in the matrix space via the succinyl-CoA synthetase enzyme and this occurs via the glutaminolytic pathway[24]. In AML cells therefore, ATP derived from glycolysis or glutaminolysis may support polarization. To test this, the effects of oligomycin on the AML $\Delta\Psi_m$ was assessed in the presence of 2-deoxyglucose or CB-839 (i.e., and inhibitor of glutaminase[131]). Despite inhibiting either glycolysis or glutaminolysis, oligomycin resulted in a similar magnitude of depolarization of the AML $\Delta\Psi_m$ (**Supp. Fig. 2H**). Collectively, these data demonstrate that inhibition of either glycolysis or glutaminolysis does not alter polarization sustained by F_1-ATPase activity in AML cells. These findings suggest that ATP synthesized in the matrix space by ATP synthase may be recycled to fuel F_1-ATPase activity, a mechanism akin to a futile cycle.

Venetoclax exposure collapses AML mitochondrial respiration and by default, polarization is sustained via F_1-ATPase activity

Polarization of the $\Delta\Psi_m$ via F_1-ATPase activity is a feature of cells with compromised respiratory function[60,22]. This mechanism confers survival to cells during respiratory disruption by preserving polarization of the $\Delta\Psi_m$[28]. As proof of concept, respiration-deficient OCI_{Rho0} cells resisted apoptosis in response to inhibition of basal respiration by IACS (i.e. a complex I inhibitor) and antimycin A (**Fig. 5A-B**). However, cytotoxicity of OCI_{Rho0} cells was observed when F_1-ATPase activity was inhibited by oligomycin, alone or in combination with the respiratory inhibitors IACS and antimycin A. (**Fig. 5A-B**). Because OCI_{Rho0} cells sustain a voltage potential via F_1-ATPase activity, we hypothesized that AML, which also sustain a voltage potential via F_1-ATPase activity, would be inherently resistant to respiratory inhibition. To test this, AML were treated with either

IACS, antimycin a, or oligomycin. AML were found to be resistant to respiratory inhibition by IACS and antimycin A, however, inhibition of F_1-ATPase activity by oligomycin resulted in AML cytotoxicity (**Fig. 5C**). These data suggest that survival of AML is contingent upon F_1-ATPase activity, therefore, we hypothesized that inhibiting F_1-ATPase mediated polarization of the $\Delta\Psi_m$ would induce AML cytotoxicity. To test this, AML were exposed to BAM15 (i.e. a mitochondrial protonophore that directly depolarizes the $\Delta\Psi_m$). Depolarization of the $\Delta\Psi_m$ by BAM15 induced dose-dependent cytotoxicity in AML (**Fig. 5D**). Taken together, these data suggest that mitochondrial respiration is dispensable for AML survival; however, disrupting mitochondrial polarization is highly cytotoxic to AML cells, suggesting that $\Delta\Psi_m$ is actionable in AML.

Disruptions in AML cell respiration is reported to occur in response to various chemotherapeutics including – doxorubicin[96], cytarabine[54], and venetoclax[69]. Venetoclax, a specific inhibitor of the anti-apoptotic Bcl-2 protein, has been shown to directly inhibit AML respiratory flux[69,110]. In our hands, 1-hour exposure to venetoclax in treatment naïve AML cells ("$MV411_{WT}$" and "OCI_{WT}") collapses respiratory capacity and OxPhos respiratory flux without overtly reducing cell viability (**Fig. 5D-G**) (**Supp. Fig. 3A-B**). We hypothesized that the collapse of respiration in response to venetoclax would also present as a loss in polarization by the proton-pumping respiratory complexes. To test this, we designed an assay that measures changes in the $\Delta\Psi_m$ of digitonin-permeabilized cells. Operating in quench mode, shifts in TMRM fluorescence can be quantified under experimentally controlled buffer conditions. Using this approach, polarization of the $\Delta\Psi_m$ induced by various substrates was measured following 1-hour exposure of treatment naïve AML cells to venetoclax. Venetoclax exposure inhibited polarization by Complex I (pyruvate/malate/glutamate or "P/M/G") and Complex II (succinate/rotenone or "S/Rot) substrates in treatment naïve AML (**Fig. 5H**) (**Supp. Fig. 3C-D**). However, polarization by F_1-ATPase activity ("ATP") was unaltered (**Fig. 5H**) (**Supp. Fig. 3C-D**). Therefore, we hypothesized that polarization of the $\Delta\Psi_m$ in response to venetoclax exposure is sustained by F_1-ATPase activity. To test this, treatment naïve AML were exposed to venetoclax for 1-hour and the $\Delta\Psi_m$

was measured using our "OxPhos Kinetics" assay. In this assay, venetoclax exposed cells were energized with pyruvate and malate, and the $\Delta\Psi_m$ was measured across a span of physiological ATP free energy (ΔG_{ATP}) values. Following this oligomycin was added to inhibit ATP synthase and FCCP was added as a negative control. Venetoclax exposure resulted in a loss of $\Delta\Psi_m$ by pyruvate and malate (**Fig. 5I**). In both groups, polarization induced by the titration of ΔG_{ATP} was inhibited by the addition of oligomycin, however, the magnitude of depolarization was greater in venetoclax exposed AML cells (**Fig. 5I**). These data indicate that the $\Delta\Psi_m$ is sustained by F_1-ATPase activity in response to venetoclax. Given that F_1-ATPase activity sustains the $\Delta\Psi_m$ of treatment naïve AML during venetoclax exposure, we hypothesized that targeting F_1-ATPase mediated polarization with oligomycin or BAM15 would synergize with venetoclax in treatment naïve AML. To test this, colony formation of OCI_{WT} cells was measured in the presence of venetoclax, in combination with either oligomycin or BAM15. Exposure to BAM15 or oligomycin in combination with venetoclax synergistically inhibited colony formation of OCI_{WT} cells (**Supp. Fig. 3E**). These data indicate that venetoclax collapses mitochondrial respiration in AML cells and by default, polarization of the AML $\Delta\Psi_m$ is sustained by F_1-ATPase activity (**Fig. 5J**). Given that polarization of the $\Delta\Psi_m$ appears critical for AML survival, these data suggest that F_1-ATPase activity may lay the groundwork for chemoresistant disease.

Downregulation of *ATP5IF1* in AML confers chemoresistance

Depolarization of the $\Delta\Psi_m$ is a known driver of cell death via apoptosis[80,48]. Herein, treatment naïve AML sustain polarization of the $\Delta\Psi_m$ by the ETS as well as ATP hydrolysis by the F_1-ATPase. However, exposure of treatment naïve AML to venetoclax resulted in a profound impairment of proton pumping by the respiratory complexes that restricted polarization of the $\Delta\Psi_m$ to F_1-ATPase activity. Based on this, we hypothesized that sustaining polarization of the $\Delta\Psi_m$ via F_1-ATPase activity allows AML cells to resist venetoclax induced cell death, in turn laying the groundwork for venetoclax resistant disease. To test our hypothesis, we developed in-vitro models

of venetoclax resistance by gradually exposing treatment naïve AML cells to increasing concentration of venetoclax until they were refractory to venetoclax ($MV411_{Vclax}$, $OCI_{Vclax,}$ and $MOLM\text{-}13_{Vclax}$). To validate our in-vitro models, venetoclax resistant AML were treated with increasing doses of venetoclax. In response to venetoclax, venetoclax resistant AML were found to oppose apoptosis (**Fig. 6A**). Having established our in-vitro models of venetoclax resistance, we then evaluated the impact of venetoclax resistance on mitochondrial OxPhos flux, membrane potential, and proteome composition. The abundance of all three of the proton-pumping respiratory complexes (Complex I/III/IV) were downregulated in $MV411_{Vclax}$ and OCI_{Vclax} (**Fig. 6B**). In $MV411_{Vclax}$ isolated mitochondria, downregulations in the respiratory complexes was accompanied by reduced expression of *ATP5IF1* (**Fig. 6C**). Given that *ATP5IF1* specifically blocks ATP hydrolysis[66,14], downregulation of *ATP5IF1* would be expected to drive increased matrix F_1-ATPase activity. Based on thermodynamic principles, we hypothesized that decreased respiratory complex abundance would be expected to favor matrix ATP uptake which, in combination with a downregulation of *ATP5IF1*, would manifest as low OxPhos flux, however, polarization of the $\Delta\Psi_m$ would be sustained by F_1-ATPase activity. To test this, OxPhos flux and $\Delta\Psi_m$ was measured in venetoclax resistant AML cells. Venetoclax resistant AML were found to be profoundly OxPhos deficient (**Fig. 6D**) (**Supp. Fig. 4A-C**). Consistent with minimal OxPhos flux, oligomycin depolarized the $\Delta\Psi_m$ of chemoresistant AML more than that in treatment naïve AML, demonstrating that enhanced F_1-ATPase activity sustained polarization of the $\Delta\Psi_m$. (**Fig. 6E**) (**Supp. Fig. 4D-F**). To confirm F_1-ATPase dependent mitochondrial polarization occurs in living venetoclax-resistant AML cells, we assessed $\Delta\Psi_m$ of intact venetoclax resistant AML cultures in the absence and presence of oligomycin, as described previously. Indeed, oligomycin resulted in a depolarization of the $\Delta\Psi_m$ in venetoclax resistant AML, indicating that venetoclax resistant AML sustain polarization via F_1-ATPase activity (**Fig. 6F**). Interestingly, cytochrome C increased $MOLM\text{-}13_{Vclax}$ state IV respiratory flux (i.e., respiratory flux stimulated by only substrates in the absence of ADP or FCCP), indicating that venetoclax resistance cells may survive despite

permeabilization of the outer mitochondrial membrane (**Supp. Fig. 4C**). Taken together, our data identify F_1-ATPase activity as a cell-intrinsic mechanism by which AML cells may resist Bcl-2 targeted therapy.

F_1-ATPase activity conferred an inherent resistance to respiratory inhibition in respiration incompetent OCI cells and AML cells (**in reference to Fig. 5B-C**). Because AML cell exposed to venetoclax present with collapsed mitochondrial respiration, we hypothesized that F_1-ATPase activity confers resistant to venetoclax. To test this, we generated an *ATP5IF1* knockdown model in treatment naive AML ("$MV411_{shCtrl}$" and "$MV411_{shIF1}$". Consistent with a loss of *ATP5IF1* expression (**Fig. 6G**) (**Supp. Fig. 4G**), F_1-ATPase activity was elevated in the *ATP5IF1* knockdown cells (**Fig. 6H-I**). Based on previous work that shows ATP5IF1 preferentially inhibits ATP hydrolysis by the F_1-ATPase[66,14], we hypothesized that *ATP5IF1* was selective for inhibiting ATP hydrolysis in AML. To test this, we leveraged our "Oxphos Kinetics" assay to capitalize on a finding from our previous publication where it was discovered that matrix ATP inhibited AML uncoupled respiratory flux[92]. The purpose of this assay was two-fold: 1) to determine if, in the presence of ATP, the F_1-ATPase can hydrolyze matrix ATP to rescue uncoupled respiration, and 2) to determine if knockdown of *ATP5IF1* increases AML "Fractional OxPhos". To begin, *ATP5IF1* knockdown cells were energized with multiple substrates (pyruvate, malate, glutamate, succinate, and octanoyl-carnitine; P/M/G/S/O) and respiration was stimulated across a physiological span of ΔG_{ATP} values. Following this, each group was provided either oligomycin, or no oligomycin, to inhibit the activity of the F_1-ATPase, and maximal respiratory flux in each group was quantified by titrating FCCP uncoupler (**Supp. Fig. 4G**). These data were normalized by making paired measurements of $MV411_{shCtrl}$ and $MV411_{shIF1}$ total respiratory capacity (**Supp. Fig. 4H**) using the same substrate conditions in an adenylate replete buffer. These experiments resulted in two pieces of evidence that demonstrate specificity of *ATP5IF1* for ATP hydrolysis: 1) the "Fractional OxPhos" ratio (represented as a percentage of total respiratory flux) was unaffected by *ATP5IF1* knockdown, indicating that increased ATP synthesis was not stimulated following by a decrease

in *ATP5IF1* expression, and 2) increased F_1-ATPase activity opposed the inhibition of uncoupled respiratory flux by matrix ATP (**Fig. 6J**). To confirm that live *ATP5IF1* knockdown cells sustain polarization via F_1-ATPase, the $\Delta\Psi_m$ of intact *ATP5IF1* knockdown cells was quantified. Depolarization in response to oligomycin indicates that polarization of the $\Delta\Psi_m$ still occurs via F_1-ATPase activity following *ATP5IF1* downregulation (**Fig. 6I**). Having validated the knockdown model, sensitivity to venetoclax was measured in the *ATP5IF1* knockdown cells. *ATP5IF1* knockdown cells resisted venetoclax-induced apoptosis (**Fig. 6K**). Furthermore, loss of *ATP5IF1* opposed reductions in colony formation of venetoclax treated *ATP5IF1* knockdown cells (**Fig. 6L-M**). Taken together, these data demonstrate that downregulation of *ATP5IF1* in AML confers chemoresistance (**Fig. 6N**).

Targeting F_1-ATPase dependent polarization of the $\Delta\Psi_m$ restores venetoclax sensitivity.

Our preliminary data place F_1-ATPase activity at the nexus of AML chemoresistance. Specifically, AML cells resistant to venetoclax appear to circumvent the effects of Bcl-2 inhibition on OxPhos flux by boosting F_1-ATPase activity. Enhanced F_1-ATPase activity sustains polarization across the inner mitochondrial membrane. Given that loss of mitochondrial polarization drives AML apoptosis, we hypothesized that targeting F_1-ATPase dependent polarization of the $\Delta\Psi_m$ would restore sensitivity to venetoclax. To test this, we leveraged mitochondrial-targeted lipophilic small molecules d-TPP and MitoQ because of their unique chemical properties. Driven by the mitochondrial voltage potential, these positively charged compounds accumulate in the negatively charged matrix where they directly interfere with mitochondrial polarization (**Fig. 7A**). Importantly, MitoQ is an over-the-counter supplement that has previously been shown to demonstrate anti-cancer effects[25], and the mitochondrial-targeted portion of MitoQ is similar to that of d-TPP (**Fig. 7A**). To demonstrate that these compounds interfere with the AML $\Delta\Psi_m$, polarization by the respiratory complexes and that by F_1-ATPase activity was measured in response to either d-TPP or MitoQ. Exposure to these compounds resulted in depolarization of $\Delta\Psi_m$ regardless of the

source of polarization (ETS or F1-ATPase) (**Fig. 7B-C**) (**Supp. Fig. 5A-F**). Consistent with depolarization of the $\Delta\Psi_m$, d-TPP also stimulates respiration similarly to mitochondrial uncouplers (**Supp. Fig. 5G**). However, unlike respiratory uncouplers, d-TPP also inhibits Complex I respiration (**Supp. Fig. 5H-I**). Taken together, these data demonstrate that the mitochondrial-targeted lipophilic small molecules d-TPP and MitoQ depolarize the AML $\Delta\Psi_m$.

Depolarization of the $\Delta\Psi_m$ by BAM15 was found to be cytotoxic to AML cells (**in reference to Fig 5C**). Therefore, we hypothesized that depolarization of the $\Delta\Psi_m$ by d-TPP would be cytotoxic to AML. To test this, treatment naïve AML were treated with increasing doses of d-TPP. Depolarization of the $\Delta\Psi_m$ by d-TPP induced single agent toxicity in treatment naïve AML (**Fig. 7D**). Having established that depolarization of the $\Delta\Psi_m$ by d-TPP is cytotoxic to treatment naïve AML, we hypothesized that d-TPP would synergize with venetoclax in treatment naïve AML. Therefore, using Healthy BMC cells, we measured colony formation in response to increasing doses of d-TPP (100nM, 250nM and 500nM), as well as 100nM d-TPP in combination with venetoclax, such that a dose of d-TPP could be identified that is preferentially cytotoxic to AML as opposed to normal blood cells. Although Healthy BMC colony formation was inhibited by high doses of d-TPP (250nM and 500nM), 100nM d-TPP alone, and in combination with venetoclax, did not interfere with Healthy BMC colony formation (**Fig. 7E**). Having established this, we tested the hypothesis that d-TPP would synergize with venetoclax in treatment naïve AML. To test this, colony formation of treatment naïve AML was measured using similar doses of d-TPP as that in the Healthy BMC assay. Unlike Healthy BMC, treatment naïve AML were highly sensitive to 100nM d-TPP, in combination with venetoclax, that profoundly inhibited colony formation (**Fig. 7F-G**). Importantly, the magnitude of colony formation inhibition by 250nM d-TPP single agent was greater in treatment naïve AML, relative to normal blood cells, and 100nM d-TPP single agent was inhibitory to colony formation of OCI_{WT}, specifically. These data demonstrate that sustaining polarization via F_1-ATPase activity during venetoclax exposure sensitizes treatment naïve AML to agents that depolarize the $\Delta\Psi_m$. Lastly, because chemoresistant AML sustain polarization via F_1-

ATPase activity, we hypothesized that d-TPP and MitoQ would restore venetoclax sensitivity. To test this, viability and colony formation of chemoresistant AML was measured in response to either d-TPP or MitoQ, and that in combination with venetoclax. Importantly, d-TPP and MitoQ restored venetoclax sensitivity in chemoresistant AML, thereby resulting in cytotoxicity and a profound impairment of colony formation (**Fig. 7H-J**) (**Supp. Fig. 5J-K**). Collectively, these data demonstrate that targeting F_1-ATPase dependent polarization of the $\Delta\Psi_m$ with d-TPP and MitoQ restores venetoclax sensitivity, thereby placing F_1-ATPase mediated polarization of the $\Delta\Psi_m$ at the nexus of chemoresistance (**Fig. 7K**). Given that chemoresistant AML cytotoxicity induced by d-TPP is enhanced by the presence of venetoclax, the effects of venetoclax appear to be retained even after the development of chemoresistant disease (**Fig. 7H-I**) (**Supp. Fig. 5J**).

DISCUSSION

Acute myeloid leukemia is often described as being overly reliant on OxPhos[76,75,74,65], however, such interpretations are based on whole cell measurements of 1) mitochondrial respiration, or 2) mitochondrial protein expression. These measurements may be reflective of an increased demand for ATP synthesis, or a decrease in OxPhos efficiency that triggers a compensatory increase in mitochondrial content. To account for differences in mitochondrial content, intact cell mitochondrial respiration and OxPhos protein abundance were normalized to mitochondrial content. By doing this, our data show that individual mitochondria within the AML cell, relative to that in normal blood cells, present with reduced maximal respiration. Within individual AML mitochondria, reductions of maximal respiration were driven, primarily, by a downregulation of Complex IV (i.e., the oxygen consuming respiratory complex). Importantly, mitochondrial ATP synthesis requires robust proton pumping by the respiratory complexes to highly polarize the $\Delta\Psi_m$. A highly polarized $\Delta\Psi_m$ provides the thermodynamic driving force necessary to cause ATP synthesis to occur at the F_1 sector of ATP synthase, thus inhibiting the hydrolysis of ATP by the F_1-ATPase[93]. The F_1-ATPase will hydrolyze ATP and pump protons

across the inner membrane if the $\Delta\Psi_m$ falls beneath the reversal potential[30] (i.e., the $\Delta\Psi_m$ where ATP synthase reverts to an F_1-ATPase). A less negative $\Delta\Psi_m$ driven by lesions in Complex IV would be expected to limit the ability of the ETS to synthesize ATP, consistent with the reduced fractional OxPhos in AML. When the AML $\Delta\Psi_m$ was assessed, we made the exciting discovery that AML cells hydrolyze ATP via the F_1-ATPase to sustain polarization. Polarization via F_1-ATPase activity appears to be a conserved feature of the myeloid lineage that, when respiratory function becomes compromised, opposes depolarization of the $\Delta\Psi_m$. Given that mitochondrial polarization was highly important for AML survival, F_1-ATPase mediated polarization by AML cells provides an inherent resistance to respiratory inhibition and a survival advantage upon chemotherapeutic exposure. For example, exposure to venetoclax profoundly inhibited respiration, however, chemoresistant AML cells survive venetoclax exposure by sustaining polarization via F_1-ATPase activity. In support of this, *ATP5IF1* knockdown in treatment naïve AML cells conferred resistance to venetoclax. Targeting F_1-ATPase activity that sustained the $\Delta\Psi_m$ during venetoclax exposure, therefore, was achieved using the mitochondrial-targeted, lipophilic small-molecules d-TPP and MitoQ. These compounds disrupted F_1-ATPase mediated polarization of the AML $\Delta\Psi_m$ that, in combination with venetoclax, resulted in profound synergistic efficacy. Importantly, this synergistic efficacy also extended to chemoresistant AML where drug sensitivity was restored. These data indicate that the effects of venetoclax remain present even after the development of chemoresistant disease.

AML cells were found to hydrolyze ATP via the F_1-ATPase despite increases in whole cell basal respiration relative to normal blood cells. These data are perplexing, as mitochondria are not currently thought to be able to both respire and hydrolyze ATP. To explain how this may occur, our previous study discovered that AML cell respiration was profoundly inhibited following the import of extramitochondrial ATP into the matrix space via ANT[92] (i.e., adenine nucleotide translocase). ANT is known to mediate the exchange of matrix ATP for ADP across the inner membrane, driven by the $\Delta\Psi_m$[30,9]. When the $\Delta\Psi_m$ is insufficient however, based on

thermodynamic principles, ANT will import ATP in exchange for matrix ADP and this exchange polarizes the $\Delta\Psi_m$[9]. Importantly, matrix ATP is an allosteric inhibitor of Complex IV[10,11] and various TCA cycle enzymes (e.g., fumarase[99], isocitrate dehydrogenase[122], and citrate synthase[59]). Consistent with the findings in our previous study[92], when these respiratory components are inhibited by matrix ATP, it would be expected to result in an inhibition of respiratory flux that further constrains polarization of the $\Delta\Psi_m$ by the ETS. For respiration to continue unopposed, ATP must be depleted from the mitochondrial matrix. Herein, matrix ATP hydrolysis by the F_1-ATPase was sufficient to rescue the inhibition of uncoupled AML respiratory flux by ATP, however, inhibition of F_1-ATPase activity by oligomycin resulted in inhibition of uncoupled respiratory flux. Taken together, we suspect that AML mitochondrial bioenergetics can be characterized by a novel bioenergetic model that resembles an alternating current (AC) circuit. In an AC circuit, the peak voltage potential is not constantly maintained, rather, the voltage potential rapidly cycles from peak to baseline and back to peak. The voltage potential generated by the AML respiratory complexes is not sufficient to export matrix ATP via ANT[92]. Thus, ANT either imports matrix ATP, or ATP synthesized in the matrix space may 1) inhibit proton pumping by the respiratory complexes, thereby reducing the "peak" voltage potential or 2) be hydrolyzed by the F_1-ATPase to sustain a "baseline" voltage potential, thereby depleting the matrix of ATP (**Fig. 8A**). However, if ATP is depleted from the matrix by the F_1-ATPase, this in turn would prevent the inhibition of respiration by ATP and return the voltage potential back towards the "peak". Alternatively, the "peak" voltage potential generated by the respiratory complexes creates a "backpressure" that opposes proton pumping by the F_1-ATPase[93,30] thereby preventing F_1-ATPase activity needed to deplete the matrix of ATP. Accumulation of ATP in the matrix then can then inhibit respiration and return the voltage potential back towards "baseline" that can be sustained again by F_1-ATPase activity. Collectively, we propose that F_1-ATPase activity and respiratory flux occur simultaneously at submaximal voltage potentials in-between the ETS induced "peak" voltage potential and the F_1-ATPase induced, "baseline" voltage potential of the AC circuit model, thus fueling respiration

that is not coupled to synthesis of ATP (**Fig. 8A**). Although ATP synthesis can be fueled by a highly polarized $\Delta\Psi_m$ in normal blood cells, AML appear to use their membrane potential to, primarily, drive non-OxPhos processes such as aspartate export, for example, which is necessary for proliferation[121]. Nonetheless, given that ATP within the matrix must be hydrolyzed by the F_1-ATPase to support substrate oxidation, we propose that AML mitochondrial bioenergetics can be described as dephosphorylative oxidation (i.e., DephOx), as opposed to OxPhos (**Fig. 8B**).

During OxPhos, mitochondrial respiration is coupled to the synthesis of ATP. Thus, the intracellular ATP/ADP acts as a signal that links mitochondrial respiration to the intracellular ATP demand. As a demand-driven process, OxPhos opposes aberrant mitochondrial metabolism. Importantly, abberant mitochondrial metabolism is a known feature of AML[43,118]. Consistent with our data, AML mitochondrial respiration is not coupled to the synthesis of ATP which would be expected to present as abberant mitochondrial metabolism that occurs independently of a demand for intracellular ATP. Rather, ATP is consumed by the AML F_1-ATPase to sustain the $\Delta\Psi_m$, inducing bioenergetic stress by being unable to contribute the intracellular ATP demand. To satisfy the intracellular ATP demand therefore, AML may rely on non-mitochondrial sources of ATP and are therefore hallmarked by increases in 1) glutaminolysis[137,49] , that produces ATP in the matrix via substrate-level phosphorylation by succinate-CoA ligase[24] and 2) glycolysis[100], that produces ATP in the cytosol via substrate-level phosphorylation by phosphoglycerate kinase[100] and pyruvate kinase[57]. Importantly, inhibition of glucose or glutamine metabolism is understood to be cytotoxic to AML[70,81], therefore, CB-839 (i.e. an inhibitor of glutaminase[131]) has been entered into clinical trials for the treatment of AML[133]. Furthermore, AML chemoresistance is associated with an increased dependence on glucose[116,117] and glutamine[130] metabolism, and importantly, this coincides with our data demonstrating an increased utilization of F_1-ATPase activity to sustain the $\Delta\Psi_m$ in chemoresistant AML.

At the nexus of AML chemoresistance, our data identify F_1-ATPase mediated polarization of the $\Delta\Psi_m$. Polarization of the $\Delta\Psi_m$ by F_1-ATPase activity is a feature of bioenergetically stressed

cells. Thus, given our extensive data demonstrating that AML mitochondria are bioenergetically stressed, targeting F_1-ATPase activity in AML cells represents an exciting opportunity to intervene on a unique AML-specific mitochondrial pathway. F_1-ATPase mediated polarization can be disrupted in one of two distinct ways: 1) direct inhibition of the F_1-ATPase, or 2) depolarization of the $\Delta\Psi_m$. For example, depolarization of the $\Delta\Psi_m$ by either d-TPP or MitoQ, in combination with venetoclax, synergistically disrupted polarization of the $\Delta\Psi_m$ in chemoresistant AML and restored venetoclax sensitivity. Venetoclax sensitivity was also enhanced in treatment naïve AML by direct F_1-ATPase inhibition with oligomycin. Given that inhibition of the F_1-ATPase is the physiological role of *ATP5IF1*[66,14], our data provides a rationale for developing a mimetic of *ATP5IF1*. However, an *ATP5IF1* mimetic should be carefully designed to mimic the conditionally-dependent mechanism of *ATP5IF1* that specifically inhibits the hydrolysis of ATP when ATP synthase reverts to an F_1-ATPase proton pump[66,14]. F_1-ATPase proton pumping occurs in bioenergetically stressed AML cells to sustain the $\Delta\Psi_m$. When the $\Delta\Psi_m$ is sustained by F_1-ATPase activity, ATP binds to the F_1 sector of ATP synthase and the hydrolysis of ATP induces a rotation of the F_1-ATPase. During this process, *ATP5IF1* can bind the F_1-ATPase enzyme, thereby preventing further rotation of the motor and disrupting F_1-ATPase mediated polarization of the $\Delta\Psi_m$[66,14]. However, when the $\Delta\Psi_m$ is highly polarized, proton reentry into the matrix through the F_0 motor can induce a counterrotation of the F_1-ATPase enzyme that fuels the synthesis of ATP. When ATP synthesis occurs, *ATP5IF1* has been shown to be ejected from it's binding site on the F_1-ATPase, thereby selectively inhibiting the hydrolysis of ATP by the F_1-ATPase[66]. Thus, inhibition of the F_1-ATPase via *ATP5IF1* provides a way to inhibit F_1-ATPase activity in AML without compromising ATP synthesis. Therefore, we suspect that a peptide mimetic of *ATP5IF1* may be an ideal approach to target F_1-ATPase mediated polarization of the $\Delta\Psi_m$ given the specificity of *ATP5IF1* for F_1-ATPase activity. With this approach, it may be possible to achieve AML-selective toxicity that would ultimately, thwart chemoresistance. Collectively, our findings present a novel and actionable AML-specific

mechanism of chemoresistance, thus highlighting the utility of using mitochondrial diagnostics to distinguish cancer from non-cancer mitochondrial phenotypes.

METHODS

All procedures involving human subjects were approved by the Institutional Review Board of the Brody School of Medicine.

Blood collection and isolation of PBMCs.

Venous blood from the brachial region of the upper arm was collected from healthy volunteers, between the ages of 18-70 years. Whole blood was collected in sodium-heparinized Cell Preparation Tubes (CPT) (BD Biosciences, Franklin Lakes, NJ) and was then centrifuged at 1,800 x *g* for 15 min. Mononuclear cells were washed in ammonium-chloride-potassium (ACK) lysis buffer to remove red blood cells and were either used immediately, or frozen in liquid nitrogen (-80°C.) prior to experimentation.

Mononuclear cell isolation from bone marrow aspirates

Bone marrow aspirates were collected from healthy donors, ages 26-33, supplied by HemaCare (Northridge, CA). For primary leukemia samples, bone marrow aspirates were collected from patients undergoing confirmatory diagnosis for a range of hematological malignancies. Patients with confirmed acute myeloid leukemia were enrolled in the study. Patient age ranged from 32-78 years. Bone marrow aspirates were collected in sodium-heparinized Cell Preparation Tubes (CPT) (BD Biosciences, Franklin Lakes, NJ) and centrifuged at 1,800 x *g* for 15 min. Mononuclear cells were isolated and then washed in ACK lysis buffer to remove red blood cells and used immediately for experiments.

CD34+ Stem/Progenitor cell collection and culture

CD34+ cells were purchased from HemaCare (Northridge, CA). These cells were isolated and purified from bone marrow aspirates of healthy donors, ages 20-39. A portion from each vial was cultured in IMDM supplemented with 15% HyClone FBS, recombinant human SCF (25ng/mL), TPO (50ng/mL), and FLT-3 (50ng/mL).

Culturing of leukemic cell lines

MV4;11, HL60, KG-1, JVM3, OCI-AML2, MM6, and U937 (ATCC, Manassas, VA) human leukemia cells were cultured in IMDM or RPMI-1640 (Thermo Fisher Scientific, Waltham, MA) supplemented with glutamax, 10% FBS, and 1% penicillin/streptomycin and incubated at 37°C in 5% CO_2. For experiments involving venetoclax resistance, MV4;11, OCI-AML2, MOLM-13, and HL60 cells were cultured in either IMDM or RPMI-1640, supplemented with glutamax, 10% FBS, and 1% penicillin/streptomycin. To model venetoclax resistance, cells were adapted in culture to 1uM venetoclax by passaging cells in increasing doses of venetoclax beginning at 10nM. After reaching an average cell density of $1x10^6$ cell per mL, maintained in 1uM venetoclax, the cells were harvested and used for experimentation.

Cell viability assays

Cell viability for mitochondrial functional assessments were quantified with viable cell counts using Trypan Blue (0.4%). For fluorescent measurements of cell viability, cells were seeded in black-wall, 96-well plates, in growth medium. After addition of agents (0.2mL final well volume), cells were incubated at 37° C, 5% CO_2, for the indicated times. Viability was determined using propidium iodide (PI). Positive control cells were permeabilized by addition of 1µl of 10.0mg/ml digitonin and incubated at 37° C, 5% CO_2, for 20min. Following this, plates were centrifuged at 1200 x *g* for 10 min. After centrifugation, plates were dumped to remove culture media and 0.100mL of a 5.0µM PI solution in PBS was added. The plate was then incubated at

37° C, 5% CO_2 for 20min, and viability was calculated as the mean fluorescence (minus permeabilized vehicle control) at 530nm excitation and 620nm emission.

OxPhos kinetics assay

OxPhos kinetics were measured using a modified version of the creatine-kinase clamp (CK Clamp). For experiments using the CK clamp assay, the free energy of ATP hydrolysis (ΔG_{ATP}) is calculated using the equilibrium constant for the CK reaction (K'_{CK}) and is based upon the addition of known concentrations of creatine (CR), phosphocreatine (PCR), and ATP in the presence of excess amounts of CK (Fisher-Wellman et al., 2018). Calculation of ΔG_{ATP} at defined PCR concentrations was done using the online resource (https://dmpio.github.io/bioenergetic-calculators/ck_clamp/) as previously described[44].

Respiratory flux in intact and permeabilized cells

Approximately $2x10^6$ cells were used for each intact and permeabilized cell respirometry experiment. Respirometry measurements were conducted using an Oroboros Oxgraph-2k (O2k; Oroboros Instruments, Innsbruck, Austria) in either a 0.5 or 1.0mL reaction volume at 37°C. Data was normalized to viable cell count unless otherwise indicated. For normalization to total protein, cell suspensions were removed from the O2k chamber following the completion of each assay and placed into microcentrifuge tubes. The cell suspension was then centrifuged at 2,000 x *g* for 10min at 4°C. Assay buffer was aspirated and the cell pellet was washed with PBS. Cells were then lysed using low-percentage detergent buffer (CelLytic M) followed by a freeze-thaw cycle on dry ice. The protein concentration was then determined using a BCA protein assay.

Respiratory flux was measured using methods described previously[44]. For intact cell measurements, cells were resuspended in Intact Cell Respiratory Media (17.7g/L Iscove's Modified Dulbecco's Medium (IMDM), 20mM HEPES, 1% Penicillin/Streptomycin, 10% FBS, pH 7.4). Basal respiration was measured, followed by the quantification of maximal respiration by

titrating FCCP uncoupler (FC; 0.5-5μM). Antimycin A (Ant; 0.5μM) was used to inhibit mitochondrial respiration.

For permeabilized cell measurements, cells were resuspended in Respiratory Buffer supplemented with creatine (105mM MES potassium salt, 30mM KCl, 8mM NaCl, 1mM EGTA, 10mM KH_2PO_4, 5mM $MgCl_2$, 0.25% BSA, 5mM creatine monohydrate, pH 7.2). Cells were permeabilized with digitonin ("Digi", 0.02mg/mL). OXPHOS respiratory kinetics were measured using the creatine kinase (CK) clamp, and respiratory capacity was quantified with FCCP titration.

For all assays using the CK clamp technique, various combinations of carbon substrates and inhibitors were utilized. Substrates and inhibitors used in each assay are indicated in the figure legends: CK (20U/mL), ATP (5mM), PCr (1mM, 6mM, 15mM, 21mM), pyruvate (Pyr or P; 5mM), malate (M; 1mM), octanoyl-carnitine (O; 0.2mM), succinate (Succ or S; 5mM), glutamate (Glut or G; 5mM), oligomycin (Oligo, 0.02μM), FCCP (0.5-2μM), rotenone (Rot or R, 0.5μM), antimycin A (Ant A, 0.5μM), venetoclax (Vclax, 0.1nM-1μM), dodecyltriphenylphosphonium (d-TPP, 0.1μM-0.5μM), FCCP (5uM), MitoQ (MitoQ, 0.1μM-0.5μM).

Isolation of mitochondria from leukemia cells

Leukemia cells were harvested and centrifuged at 300 x *g* for 7 min, washed in ice cold PBS, and centrifuged again at 500 x *g* for 10 min. Cell pellets were then resuspended in Mitochondrial Isolation Buffer with BSA (100mM KCl, 50mM MOPS, 1mM EGTA, 5mM $MgSO_4$, 0.2% BSA, pH 7.1) and homogenized using a borosilicate glass mortar and Teflon pestle. Cell homogenate was centrifuged at 800 x g for 10min at 4°C. Following this, supernatant was collected and centrifuged at 10,000 x *g* for 10 min at 4°C to pellet the mitochondrial fraction. The mitochondrial fraction was resuspended in Mitochondrial Isolation Buffer without BSA, transferred to a microcentrifuge tube and centrifuged again at 10,000 x *g*. The mitochondrial pellet was then resuspended in ~200μL of Mitochondria Isolation Buffer and protein was quantified using the Pierce BCA assay.

Isolation of mitochondria from mouse heart

Heart was dissected and placed in ice-cold Mitochondrial Isolation Buffer with BSA (100mM KCl, 50mM MOPS, 1mM EGTA, 5mM $MgSO_4$, 0.2% BSA, pH 7.1). Tissue was then minced, resuspended in 10mL of Mitochondrial Isolation Buffer and homogenized for ~10 passes via a Teflon pestle and borosilicate glass vessel. The homogenate was transferred to a 15mL tube, the volume was brought to 12mL, and sample was centrifuged at 800 x *g* for 10 min at 4°C. The supernatant was transferred to a fresh 15mL tube and spun at 10,000 x *g* for 10 min at 4°C. Mitochondrial pellet was washed in 1.4mL of Mitochondrial Isolation Buffer without BSA (100mM KCl, 50mM MOPS, 1mM EGTA, 5mM $MgSO_4$, pH 7.1) and spun at 10,000 x *g* for 10min at 4°C. The resulting pellet was resuspended in Mitochondrial Isolation Buffer without BSA. Protein content was determined using the Pierce BCA assay.

Assessment of mitochondrial membrane potential in whole intact cells using flow cytometry

Cells were harvested and resuspended in IMDM media ($1x10^6$ cell per mL). After this, cells were treated with FCCP (5uM), Rotenone/Antimycin A [0.5uM/0.5uM], Oligomycin [5uM] or DMSO (Vehicle) for 15 minutes at room temperature. The cells were stained with TMRM (10nM) and incubated for 30 minutes at 37^0C with 5% CO_2. Thereafter, DAPI (1ug/mL) was added. Samples were then analyzed with a Cytek Aurora flow cytometer. Data analysis included gating and analysis of fluorescence intensity to determine mitochondrial membrane potential using FlowJo software v10.9.0 (Treestar, USA).

Assessment of Isolated Mitochondrial Membrane Potential Using Flow Cytometry

Mitochondria isolated from mouse heart or HL60 AML cells were treated with either 1) H_2O (Vehicle), 2) pyruvate (Pyr or P; 5mM) and malate (M; 1mM), 3) P/M, CK (20U/mL), ATP (5mM), and PCr (21mM), 3) P/M, CK (20U/mL), ATP (5mM), PCr (21mM) and Oligo (5uM), or 4) P/M, CK (20U/mL), ATP (5mM), PCr (21mM), Oligo (5uM) and FCCP (5uM) for 15 minutes at room

temperature. The cells were stained with TMRM (10nM) and incubated for 30 minutes at 37^0C with 5% CO_2. Samples were then analyzed with a Cytek Aurora flow cytometer. Data analysis included gating and analysis of fluorescence intensity to determine mitochondrial membrane potential using FlowJo software v10.9.0 (Treestar, USA).

Mitochondrial membrane potential (ΔΨ) in permeabilized cells

Mitochondrial membrane potential was performed using methods described previously[44] with some adaptations. Fluorescent determination of $\Delta\Psi_m$ using permeabilized cells was performed using a QuantaMaster Spectrofluorometer (QM-400; Horiba Scientific). Quantification of ΔΨ via TMRM (operating in quench mode) was conducted as described previously (Fisher-Wellman et al., 2018). Cells were harvested, centrifuged at 300 x *g* for 7 minutes then washed with PBS and centrifuged again at 300 x *g*. Following this, cells were resuspended in 1mL of assay buffer and viable cells were counted with trypan blue. Cells were then permeabilized with digitonin (Digi; 0.02mg/mL) for 10 minutes at room temperature. From the permeabilized cell suspension, ~3 million cells were added to a microcentrifuge tube and centrifuged at 1,500 x *g* for 10 minutes. Cell pellet was resuspended in fresh assay buffer and loaded with 200nM TMRM. Optimal excitation and emission parameters for each cell type were determined using an excitation emission scan to determine the fluorescence ratio. Membrane potential was then quantified using a fluorescence ratio of the experimentally determined excitation and emission parameters.

ATP5IF1 knockdown in MV4;11 cells

MV4;11 cells were cultured in IMDM (Thermo Fisher Scientific, Waltham, MA) supplemented with glutamax, 10% FBS, and 1% penicillin/streptomycin and incubated at 37°C in 5% CO_2. Human shRNA lentiviral particles cloned into pLKO.1 vector (18mer *ATP5IF1*-specific shRNA 5' GGCTGAAGAGGAACGATA 3'), and one scramble control; 0.5mL each,>10^7 TU/ml) were purchased from Addgene (CAT#: 10878). To facilitate infection, cells and lentiviral particles

were co-cultured at a seeding density of $5x10^5$ cells per mL in a retronectin dish. Following 72 hours of infection, cultures were then subjected to puromycin selection by continuous exposure to 2 µg/mL puromycin in the culture media. Confirmation of *ATP5IF1* knockdown was performed via western blotting and analyzed with densitometry using ImageJ software.

Determination of ATP hydrolytic activity of Complex V

Complex V activity was assessed as described previously (Fisher-Wellman et al., 2018). Mitochondrial lysates for the assay were prepared via dilution of the final isolated mitochondrial suspensions in CelLytic M (Sigma-Aldrich; C2978) at a protein concentration of 2mg/ml. Buffer for the assay was supplemented with lactate dehydrogenase/pyruvate kinase (10U/ml), phosphoenoyl-pyruvate (5mM), rotenone (0.005mM) and NADH (0.2mM). Assay buffer (200µL) was loaded into individual wells of a 96-well plate, followed by mitochondrial lysate (2µg/well). Assays were done in the absence and presence of oligomycin (0.005mM) in order to calculate the oligomycin-sensitive rates of ATP hydrolysis. The assay was initiated with the addition of ATP (5mM). In the assay, NADH oxidation and ATP hydrolysis occur at a 1:1 stoichiometry and thus Complex V activity (pmoles of ATP/sec/mg) was determined via tracking the degradation in the NADH auto-fluorescence (Ex:Em 376/450) signal upon ATP addition. Fluorescence values were converted to pmoles of NADH via an NADH standard curve.

Sample prep for label-free proteomics

Cell pellets or isolated mitochondria pellets were lysed in urea lysis buffer (8M urea in 40mM Tris, 30mM NaCl, 1mM $CaCl_2$, 1 x cOmplete ULTRA mini EDTA-free protease inhibitor tablet; pH=8.0), as described previously. The samples were subjected to two freeze-thaw cycles, and sonicated with a probe sonicator in three 5s bursts (Q Sonica #CL-188; amplitude of 30). Samples were centrifuged at 10,000 x *g* for 10min at 4°C. Protein concentration was determined by BCA. Equal amounts of protein were reduced with 5mM DTT at 37°C for 30min, and then alkylated with 15mM iodoacetamide for 30min in the dark. Unreacted iodoacetamide was quenched with DTT (15mm). Reduction and alkylation reaction were carried out at room

temperature. Initial digestion was performed with Lys C (1:100 w:w) for 4hr at 32°C. Following dilution to 1.5M urea with 40mM Tris (pH=8.0), 30mM NaCl, 1mM $CaCl_2$, samples were digested overnight with sequencing grade trypsin (50:1 w/w) at 32°C. Samples were acidified to 0.5% TFA and then centrifuged at 4,000 x *g* for 10min at 4°C. Supernatant containing soluble peptides was desalted and then eluate was frozen and subjected to speedvac vacuum concentration.

nLC-MS/MS for label-free proteomics

Final peptides were resuspended in 0.1% formic acid, quantified (ThermoFisher Cat# 23275), and diluted to a final concentration of 0.25µg/µL. Samples were subjected to nanoLC-MS/MS analysis using an UltiMate 3000 RSLCnano system (ThermoFisher) coupled to a Q Exactive Plus Hybrid Quadrupole-Orbitrap mass spectrometer (ThermoFisher) via a nanoelectrospray ionization source. For each injection, 4µL (1µg) of sample was first trapped on an Acclaim PepMap 100 20mm x 0.075mm trapping column (ThermoFisher Cat# 164535; 5µL/min at 98/2 v/v water/acetonitrile with 0.1% formic acid). Analytical separation was performed over a 95min gradient (flow rate of 250nL/min) of 4-25% acetonitrile using a 2µm EASY-Spray PepMap RSLC C18 75µm x 250mm column (ThermoFisher Cat# ES802A) with a column temperature of 45ºC. MS1 was performed at 70,000 resolution, with an AGC target of $3x10^6$ ions and a maximum injection time (IT) of 100ms. MS2 spectra were collected by data-dependent acquisition (DDA) of the top 15 most abundant precursor ions with a charge greater than 1 per MS1 scan, with dynamic exclusion enabled for 20s. Precursor ions isolation window was 1.5m/z and normalized collision energy was 27. MS2 scans were performed at 17,500 resolution, maximum IT of 50ms, and AGC target of $1x10^5$ ions.

Data analysis for label-free proteomics

As described previously with some modification, Proteome Discoverer 2.2 (PDv2.2) was used for raw data analysis, with default search parameters including oxidation (15.995 Da on M) as a variable modification and carbamidomethyl (57.021 Da on C) as a fixed modification. Data were searched against the Uniprot Homo Sapiens reference proteome (Proteome ID:

UP000005640), as well as the Human Mito Carta 3.0 database. PSMs were filtered to a 1% FDR and grouped to unique peptides while maintaining a 1% FDR at the peptide level. Peptides were grouped to proteins using the rules of strict parsimony and proteins were filtered to 1% FDR. Peptide quantification was done using the MS1 precursor intensity. Imputation was performed via low abundance resampling. Using only high confidence master proteins, mitochondrial enrichment factor (MEF) was determined as previously described by comparing mitochondrial protein abundance (i.e., proteins identified to be mitochondrial by cross-reference with the MitoCarta 3.0 database) to total protein abundance.

Statistical evaluation of label-free proteomics

All proteomics samples were normalized to total protein abundance, and the protein tab in the PDv2.2 results was exported as a tab delimited .txt. file and analyzed. Protein abundance was converted to the Log2 space. For pairwise comparisons, tissue mean, standard deviation, p-value (p; two-tailed Student's t-test, assuming equal variance), and adjusted p-value (Benjamini Hochberg FDR correction) were calculated35. Mitochondrial functional assay results are expressed as the mean ± SEM (error bars). Data were normalized to viable cell counts and then corrected for the group mean MEF, with the final values expressed as pmol/s/million cells/MEF18. Throughout the paper, differences between groups were assessed by t-test, or one-way ANOVA, followed by Tukey's test where appropriate using GraphPad Prism 8 software (Version 8.4.2). Other statistical tests used are described in the figure legends. Statistical significance in the figures is indicated as follows: *$p < 0.05$; **$p < 0.01$; ***$p < 0.001$; ****$p < 0.0001$. Unless otherwise stated, figures were generated using GraphPad Prism 8 software (Version 8.4.2) or Biorender

Statistical analysis and software

Statistical analysis was performed using GraphPad Prism 8.4. All data are represented as mean ± SEM and analysis were conducted with a significance level set at $p<0.05$. Details of statistical analysis are included within figure legends. Figures were generated using Biorender and GraphPad Prism 8.4.

Figure 3. Intrinsic lesions in respiratory complex IV limit OxPhos flux in AML cells. All experiments were performed using whole cells and digitonin-permeabilized cells (A) Comparison of fractional OXPHOS of normal blood cells, patient AML, AML cell lines, chemoresistant AML, and mouse AML calculated as the ratio of JH^{+}_{OXPHOS} to JH^{+}_{Total} (B) Volcano plot comparing mitochondrial and non-mitochondrial proteome of AML and Mobilized PBMC cells. (C) Comparison of mitochondrial content in AML and Mobilized PBMC cells. (D) Comparison of whole cell respiratory capacity in Mobilized PBMC, $MV411_{WT}$ and OCI_{WT} cells normalized to milligrams of protein. (E) Comparison of the OXPHOS proteome between Mobilized PBMC and AML cells. (F) Comparison of whole cell respiratory capacity in Mobilized PBMC, $MV411_{WT}$ and OCI_{WT} cells normalized to milligrams of mitochondrial protein (G) Schematic depicting complex IV lesions and reduced respiration of individual AML mitochondria. Data are presented as mean ±SEM and analyzed by two-way ANOVA (E,F) and one-way ANOVA (A,C,D). *p<0.05, **p<0.01, ***p<0.001, ****p<0.0001.

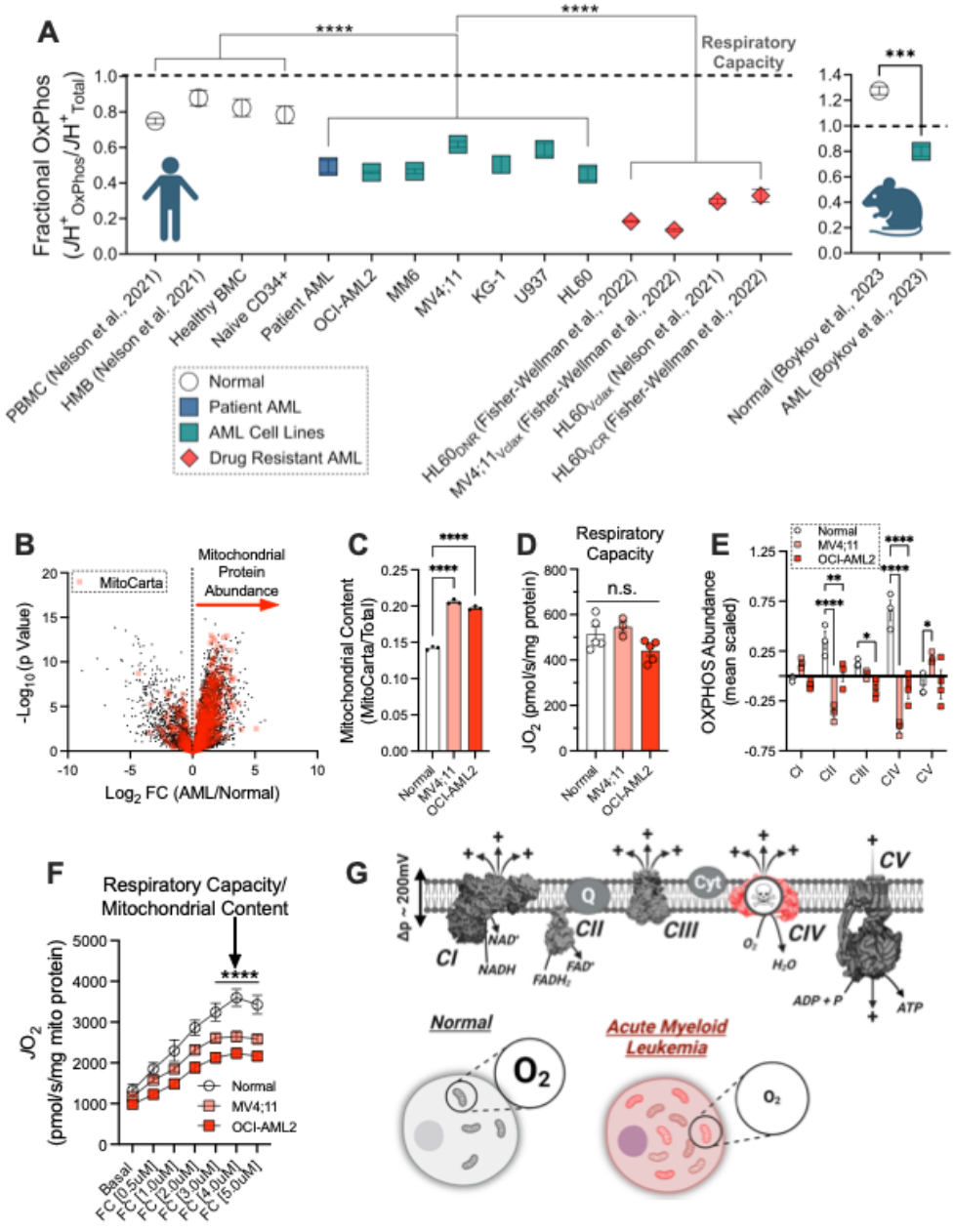

Figure 4. Mitochondria in AML cells consume cellular ATP to sustain mitochondrial polarization. All experiments were performed using whole intact cells. (A) Schematic depicting strategy to determine functional OxPhos in $\Delta\Psi_m$ assays. (B) Representative image from flow cytometric analysis of intact cell $\Delta\Psi_m$ using OCI_{Rho0}. (C) Flow cytometric analysis of intact cell $\Delta\Psi_m$ in OCI_{Rho0} cells. (D) Flow cytometric analysis of intact cell $\Delta\Psi_m$ in Healthy BMC. (E) Flow cytometric analysis of intact cell $\Delta\Psi_m$ in myeloid and lymphoid populations sorted from PBMC. (F) Flow cytometric analysis of intact cell $\Delta\Psi_m$ in AML cell lines. (G). Flow cytometric analysis of intact cell $\Delta\Psi_m$ in patient AML. (H) Flow cytometric analysis of intact cell $\Delta\Psi_m$ in OCI-AML2 cells using HPLM media. (I) Schematic depicting functional OxPhos or F_1-ATPase activity in normal blood cells or AML, respectively. Data are presented as mean ±SEM and analyzed by two-way ANOVA in (E,F) and one-way ANOVA in (C,D,G,H). *p<0.05, **p<0.01, ***p<0.001, ****p<0.0001.

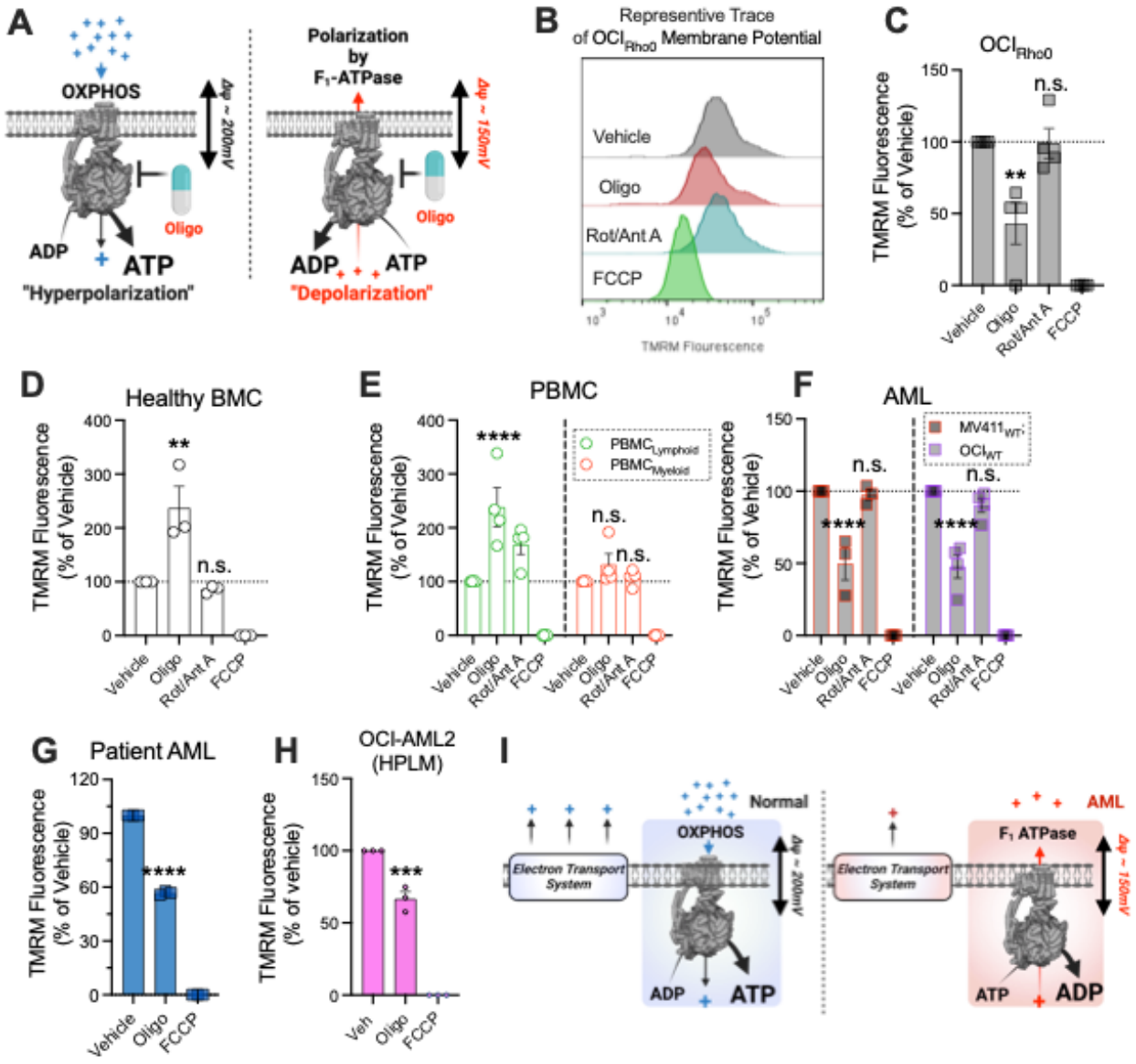

Figure 5. Venetoclax exposure collapses AML mitochondrial respiration and by default, polarization is sustained via F_1-ATPase activity. All experiments were performed using whole intact cells or digitonin permeabilized cells. (A) Schematic depicting mechanism of IACS-010759, Antimycin A, BAM15, and oligomycin on the electron transport system. (B) Effect of either IACS-010759, Antimycin A, oligomycin or that in combination, on OCI_{Rho0} cell viability. (C) Effect of either IACS-010759, Antimycin A, oligomycin, or BAM15 on OCI-AML2 cell viability (D) Schematic depicting characterization of AML cells exposed to venetoclax for 1 hour. (E) Effect of 1 hour venetoclax exposure on AML cell viability. (F) Effect of 1 hour exposure to 1uM venetoclax on respiratory capacity in AML (G) Effect of 1 hour exposure to 100nM venetoclax on OxPhos capacity in AML (H) Effect of 1 hour exposure to 100nM venetoclax on polarization induced by Complex I substrates (P/M/G), Complex II substrates (S/R), or Complex V substrates (ATP) in AML (I) Effect of 1 hour exposure to 100nM venetoclax on $\Delta\Psi_m$ in AML.(J) Schematic depicting effect of venetoclax on the AML electron transport system. Data are presented as mean ±SEM and analyzed by two-way ANOVA (F,G,H,I) or one-way ANOVA (B,C,E). *p<0.05, **p<0.01, ***p<0.001, ****p<0.0001.

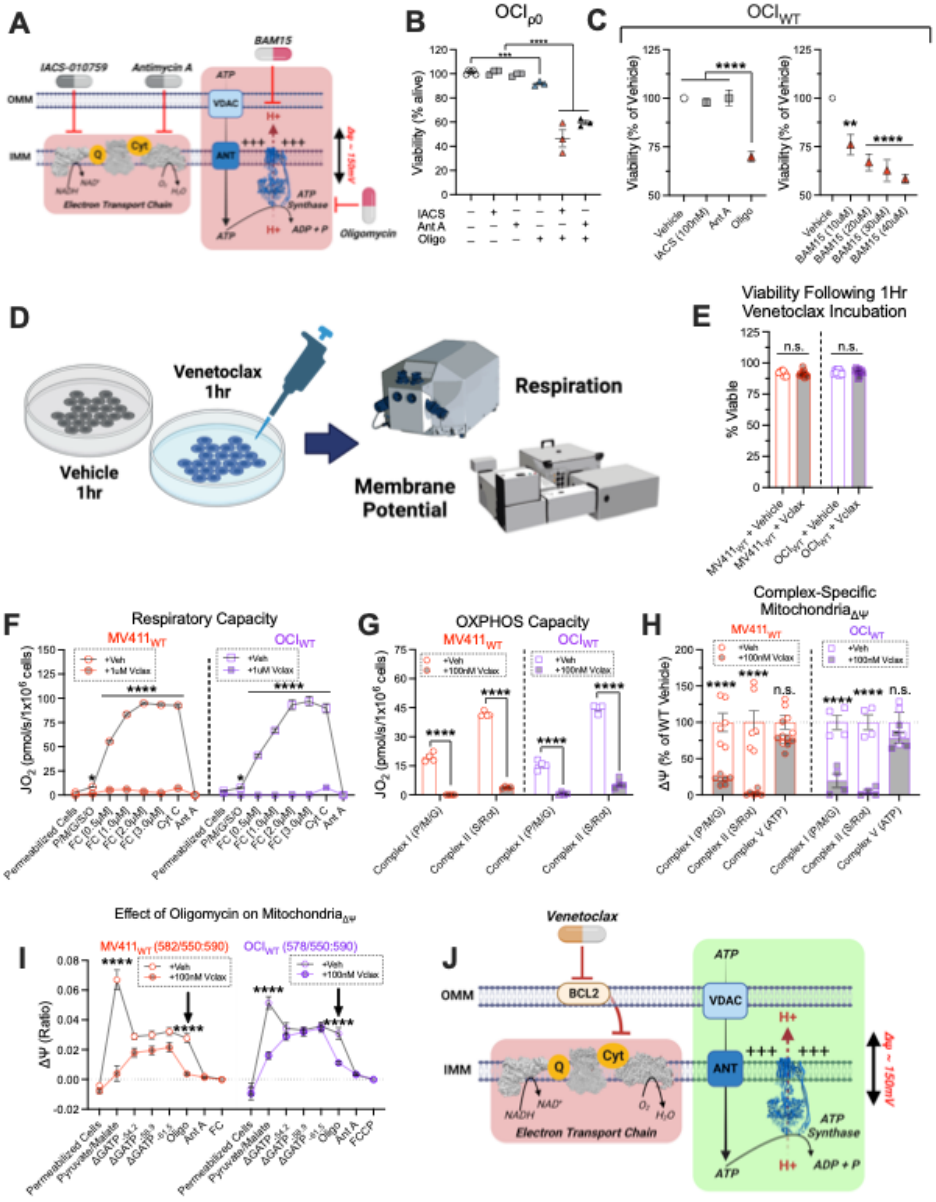

Figure 6. Downregulation of *ATP5IF1* in AML confers chemoresistance. All experiments were performed using whole intact cells, permeabilized cells, or isolated mitochondria. (A) Effect of venetoclax on treatment naïve AML and chemoresistant AML cell viability. (B) Comparison of OxPhos proteome in permeabilized treatment naïve AML and chemoresistant AML cells. (C) Comparison of *ATP5IF1* expression in mitochondria isolated from $MV411_{WT}$ and $MV411_{Vclax}$. (D) Comparison of OxPhos capacity in permeabilized treatment naïve AML and chemoresistant AML cells. (E) Effect of oligomycin on $\Delta\Psi_m$ in permeabilized treatment naïve AML and chemoresistant AML cells. (F) Flow cytometric analysis of intact cell $\Delta\Psi_m$ in chemoresistant AML. (G) Comparison of *ATP5IF1* expression $MV411_{shCtrl}$ or $MV411_{shIF1}$ cells. (H) Flow cytometric analysis of intact cell $\Delta\Psi_m$ in $MV411_{shCtrl}$ or $MV411_{shIF1}$. (I) Comparison of ATP hydrolysis by the F_1-ATPase in permeabilized $MV411_{shCtrl}$ or $MV411_{shIF1}$ cells. (J) Comparison of OxPhos respiratory kinetics in permeabilized $MV411_{shCtrl}$ or $MV411_{shIF1}$ cells. (K) Effect of venetoclax on $MV411_{shCtrl}$ or $MV411_{shIF1}$ cell viability. (L) Effect of venetoclax on $MV411_{shCtrl}$ or $MV411_{shIF1}$ colony formation. (M) Representative image of $MV411_{shCtrl}$ or $MV411_{shIF1}$ colony formation in response to venetoclax (from Fig. 4L). (N) Schematic depicting mechanism of chemoresistance conferred by *ATP5IF1* knockdown in treatment naïve AML. Data are presented as mean ±SEM and analyzed by two-way ANOVA (A,F,H-L), one-way ANOVA (D,E) or unpaired t-tests (C,G). *p<0.05, **p<0.01, ***p<0.001, ****p<0.0001.

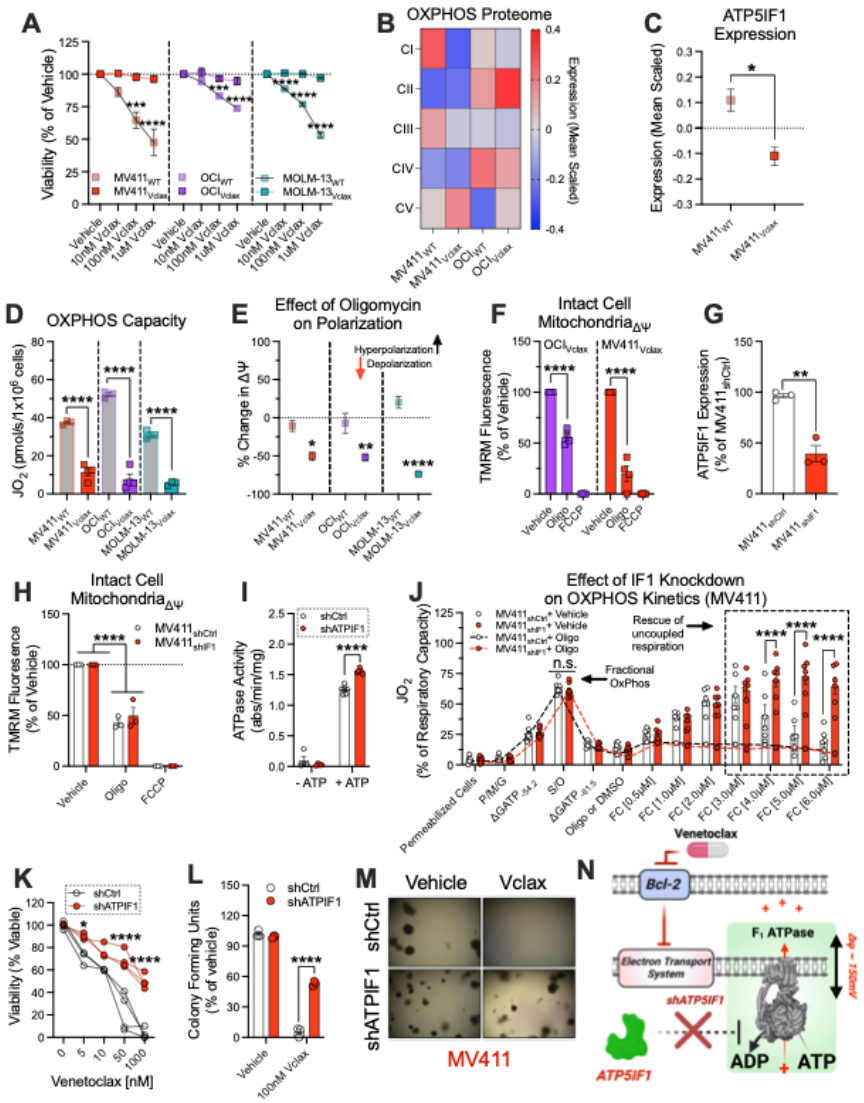

Figure 7. Targeting F_1-ATPase dependent polarization of the $\Delta\Psi_m$ restores venetoclax sensitivity. All experiments were performed using whole intact cells or digitonin-permeabilized cells. (A) Schematic depicting mechanism of action of organic cations and the structure of d-TPP compared to MitoQ. (B) Effect of MitoQ on $\Delta\Psi_m$ polarization induced from Complex I substrates (P/M/G), Complex II substrates (S/R), or Complex V substrates (ATP) in OCI_{WT} cells. (C) Effect of d-TPP on $\Delta\Psi_m$ polarization induced from Complex I substrates (P/M/G), Complex II substrates (S/R), or Complex V substrates (ATP) in AML cells. (D) Effect of single agent d-TPP on OCI_{WT} cell viability. Effect of venetoclax and d-TPP as single agents, or in combination, on colony formation of (E) Healthy BMC, (F) OCI_{WT} , (G) $HL60_{WT}$ cells. (H) Effect of d-TPP on MOLM-13_{WT} and MOLM-13_{Vclax} cell viability. (I) Effect of either d-TPP as a single agent, or in combination with venetoclax, on $MV411_{WT}$ and $MV411_{Vclax}$ cell viability (J) Effect of 100nM d-TPP in combination with 1uM Vclax on colony formation of chemoresistant AML. Data are presented as mean ±SEM and analyzed by two-way ANOVA (B,C,E-J) or one-way ANOVA (D). *p<0.05, **p<0.01, ***p<0.001, ****p<0.0001.

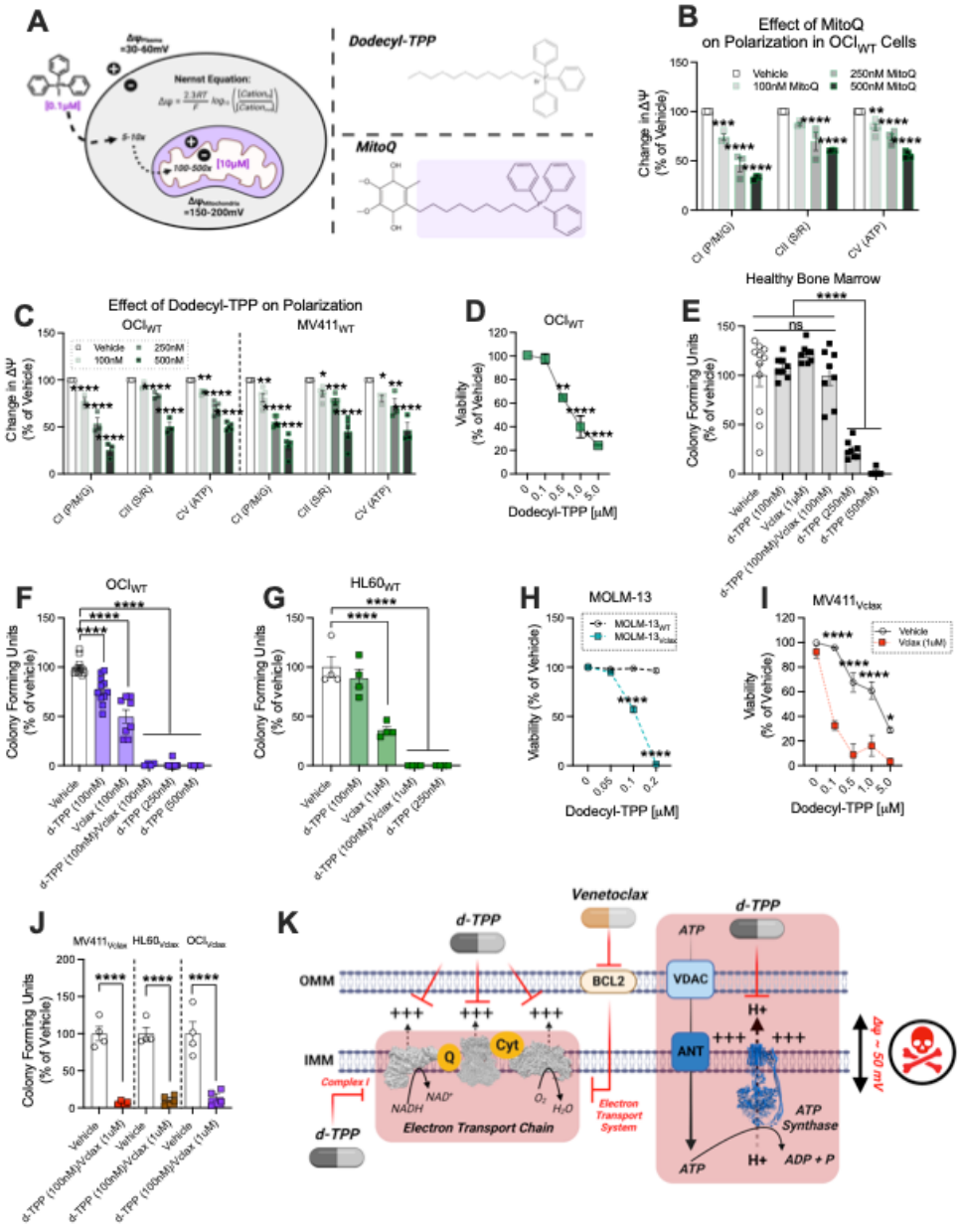

Figure 8. AML mitochondrial bioenergetics mimic an alternating current circuit model. (A) Schematic depicting AML mitochondrial bioenergetics as an alternating current model. (B) Schematic depicting the mechanism of dephosphorylative oxidation in AML.

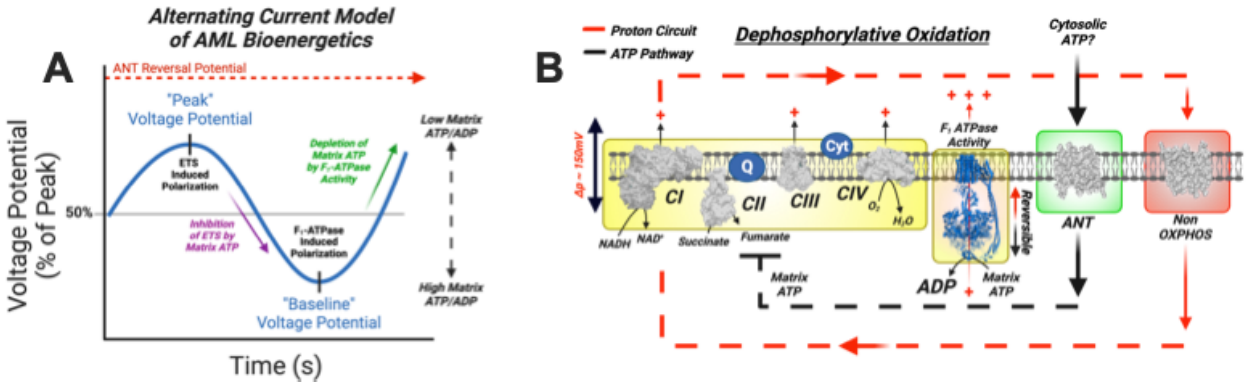

Supplementary Figure 1. Respiratory capacity and OXPHOS kinetics profiling of AML and healthy hematopoietic cells. (Related to Figure 1). All experiments were performed using whole intact or digitonin-permeabilized cells. Respiratory capacity was measured using (A) Healthy BMC, (B) OCI_{WT}, (C) $MV411_{WT}$, (D) MM6 cells. OXPHOS respiratory kinetics were measured using (E) Healthy BMC, (F) OCI_{WT}, (G) $MV411_{WT}$, (H) MM6 cells. (I) Comparison of Complex I subunit expression in Mobilized PBMC and AML cells. (J) Comparison of Complex II subunit expression in Mobilized PBMC and AML cells. (K) Comparison of Complex III subunit expression in Mobilized PBMC and AML cells. (L) Comparison of Complex IV subunit expression in Mobilized PBMC and AML cells. (M) Comparison of Complex V subunit expression in Mobilized PBMC and AML cells.

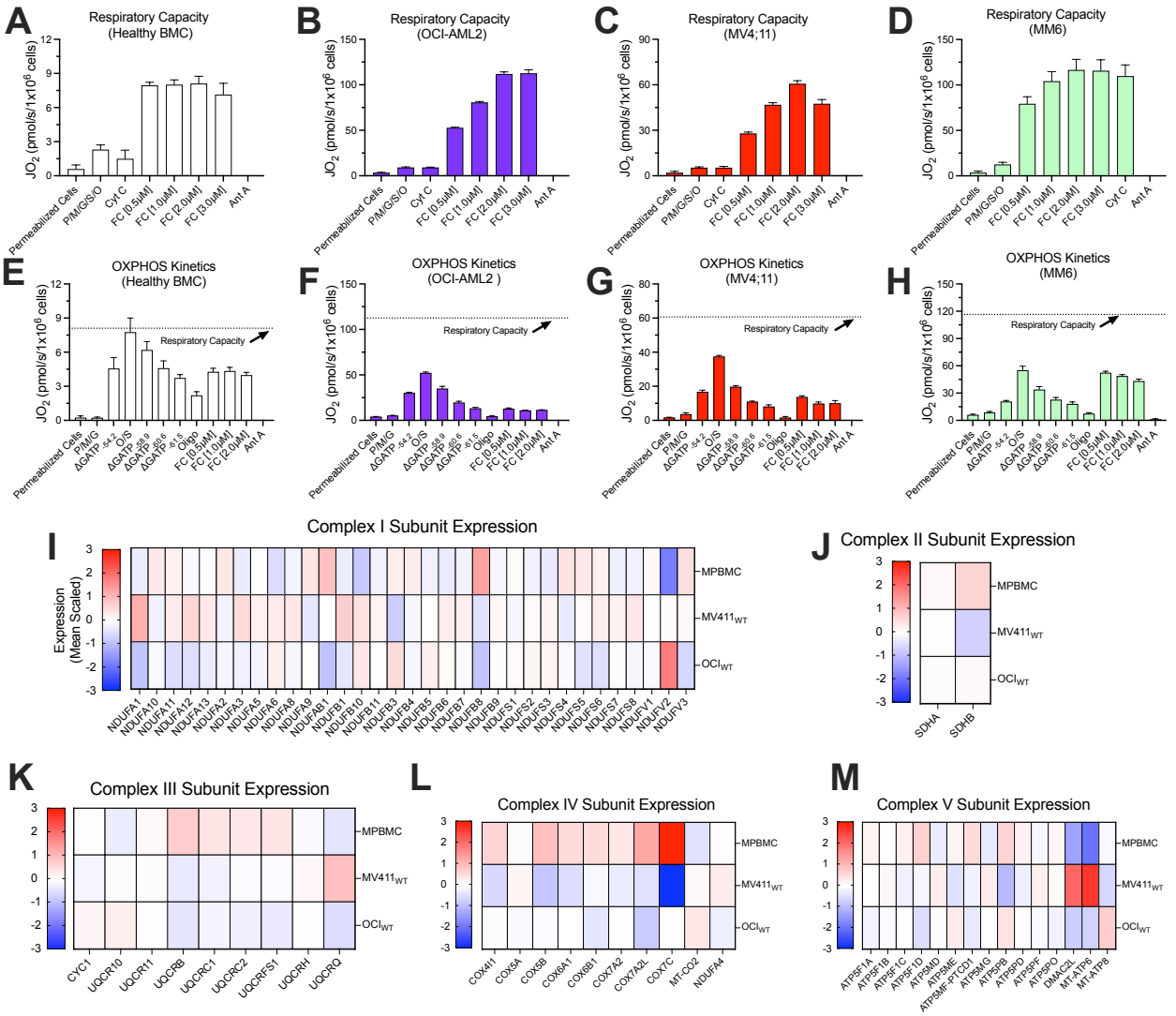

Supplementary Figure 2. Validation of p^0 OCI-AML2 cells. (Related to Figure 2). All experiments were performed using whole intact cells or isolated mitochondria. (A) Comparison of basal respiration of OCI_{Rho0} or OCI_{WT} cells. (B) Comparison of NADH autofluorescence of OCI_{Rho0} or OCI_{WT} cells. (C) Comparison of membrane potential of isolated mitochondria derived from mouse heart or HL60 cells measured using flow cytometry (D) Comparison of oligomycin induced polarization of isolated mitochondria derived from mouse heart or HL60 (E) Change in TMRM fluorescence of individual mitochondria in whole mitochondrial populations derived from mouse heart or HL60 before and after oligomycin addition during flow cytometry analysis. (F) Comparison of intact cell basal respiration of AML and MPBMC. (G) Effect of oligomycin, 2-deoxyglucose (2-DG), rotenone/antimycin A (R/A), or those in combination, on intact cell $\Delta\Psi_m$ of p^0 OCI-AML2 cells. (H) Effect of CB839 or 2-DG on oligomycin induced depolarization of OCI-AML2 intact cell $\Delta\Psi_m$. Data are presented as mean ±SEM and analyzed by two-way ANOVA (C,G,H), one-way ANOVA (F) or unpaired t-test (A,B,D) *p<0.05, **p<0.01, ***p<0.001, ****p<0.0001.

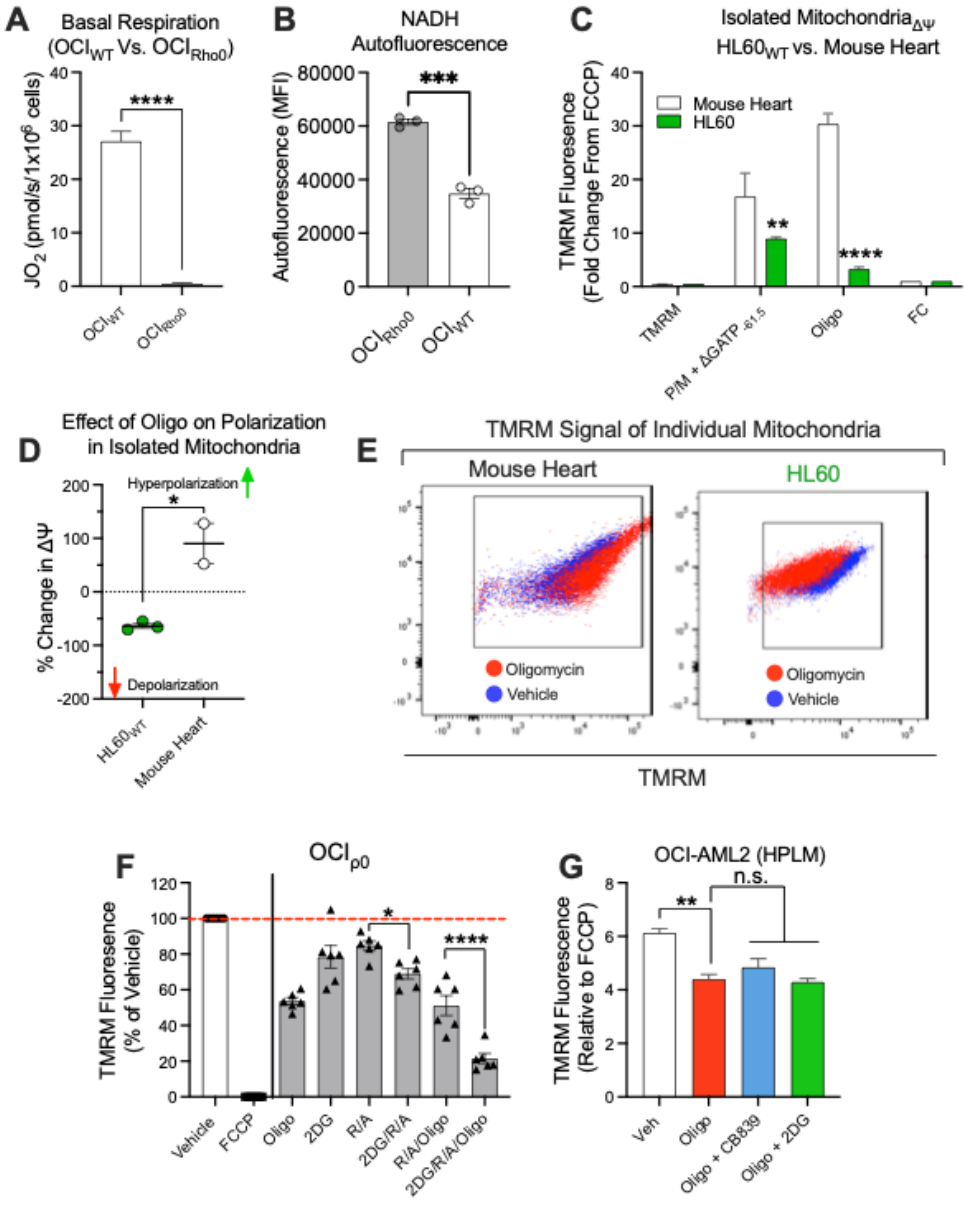

Supplementary Figure 3. Mitochondrial$_{\Delta\Psi}$ profiling of venetoclax-exposed AML cells. (Related to Figure 3). All experiments were performed using whole intact and digitonin-permeabilized cells. Effect of 1 hour exposure to 100nM venetoclax on polarization induced by Complex I substrates (P/M/G) or Complex II substrates (S/R) in (A) MV411$_{WT}$ and (B) OCI$_{WT}$ cells. Effect of 1 hour exposure to 100nM venetoclax on polarization induced by Complex V substrates (ATP) in (C) MV411$_{WT}$ and (D) OCI$_{WT}$ cells. (E) Effect of BAM15 and oligomycin as single agents, or in combination with venetoclax, on colony formation of OCI$_{WT}$ cells. Data are presented as mean ±SEM and analyzed by two-way ANOVA (A-D) or one-way ANOVA (E). *p<0.05, **p<0.01, ***p<0.001, ****p<0.0001.

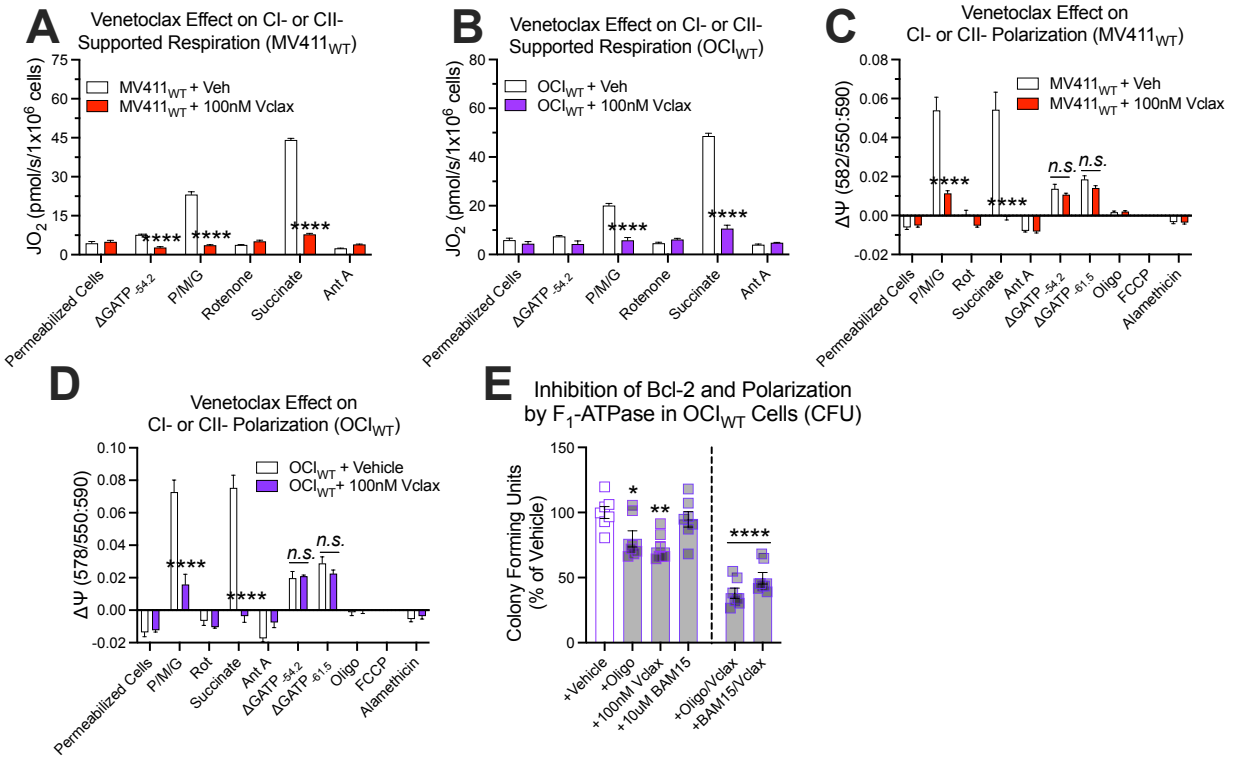

Supplementary Figure 4. OxPhos profiling of chemoresistant AML and *ATP5IF1* knockdown AML cell lines. (Related to Figure 4). All experiments were performed using whole intact or digitonin-permeabilized cells. OxPhos respiratory kinetics were measured in (A) $MV411_{Vclax}$, (B) OCI_{Vclax} and (C) $MOLM\text{-}13_{WT}$ or $MOLM\text{-}13_{Vclax}$ cells. Comparisons of the $\Delta\Psi_m$ was measured in (D) $MV411_{WT}$ or $MV411_{Vclax}$, (E) OCI_{WT} or OCI_{Vclax} and (F) $MOLM\text{-}13_{WT}$ or $MOLM\text{-}13_{Vclax}$ cells. (G) Western blot image of *ATP5IF1* protein of $MV411_{shCtrl}$ and $MV411_{shIF1}$ cells. (H) Comparison of OxPhos respiratory kinetics in $MV411_{shCtrl}$ and $MV411_{shIF1}$ cells. (I) Comparison of respiratory capacity in $MV411_{shCtrl}$ and $MV411_{shIF1}$ cells. Data are presented as mean ±SEM and analyzed by two-way ANOVA (C-F, H, I). *p<0.05, **p<0.01, ***p<0.001, ****p<0.0001.

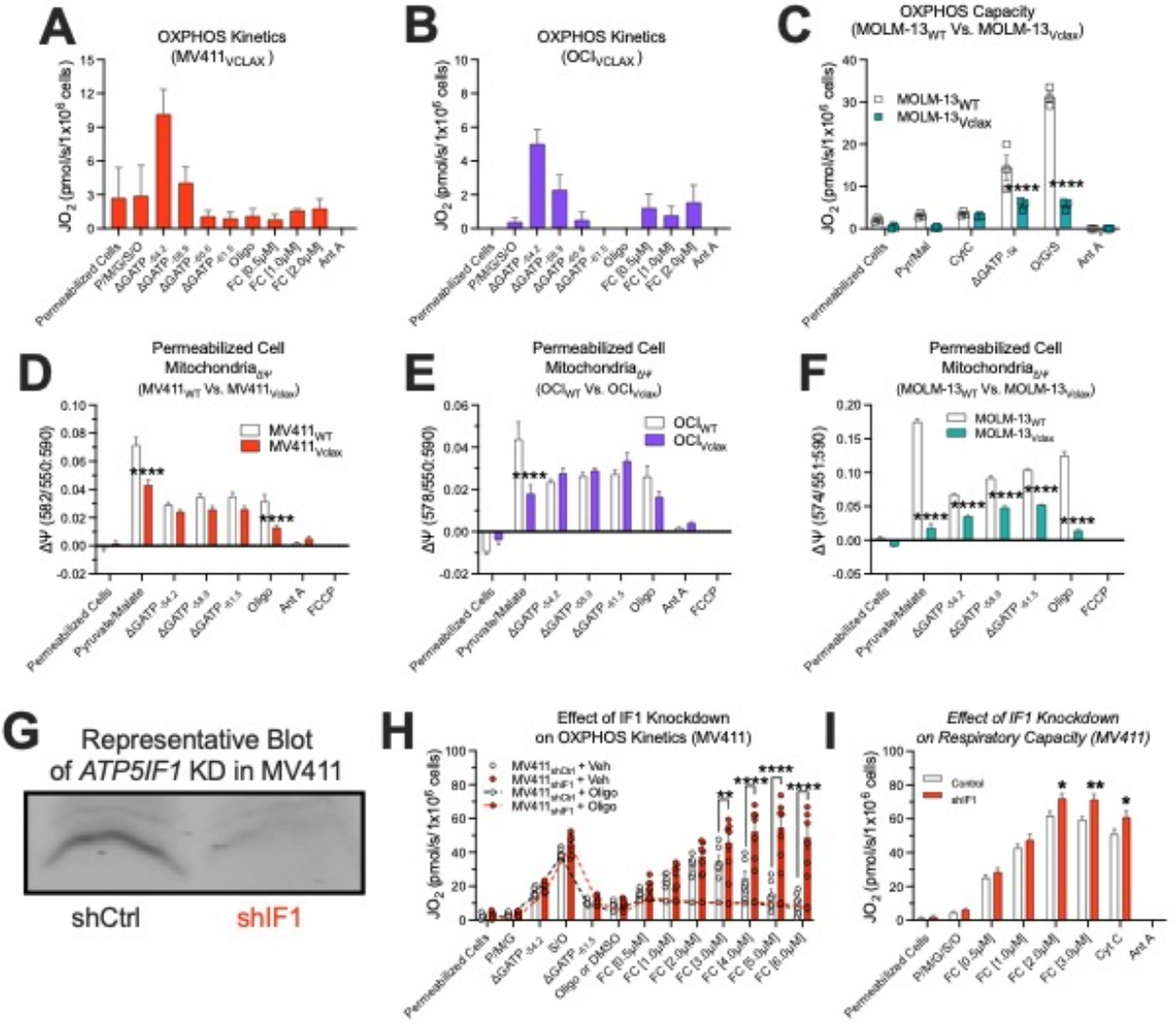

Supplementary Figure 5. MitoQ and d-TPP depolarize the AML $\Delta\Psi_m$. (Related to Figure 5). All experiments were performed using whole intact or digitonin-permeabilized cells. (A) Effect of increasing doses of MitoQ on polarization induced by Complex I substrates (P/M/G) or Complex II substrates (S/R) in OCI_{WT} cells. (B) Effect of increasing doses of MitoQ on polarization induced by Complex V substrates (ATP) in OCI_{WT} cells. (C) Effect of increasing doses of d-TPP on polarization induced by Complex I substrates (P/M/G) or Complex II substrates (S/R) in OCI_{WT} cells. (D) Effect of increasing doses of MitoQ on polarization induced by Complex V substrates (ATP) in OCI_{WT} cells. (E) Effect of increasing doses of d-TPP on polarization induced by Complex I substrates (P/M/G) or Complex II substrates (S/R) in $MV411_{WT}$ cells. (F) Effect of increasing doses of MitoQ on polarization induced by Complex V substrates (ATP) in $MV411_{WT}$ cells (G) Effect of increasing doses of d-TPP on respiratory capacity using OCI_{WT} cells. (H) Respiration-stimulating effects of d-TPP during the substrate preference assay using OCI_{WT} cells. (I) Stimulation of Complex II respiration by d-TPP using OCI_{WT} cells. (J) Effect of venetoclax and d-TPP as single agents, or in combination, on colony formation in OCI_{Vclax} cells. (K) Effect of venetoclax and MitoQ as single agents, or in combination, on colony formation in OCI_{Vclax} cells. Data are presented as mean ±SEM and analyzed by two-way ANOVA (A-K). *p<0.05, **p<0.01, ***p<0.001, ****p<0.0001.

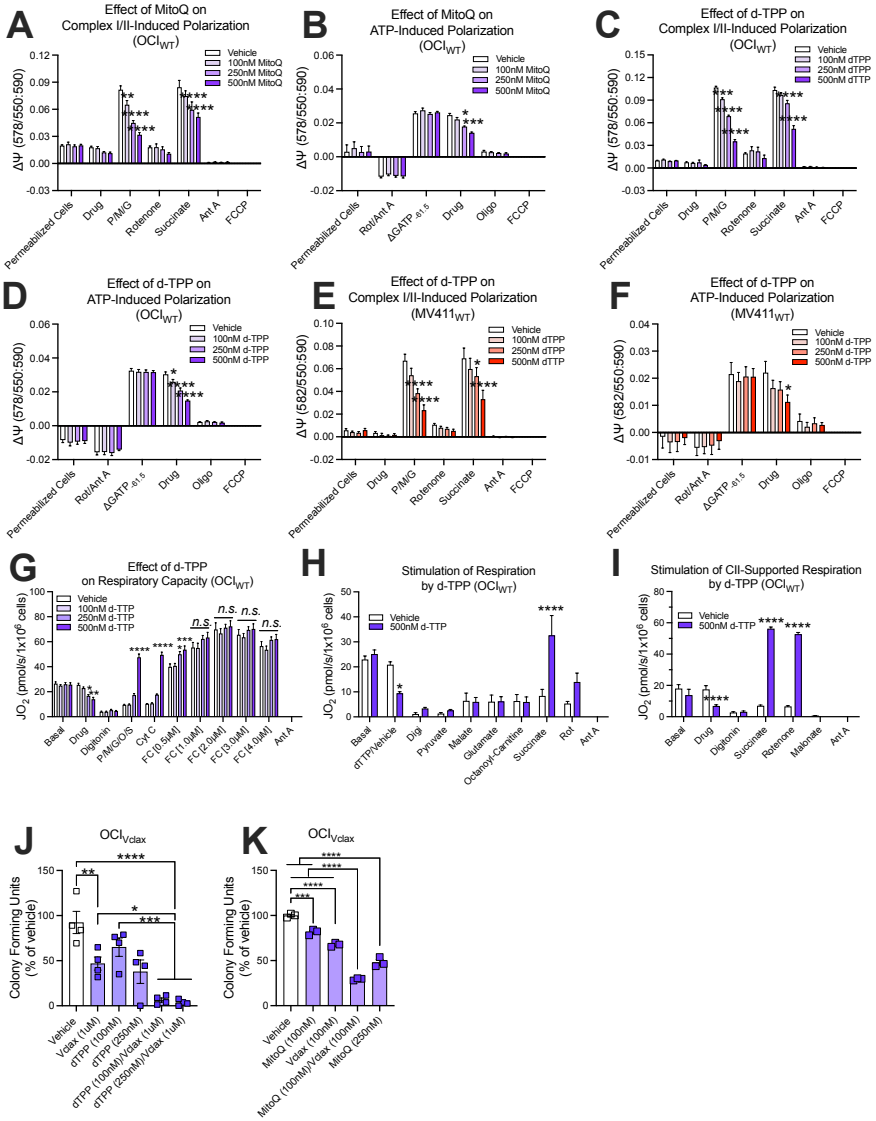

Chapter 3: BAI1 reactivates AML OxPhos independently of BAX expression

ABSTRACT

BAI1 is a small-molecule inhibitor of the pro-apoptotic BAX protein. BAX mediates apoptosis by permeabilizing the outer mitochondrial membrane, thereby facilitating the release of cytochrome C. Cytochrome C is an electron carrier that shuttles electrons from Complex III to Complex IV of the electron transport system (ETS). Importantly, respiratory function is known to become impaired following BAX activation, potentially implicating BAX in deficiencies of oxidative phosphorylation (OxPhos). Given that OxPhos deficiency is an intrinsic phenotype of acute myeloid leukemia (AML), we leveraged BAI1 to determine if BAX activity contributes to the intrinsic OxPhos limitations of AML. When AML were exposed to BAI1, OxPhos was reactivated. However, reactivation of OxPhos by BAI1 was cytotoxic to AML, and this is not an effect that would be expected to result from BAI1-mediated inhibition of the pro-apoptotic BAX protein. When BAX protein expression was knocked down in AML, however, it was discovered that OxPhos reactivation and cytotoxicity induced by BAI1 occurred independently of BAX. Although BAX activity was not found to contribute to intrinsic OxPhos deficiency in AML, BAX activity was found to inhibit respiration independently of cytochrome C release in the presence of venetoclax, a Bcl-2 inhibitor and a mediator of BAX/BAK-dependent apoptosis.

INTRODUCTION

Classified as the deadliest blood cancer in adults, acute myeloid leukemia (AML) is characterized by rapidly expanding abnormal blood cells[109,37,38]. Relative to normal blood cells, AML cells present with intrinsic limitations in their respiratory network that hinders the ability of AML cells to perform OxPhos[92]. Importantly, oxidative ATP synthesis requires an efficient respiratory network that can generates a mitochondrial membrane potential ($\Delta\Psi_m$). The $\Delta\Psi_m$ provides the thermodynamic driving force that fuels ATP synthesis as well as the export of ATP

from the mitochondrial matrix via the adenine nucleotide translocase (ANT)[30]. In our previous publication, ANT was found to import extramitochondrial ATP into the AML matrix space where it inhibited maximal uncoupled respiratory flux[92]. Those findings suggest that the AML mitochondrial phenotype is reflective of an "ATP consumer" as opposed to an "ATP producer". Intrinsic OxPhos deficiency of AML cells may be multifactorial - the mitochondrial proteome consists of ~1100-1400 proteins[89] and many of those proteins are known to influence energy transduction of the electron transport system (ETS) such as UCP2[126] (i.e., uncoupling protein 2), Bcl-2[29] (i.e., an anti-apoptotic protein), the mtDNA encoded proteins, and the pro-apoptotic, pore-forming BAX[51,8] protein.

The BAX protein has previously been shown to inhibit components of the ETS[8,15], in addition to it's understood role in mediating the intrinsic pathway of apoptosis[98]. During apoptotic induction, the BAX protein is known to permeabilize the outer mitochondrial membrane, thereby promoting mitochondrial permeability transition and the release of cytochrome C. Cytochrome C functions at the inner mitochondrial membrane where it functions as an electron carrier, shuttling electrons from Complex III to Complex IV at the terminal end of the (ETS). Because respiratory function is known to become impaired following the activation of BAX[8], BAX activity is a potential culprit for the intrinsic deficiencies of AML OxPhos. We hypothesized that intrinsic reductions in respiratory function of AML mitochondria may be a result of BAX activity, either as a result of cytochrome C release, or as a result of BAX-mediated inhibition of respiratory chain components. To this end, we made use of the small molecule allosteric inhibitor of the BAX protein, BAI1. BAI1 has previously been shown to be a selective inhibitor of the BAX protein, thereby inhibiting BAX activity to mitigate doxorubicin-induced cardiomyopathy[7]. Herein, we leveraged a novel mitochondrial phenotyping and diagnostics assay platform[44] to investigate the effects of BAI1-mediated inhibition of the BAX protein on the intrinsic OxPhos deficiency of AML.

The current investigation sought to 1) determine the effects of BAI1 on AML mitochondrial respiratory function and 2) determine if the effects of BAI1 in AML are dependent on BAX protein expression. In our preliminary investigation, we discovered that the presence of BAI1 prevented

the collapse of uncoupled respiration in intact AML cells. When AML cells were permeabilized so that OxPhos function could be directly assessed under experimentally controlled buffer conditions, the presence of BAI1 increased OxPhos respiratory kinetics. Improvements of respiratory function induced by BAI1 corresponded to a shift in the AML mitochondrial phenotype from an ATP "consumer" to an ATP "producer" when the mitochondrial membrane potential ($\Delta\Psi_m$) was assessed – indicative of OxPhos "reactivation". However, reactivation of OxPhos by BAI1 resulted in cytotoxicity towards AML cells, suggesting that the effects of BAI1 in AML cells occurred independently of BAX protein expression. Related to this, our previous publication discovered that 17-AAG (i.e., an inhibitor of TRAP1) reactivated AML OxPhos and induced cytotoxicity, however these effects occurred independently of TRAP1 expression[92]. Similarly, when expression of the BAX protein was knocked down in AML cells, we discovered that OxPhos reactivation and the underlying cytotoxicity induced by BAI1 occurred independently of the BAX protein. When BAX protein activity was stimulated using venetoclax, an inhibitor of the anti-apoptotic Bcl-2 protein and a mediator of BAX/BAK-dependent apoptosis[105], we discovered that BAX activity inhibited AML respiration independently of cytochrome C release. Collectively, these findings demonstrate that BAX activity is not causal to intrinsic OxPhos deficiency in AML and implicate BAI1 as a novel drug that exerts AML cell cytotoxicity by reactivating AML OxPhos independently of BAX protein expression.

RESULTS

BAI1 stabilizes uncoupled respiration of intact AML cells

The pro-apoptotic, pore-forming BAX protein has been suggested to impair mitochondrial respiration in two different ways: 1) release of cytochrome C following BAX-mediated permeabilization of the outer mitochondrial membrane[8,98], or 2) BAX-mediated inhibition of respiratory components[8,15]. Either of these BAX-mediated effects may reduce the efficiency of energy transduction by the respiratory complexes, thereby interfering with polarization of the $\Delta\Psi_m$

that drives ATP synthesis. Furthermore, prior research has demonstrated that, compared to normal blood cells, expression of the BAX protein is frequently elevated in AML[94]. As proof of concept, BAX expression in two distinct AML cell lines, OCI-AML2 ("OCI") and MV4;11 ("MV411") was elevated relative to mobilized peripheral blood mononuclear cells (MPBMC) isolated from bone marrow (**Supp. Fig. 6A**). Given that BAX protein expression is elevated in AML, we hypothesized that BAX activity contributes to intrinsic OxPhos deficiency in AML, a phenotype that we have consistently observed in prior studies[92,45].

To begin to determine if there is a role for the BAX protein in intrinsic OxPhos deficiency of AML cells, we leveraged the small molecule allosteric inhibitor of the BAX protein, BAI1. Taking a discovery-based approach, we first sought to determine the effects of BAI1 on intact cell respiration using MV4;11 (MV411), OCI-AML2 (OCI) and HL60 (HL60) AML cells (**Fig. 9A**). In this assay, basal respiration was quantified followed by the addition of BAI1. After BAI1 addition, ATP synthase was inhibited by oligomycin ("Oligo") and then respiratory capacity (i.e. maximal respiration) was quantified by titrating FCCP (i.e., "FC", a mitochondrial uncoupler). Although BAI1 did not impact basal respiration or respiratory capacity in AML cell lines, BAI1 opposed the collapse of uncoupled respiration at the end of the FCCP titration (**Fig. 9B-D**). Collectively, these data demonstrate that BAI1 stabilizes uncoupled respiration of intact AML cells.

BAI1 reactivates OxPhos in AML

Stabilization of AML uncoupled respiration by BAI1 is reminiscent of findings in our previous investigation that showed extramitochondrial ATP/ADP (i.e., ΔG_{ATP}; the free energy of ATP hydrolysis) inhibits AML respiration following the import of ATP into the mitochondrial matrix[92]. The mechanism by which this occurs involves ANT-mediated (i.e., adenine nucleotide translocase) import of ATP in exchange for ADP, a reversal of the canonical ANT-mediated adenylate exchange (i.e., matrix ATP export in exchange for ADP) that is indicative of matrix ATP consumption. Although our previous findings were observed in permeabilized AML cells and

isolated mitochondria derived from AML, intact cells sustain an intracellular ΔG_{ATP} that must be sufficient to drive thermodynamically unfavorable intracellular processes required for cell survival[132]. Because of this, we hypothesized that BAI1 stabilization of intact cell uncoupled respiration indicates that BAI1 opposes the inhibition of uncoupled respiration by ΔG_{ATP} in AML. To test this, we conducted paired measurements of respiratory capacity and OxPhos respiratory kinetics using permeabilized AML cells in the presence or absence of BAI1 (**Fig. 10A**). To measure OxPhos respiratory kinetics, permeabilized AML cells were first provided Complex I-linked carbon substrates (i.e., pyruvate, malate, and glutamate "P/M/G/") and respiration was stimulated by clamping the ΔG_{ATP} value at -54.2 kJ/mol, a free energy of ATP hydrolysis expected to stimulate maximal OxPhos respiratory flux (i.e. OxPhos capacity). Following this, Complex II-linked carbon substrates (i.e., succinate and octanoyl-carnitine; "S/O") were added to saturate the carbon pool, followed by a titration of the ΔG_{ATP} across a physiologically relevant span of ATP free energy values ending at -61.5 kJ/mol. At the end of the ΔG_{ATP} titration, oligomycin was added to inhibit ATP synthase and FCCP was titrated to measure maximal uncoupled respiration in the presence of ΔG_{ATP}. Simultaneous measurements of respiratory capacity in permeabilized AML cells was assessed using a buffer containing identical carbon substrates in the absence of ΔG_{ATP}, and OxPhos respiratory kinetics were then normalized to a percentage of total respiratory capacity. Normalization of the OxPhos respiratory kinetics assay to the total respiratory capacity was performed to reflect the maximal uncoupled respiration in the presence of ΔG_{ATP} as a percentage of the total respiratory capacity. By doing this, losses of maximal uncoupled respiration caused by an ATP-dependent inhibition of total respiratory flux can easily be quantified. In these assays, BAI1 did not affect the total respiratory capacity of AML cells (**Fig. 10B**) (**Supp. Fig. 7A-C**), however, BAI1 dose-dependently increased respiratory flux across a span of ΔG_{ATP} and rescued the inhibition of uncoupled respiratory flux by ΔG_{ATP}. (**Fig. 10C-E**) (**Supp. Fig. 7D-F**). Because OxPhos deficiency is an intrinsic feature of AML relative to normal blood cells[92], we hypothesized that increases in OxPhos respiratory kinetics by BAI1 is specific to AML. To test

this, we measured OxPhos respiratory kinetics in permeabilized peripheral blood mononuclear cells (PBMC). In PBMC, BAI1 did not increase OxPhos respiratory kinetics, however, BAI1 did increase maximal uncoupled respiration in the presence of ΔG_{ATP} albeit at a lower magnitude than that in AML (**Supp. Fig. 7G**). Because respiratory capacity of AML cells in the adenylate-replete buffer was unaffected by BAI1, we hypothesized that the effects of BAI1 on AML OxPhos kinetics were dependent upon ΔG_{ATP}. To test this, an OxPhos kinetics assay was repeated in MV411 cells using ADP, rather than ΔG_{ATP}, to stimulate OxPhos respiratory flux. In this assay, BAI1 did not affect OxPhos respiratory kinetics nor maximal uncoupled respiration, demonstrating that the effects of BAI1 on AML respiration are dependent upon ΔG_{ATP}.

The increase in OxPhos respiratory kinetics and the rescue of maximal uncoupled respiration by BAI1 suggests that BAI1 reactivates AML OxPhos by reversing limitations of AML energy transduction. Efficient energy transduction supports ATP synthesis by polarizing the $\Delta\Psi_m$ (indicative of an “ATP producer”). When the $\Delta\Psi_m$ is insufficient to cause ATP synthesis to occur however, ATP synthase will revert into an F_1-ATPase that hydrolyzes ATP to pump protons across the inner membrane to sustain polarization[5] (indicative of an ”ATP consumer”). Therefore, we hypothesized that BAI1 shifts AML mitochondrial phenotype from being an “ATP consumer” to an “ATP producer”. To test this, we designed an assay that measures the $\Delta\Psi_m$ of permeabilized AML cells by quantifying changes in TMRM fluorescence operating in quench mode[44]. The $\Delta\Psi_m$ was measured during the OxPhos kinetics assay described previously, with the exception that pyruvate and malate were used as carbon fuel sources (**Fig. 10G**). Following the titration of ΔG_{ATP}, oligomycin was added to inhibit the activity of ATP synthase. The change in TMRM fluorescence following the addition of oligomycin was used to determine if ATP synthase was consuming the $\Delta\Psi_m$ to synthesize ATP (indicative of an “ATP producer”) or if ATP synthase was operating as an F_1-ATPase (indicative of an “ATP consumer”) (**Fig. 10G**). In AML cells, BAI1 dose-dependently shifted the oligomycin induced changes in TMRM fluorescence away from depolarization, in favor of hyperpolarization (**Fig. 10H**) (**Supp. Fig. 7H-J**). Collectively, these data indicate that BAI1

reactivates AML OxPhos, thereby shifting the AML mitochondrial phenotype from favoring an "ATP consumer" to favoring an "ATP producer" (**Fig. 10I**).

BAI1-mediated reactivation of AML OxPhos and the underlying AML cell cytotoxicity occur independently of BAX expression

The BAX inhibitor BAI1 reactivates AML OxPhos, a finding that is consistent with our overarching hypothesis that BAX activity contributes to intrinsic OxPhos deficiency in AML. Given that BAI1 has been shown to inhibit BAX-dependent apoptosis[7], we hypothesized that reactivation of OxPhos by BAI1 would not be cytotoxic to AML. To test this, AML cell viability was assessed in response to increasing doses of BAI1 that correspond with doses required to reactivate AML OxPhos. Surprisingly however, BAI1 was profoundly cytotoxic to AML at doses that reactivate OxPhos (**Fig. 11A**). These data are perplexing, as BAI1-mediated inhibition of the BAX protein would not be anticipated to result in AML cytotoxicity. Prior to testing our hypothesis that BAX activity contributes to AML OxPhos deficiency therefore, we first wanted to determine specificity of BAI1 for BAX expression. To begin to test this, BAX knockdown OCI cells ("OCI_{shBAX}") were generated in addition to a scramble control ("$OCI_{shScramble}$"). To validate the BAX knockdown model, we first measured BAX expression which was found to be reduced in OCI_{shBAX} cells (**Fig. 11B**) (**Supp. Fig. 8A**). For additional validation, we leveraged venetoclax, an inhibitor of the pro-apoptotic Bcl-2 protein and a mediator of BAX/BAK dependent apoptosis[105]. Given that BAX/BAK-dependent apoptosis of AML cells is induced by venetoclax, loss of BAX is known to confer resistance to venetoclax[90]. As proof of concept, viability and colony formation of BAX knockdown AML cells was quantified in response to increasing doses of venetoclax. In response to venetoclax, OCI_{shBAX} were highly resistant to apoptosis and losses of colony formation induced by venetoclax relative to $OC_{shScramble}$ (**Fig. 11C-D**).

Having validated our BAX knockdown model, we used the BAX knockdown AML cells to: 1) test our overarching hypothesis that BAX activity contributes to intrinsic AML OxPhos deficiency

and 2) determine specificity of BAI1 for the BAX protein. To do this, we leveraged our OxPhos kinetics assay, respiratory capacity assay, and intact cell respiration assays, conducted previously herein, using BAX knockdown cells. To begin, intact cell respiration in response to BAI1 was measured in BAX knockdown AML cells. Despite a reduction of BAX expression, however, stabilization of uncoupled respiration in response to BAI1 was similar in both OCI_{shBAX} and $OCI_{shScramble}$ cells (**Fig. 11E**). Furthermore, loss of BAX did not result in any differences of intact cell respiration even in the vehicle control groups, suggesting that BAX knockdown does not impact intact cell respiration (**Fig. 11E**). Following this, OxPhos respiratory kinetics, measured in the presence or absence of BAI1, and respiratory capacity were quantified in permeabilized BAX knockdown cells. As described previously, respiratory capacity was used for normalization of OxPhos respiratory kinetics (i.e., as a percentage of total respiratory capacity). Although reduction of BAX expression resulted in an increase in respiratory capacity (**Fig. 11F**) (**Supp. Fig. 8B**), OxPhos respiratory kinetics in the presence and absence of BAI1 were both unchanged between both OCI_{shBAX} and $OCI_{shScramble}$ cells (**Fig. 11G**) (**Supp. Fig. 8C**). These data suggest that reactivation of OxPhos by BAI1 is not dependent on BAX expression, and that BAX activity does contribute to intrinsic OxPhos deficiency in AML cells. To confirm this, the $\Delta\Psi_m$ was measured in BAX knockdown cells during our OxPhos kinetics assay in the presence or absence of BAI1. A reduction of BAX expression did not affect the magnitude of oligomycin-induced changes in polarization in the presence or absence of BAI1 (**Fig. 11H**) (**Supp. Fig. 8D-E**). Thus, OCI_{shBAX} and $OCI_{shScramble}$ cells were both characterized by a mitochondrial phenotype indicative of an “ATP consumer” that, in the presence of BAI1, was shifted towards a mitochondrial phenotype reflective of an “ATP producer”. Because BAI1 reactivation of AML OxPhos was independent of BAX protein expression, we hypothesized that reactivation of AML OxPhos by BAI1 is cytotoxic to AML cells in a BAX-independent manner. To test this, viability of BAX knockdown cells was measured in response to increasing doses of BAI1. This experiment revealed that, despite a reduction in BAX expression, cytotoxicity of BAI1 towards BAX knockdown AML cells was unaltered (**Fig. 11I**).

Collectively, these data suggest that reactivation of AML OxPhos by BAI1 and the underlying cytotoxicity are independent of BAX expression (**Fig. 11J**). Therefore, these data argue against our hypothesis that BAX activity contributes to intrinsic OxPhos deficiency of AML.

BAX inhibits AML respiration independently of cytochrome C release in response to venetoclax

Reactivation of AML OxPhos by BAI1 was found to be cytotoxic and occurred independently of BAX expression. Although BAX activity does not appear to play a role in intrinsic OxPhos deficiency of AML, BAX has previously been shown to inhibit components of the ETS[8,15] in addition to it's known role in permeabilizing the outer mitochondrial membrane to facilitate the release of cytochrome C[8,98]. Cytochrome C release is known to occur following inhibition of pro-apoptotic Bcl-2 by venetoclax that mediates BAX/BAK dependent apoptosis[101]. In addition to these effects, venetoclax is also known to inhibit respiration in AML[69]. As proof of concept, we measured OxPhos capacity of permeabilized AML cells or peripheral blood mononuclear (PBMC) cells in the presence or absence of venetoclax. Venetoclax inhibited OxPhos capacity in AML cells and PBMC, however, the magnitude of inhibition was more pronounced in AML cells relative to PBMC (**Fig. 12A**) (**Supp. Fig. 9A-D**). Given that venetoclax mediates BAX/BAK dependent apoptosis, losses in respiration may be multifactorial, thus 1) Bcl-2 inhibition, 2) BAX/BAK activity, and 3) other apoptotic events may play a role in venetoclax-mediated inhibition of respiration during apoptosis. Although the precise mechanism of the intrinsic apoptotic pathway remains relatively controversial, prior research has suggested that BAX induces apoptosis, specifically, by permeabilizing the outer mitochondrial membrane and facilitating the induction of mitochondrial permeability transition[64]. Mitochondrial permeability transition occurs when the inner mitochondrial membrane becomes permeable to solutes with a molecular mass under 1.5kDa and this process is mediated by cyclophilin D[17]. Inhibition of cyclophilin D by cyclosporin A (CSA), therefore, is known to prevent mitochondrial permeability transition and block apoptosis[73]. We

hypothesized that induction of mitochondrial permeability transition may be a potential mechanism whereby venetoclax inhibits AML respiration. To test this, we leveraged our OxPhos kinetics assay to measure permeabilized AML cell respiration in the presence or absence of venetoclax and CSA. In this assay, CSA did not rescue venetoclax-induced losses of respiratory flux, suggesting that mitochondrial permeability transition is not necessary for inhibition of AML respiratory flux in response to venetoclax (**Fig. 12B**).

Venetoclax is known to promote apoptosis in AML cells by inducing BAX-mediated release of cytochrome C[101]. Because cytochrome C shuttles electrons from Complex III to Complex IV at the terminal end of the electron transport system (ETS), we hypothesized that inhibition of AML respiration by venetoclax may be driven by the release of cytochrome C following BAX-mediated permeabilization of the outer mitochondrial membrane. To test this, we leveraged our respiratory capacity assay to measure maximal respiratory flux of permeabilized $OCI_{shScramble}$ in the presence or absence of venetoclax and cytochrome C. Adding cytochrome C directly to the assay buffer was intended to test the integrity of the outer mitochondrial membrane. When the outer mitochondrial membrane becomes damaged, by BAX activity for example, supplying cytochrome C will increase respiratory flux[8,127]. In this assay, inhibition of maximal respiratory flux of $OCI_{shScramble}$ by venetoclax was not rescued by the presence of cytochrome C (**Fig. 12C**). These data indicate that venetoclax inhibits respiratory flux independently of cytochrome C release. Interestingly, neither cytochrome C nor CSA rescued the inhibition of AML cell respiration by venetoclax, suggesting that losses of respiration by venetoclax may be driven by either 1) inhibition of Bcl-2 or 2) activation of pro-apoptotic proteins such as BAX/BAK. Given that BAX knockdown confers resistance to venetoclax, but not BAK alone[90] (Fig. 3C-D), we hypothesized that BAX also inhibits respiration in response to venetoclax. To test this, we measured the OxPhos capacity and respiratory capacity of BAX knockdown cells in the presence or absence of venetoclax. In these assays, OCI_{shBAX} were more resistant to venetoclax-mediated inhibition of respiratory capacity and OxPhos capacity relative to $OCI_{shScramble}$ (**Fig. 12D**) (**Supp. Fig. 9E-H**).

Importantly, cytochrome C addition at the end of the respiratory capacity assay did not result in an increase in respiration of either $OCI_{shScramble}$ or OCI_{shBAX} (**Supp. Fig. 9G-H**). Collectively, these data indicate that BAX inhibits AML respiration in response to venetoclax, and this loss of respiration is independent of cytochrome C release.

DISCUSSION

AML cells present with intrinsic deficiencies in OxPhos that reduce the ability of AML to synthesize ATP[92]. Reduction of ATP synthesis in AML appears to involve intrinsic limitations in the ability of the electron transport system to polarize the $\Delta\Psi_m$. The $\Delta\Psi_m$ provides the thermodynamic driving force to cause ATP synthesis to occur at the F_1 sector of ATP synthase. However, the ATP synthase will revert to an F_1-ATPase proton pump when the $\Delta\Psi_m$ falls beneath the reversal potential[30]. Below the reversal potential, the F_1-ATPase will hydrolyze ATP to pump protons across the inner membrane to sustain polarization. In addition to this, the $\Delta\Psi_m$ also fuels the export of matrix ATP via ANT[30]. In our previous publication, ANT was found to import extramitochondrial ATP into the matrix space where it inhibited AML uncoupled respiratory flux[92], a mitochondrial phenotype indicative of an "ATP consumer". We hypothesized, therefore, that BAX activity may contribute to OxPhos deficiency in AML by compromising efficient energy transduction via 1) BAX-induced outer membrane permeabilization and subsequent cytochrome C release or 2) BAX-dependent inhibition of respiratory components. Herein, OxPhos was reactivated in AML in the presence of the BAX inhibitor, BAI1. Specifically, BAI1 was found to stabilize uncoupled respiration in intact AML cells. When AML cells were permeabilized, it was discovered that BAI1 stabilization of intact cell uncoupled respiration was related to BAI1-mediated restoration of OxPhos respiratory flux that prevented ATP-dependent inhibition of AML uncoupled respiration. These effects of BAI1 were also reflected in measurements of the AML $\Delta\Psi_m$. Although the $\Delta\Psi_m$ of AML was sustained via F_1-ATPase activity, indicated by a depolarization in response to oligomycin, the presence of BAI1 altered the AML mitochondrial

phenotype to favor ATP production, indicated by a shift towards hyperpolarization in response to the addition of oligomycin. These data demonstrate that BAI1 reactivates OxPhos in AML, thereby shifting the AML mitochondrial phenotype from an “ATP consumer”, to a mitochondrial phenotype indicative of an “ATP producer”. This phenotypic shift induced by BAI1 was found to be cytotoxic to AML, which is counterintuitive to BAI1 inhibition of the BAX protein. When BAX protein expression was knocked down in AML, it was discovered that reactivation of AML OxPhos and the underlying cytotoxicity of BAI1 in AML cells occurred independently of BAX activity. Although BAX activity was not found to be causal to the intrinsic OxPhos deficiency of AML, BAX activity has been previously suggested to inhibit respiration independently of cytochrome C release. To this end, we stimulated BAX activity in BAX knockdown cells by leveraging the chemotherapeutic venetoclax, an inhibitor of the Bcl-2 protein and a mediator of BAX/BAK-dependent apoptosis[105,90]. By doing this, we discovered that BAX activity inhibits AML respiration independently of cytochrome C release. Collectively, these data demonstrate that although BAX activity is not causal to intrinsic OxPhos deficiency in AML, BAI1 appears to be a novel agent that induces cytotoxicity via BAX-independent reactivation of AML OxPhos.

OxPhos deficiency in AML appears to result from intrinsic limitations in the ETS that hinders the ability to polarize the $\Delta\Psi_m$, therefore, the $\Delta\Psi_m$ of AML cells is sustained by hydrolyzing ATP via the F_1-ATPase. Before the F_1-ATPase hydrolyzes ATP, however, ATP synthesized in the matrix space, or imported via ANT, can allosterically regulate respiratory components[92]. Importantly, respiration in AML is inhibited following the matrix import of ATP[92]. Given that ATP-dependent inhibition is rescued by BAI1, resulting in cytotoxicity, AML appear to be dependent upon ATP-dependent allosteric regulation of the ETS. We suspect that allosteric regulation of the ETS by matrix ATP is a cytoprotective mechanism in AML that mitigates the production of cytotoxic reactive oxygen species (ROS). Consistent with this, ROS production is known to be reduced by ATP-dependent allosteric regulation of Complex IV[102]. The allosteric regulation of Complex IV maintains a low $\Delta\Psi_m$, thereby reducing the “backpressure” placed on proton-pumping by the

respiratory complexes during electron transport[102]. When electron transport is slowed by a highly polarized $\Delta\Psi_m$, electrons tend to "leak" from the respiratory complexes onto molecular oxygen and this results in the production of superoxide (i.e., a reactive oxygen species). Therefore, ROS production is reduced when the $\Delta\Psi_m$ is sustained at low voltage potentials by the ATP-dependent allosteric regulation of Complex IV. Allosteric regulation of Complex IV seems to be important for AML cells that present with abberant mitochondrial metabolism[43] and increases in mitochondrial content[91], potentially sensitizing AML cells to cytotoxic ROS production when OxPhos is reactivated. Related to this, a cytotoxic reactivation of AML OxPhos was first observed in our previous study in response to either 17-AAG (i.e., an inhibitor of TRAP1) or curcumin[92] (i.e., a plant polyphenolic compound). Importantly, curcumin is known to induce apoptosis of AML cells by stimulating the production of ROS[123], which we would expect to result following the reactivation of OxPhos in AML. However, more work is needed to fully elucidate the underlying mechanism(s) that underlie AML cell cytotixicity following the reactivation of OxPhos in AML.

Herein, AML present with increases in expression of the pro-apoptotic BAX protein relative to MPBMC, suggesting a link between BAX-mediated mitochondrial damage and intrinsic OxPhos deficiency. Although the intrinsic OxPhos deficiency of AML was not found to be related to increases in BAX protein expression, BAX activity was found to play a role in venetoclax-induced losses of respiration. Losses of respiration by BAX activity in the presence of venetoclax however, were found to be independent of cytochrome C. These data are intriguing, but it is not currently clear how BAX mediates respiration in this context. Previous research has implicated the adenine nucleotide translocase[15] as a protein directly inhibited by BAX, however, inhibition of ANT does not appear to explain the BAX-mediated inhibition of uncoupled respiration in AML herein. Other research has reported that the voltage-dependent anion channel (i.e., VDAC) is involved in BAX-mediated apoptosis, by direct interactions with the BAX protein[113,2,112]. These studies suggest that BAX mediates the conformation of VDAC, a gatekeeper of the mitochondrion, to facilitate the release of cytochrome C. Given that cytochrome C release was unrelated to BAX-mediated

respiratory inhibition herein, it may be that modulating the conformation of VDAC by BAX alters substrate uptake, thereby reducing respiration. Unsurprisingly however, respiratory inhibition of AML cells in response to venetoclax was not fully rescued by the knockdown of BAX protein. These data suggest that, notwithstanding residual BAX expression, other pro-apoptotic proteins (e.g. BAK) may inhibit mitochondrial respiration in response to venetoclax, as well as inhibition of Bcl-2 itself. Importantly Bcl-2 is also known to interact with the VDAC[111] and Complex IV[32] of the electron transport system to support either polarization of the $\Delta\Psi_m$ or mitochondrial respiration, respectively. These studies implicate Bcl-2 inhibition as a potential driver of respiratory inhibition in response to venetoclax. Ultimately however, more work is needed to delineate the mechanism(s) by which venetoclax and BAX activity inhibits AML cell respiration independently of cytochrome C release. Collectively, our data provide novel insight into the mechanism of action of venetoclax and highlight the impacts of BAI1 on AML mitochondrial bioenergetics.

METHODS

All procedures involving human subjects were approved by the Institutional Review Board of the Brody School of Medicine.

Blood collection and isolation of PBMCs.

Venous blood from the brachial region of the upper arm was collected from healthy volunteers, between the ages of 18-70 years. Whole blood was collected in sodium-heparinized Cell Preparation Tubes (CPT) (BD Biosciences, Franklin Lakes, NJ) and was then centrifuged at 1,800 x *g* for 15 min. Mononuclear cells were washed in ammonium-chloride-potassium (ACK) lysis buffer to remove red blood cells and were either used immediately, or frozen in liquid nitrogen (-80°C.) prior to experimentation.

Culturing of leukemic cell lines

MV4;11, HL60, KG-1, JVM3, OCI-AML2, MM6, and U937 (ATCC, Manassas, VA) human leukemia cells were cultured in IMDM or RPMI-1640 (Thermo Fisher Scientific, Waltham, MA) supplemented with glutamax, 10% FBS, and 1% penicillin/streptomycin and incubated at 37°C in 5% CO_2. For experiments involving venetoclax resistance, MV4;11, OCI-AML2, MOLM-13, and HL60 cells were cultured in either IMDM or RPMI-1640, supplemented with glutamax, 10% FBS, and 1% penicillin/streptomycin. To model venetoclax resistance, cells were adapted in culture to 1uM venetoclax by passaging cells in increasing doses of venetoclax beginning at 10nM. After reaching an average cell density of $1x10^6$ cell per mL, maintained in 1uM venetoclax, the cells were harvested and used for experimentation.

Cell viability assays

Cell viability for mitochondrial functional assessments were quantified with viable cell counts using Trypan Blue (0.4%). For fluorescent measurements of cell viability, cells were seeded in black-wall, 96-well plates, in growth medium. After addition of agents (0.2mL final well volume), cells were incubated at 37° C, 5% CO_2, for the indicated times. Viability was determined using propidium iodide (PI). Positive control cells were permeabilized by addition of 1µl of 10.0mg/ml digitonin and incubated at 37° C, 5% CO_2, for 20min. Following this, plates were centrifuged at 1200 x *g* for 10 min. After centrifugation, plates were dumped to remove culture media and 0.100mL of a 5.0µM PI solution in PBS was added. The plate was then incubated at 37° C, 5% CO_2 for 20min, and viability was calculated as the mean fluorescence (minus permeabilized vehicle control) at 530nm excitation and 620nm emission.

OxPhos kinetics assay

OxPhos kinetics were measured using a modified version of the creatine-kinase clamp (CK Clamp). For experiments using the CK clamp assay, the free energy of ATP hydrolysis (ΔG_{ATP}) is calculated using the equilibrium constant for the CK reaction (K'_{CK}) and is based upon

the addition of known concentrations of creatine (CR), phosphocreatine (PCR), and ATP in the presence of excess amounts of CK[44]. Calculation of ΔG_{ATP} at defined PCR concentrations was done using the online resource (https://dmpio.github.io/bioenergetic-calculators/ck_clamp/) as previously described[44].

Respiratory flux in intact and permeabilized cells

Approximately 2 x 10^6 cells were used for each intact and permeabilized cell respirometry experiment. Respirometry measurements were conducted using an Oroboros Oxgraph-2k (O2k; Oroboros Instruments, Innsbruck, Austria) in either a 0.5 or 1.0mL reaction volume at 37°C. Data was normalized to viable cell count unless otherwise indicated. For normalization to total protein, cell suspensions were removed from the O2k chamber following the completion of each assay and placed into microcentrifuge tubes. The cell suspension was then centrifuged at 2,000 x *g* for 10min at 4°C. Assay buffer was aspirated and the cell pellet was washed with PBS. Cells were then lysed using low-percentage detergent buffer (CelLytic M) followed by a freeze-thaw cycle on dry ice. The protein concentration was then determined using a BCA protein assay.

Respiratory flux was measured using methods described previously[44] (Fisher-Wellman et al., 2018). For intact cell measurements, cells were resuspended in Intact Cell Respiratory Media (17.7g/L Iscove's Modified Dulbecco's Medium (IMDM), 20mM HEPES, 1% Penicillin/Streptomycin, 10% FBS, pH 7.4). Basal respiration was measured, followed by the quantification of maximal respiration by titrating FCCP uncoupler (FC; 0.5-5μM). Antimycin A (Ant; 0.5μM) was used to inhibit mitochondrial respiration.

For permeabilized cell measurements, cells were resuspended in Respiratory Buffer supplemented with creatine (105mM MES potassium salt, 30mM KCl, 8mM NaCl, 1mM EGTA, 10mM KH_2PO_4, 5mM $MgCl_2$, 0.25% BSA, 5mM creatine monohydrate, pH 7.2). Cells were

permeabilized with digitonin ("Digi", 0.02mg/mL). OXPHOS respiratory kinetics were measured using the creatine kinase (CK) clamp, and respiratory capacity was quantified with FCCP titration.

For all assays using the CK clamp technique (respiration assays and measurements of permeabilized cell $\Delta\Psi_m$), various combinations of carbon substrates and inhibitors were utilized. Substrates and inhibitors used in each assay are indicated in the figure legends: CK (20U/mL), ATP (5mM), PCr (1mM, 6mM, 15mM, 21mM), pyruvate (Pyr or P; 5mM), malate (M; 1mM), octanoyl-carnitine (O; 0.2mM), succinate (Succ or S; 5mM), glutamate (Glut or G; 5mM), oligomycin (Oligo, 0.02μM), FCCP (0.5-2μM), rotenone (Rot or R, 0.5μM), antimycin A (Ant A, 0.5μM), venetoclax (Vclax, 0.1nM-1μM), BAI1 (BAI1, 1μM-30μM), FCCP (5uM).

Mitochondrial membrane potential (ΔΨ) in permeabilized cells

Fluorescent determination of $\Delta\Psi_m$ using permeabilized cells was performed using a QuantaMaster Spectrofluorometer (QM-400; Horiba Scientific). Quantification of $\Delta\Psi_m$ via TMRM (operating in quench mode) was conducted as described previously[44]. Cells were harvested, centrifuged at 300 x *g* for 7 minutes then washed with PBS and centrifuged again at 300 x *g*. Following this, cells were resuspended in 1mL of assay buffer and viable cells were counted with trypan blue. Cells were then permeabilized with digitonin (Digi; 0.02mg/mL) for 10 minutes at room temperature. From the permeabilized cell suspension, ~3 million cells were added to a microcentrifuge tube and centrifuged at 1,500 x *g* for 10 minutes. Cell pellet was resuspended in fresh assay buffer and loaded with 200nM TMRM. Optimal excitation and emission parameters for each cell type were determined using an excitation emission scan to determine the fluorescence ratio. Membrane potential was then quantified using a fluorescence ratio of the experimentally determined excitation and emission parameters. The buffer for used for this assay was Respiratory Buffer supplemented with creatine (105mM MES potassium salt, 30mM KCl, 8mM NaCl, 1mM EGTA, 10mM KH_2PO_4, 5mM $MgCl_2$, 0.25% BSA, 5mM creatine monohydrate, pH 7.2).

For all assays using the CK clamp technique, various combinations of carbon substrates and inhibitors were utilized. Substrates and inhibitors used in each assay are indicated in the figure legends: CK (20U/mL), ATP (5mM), PCr (1mM, 6mM, 15mM, 21mM), pyruvate (Pyr or P; 5mM), malate (M; 1mM), octanoyl-carnitine (O; 0.2mM), succinate (Succ or S; 5mM), glutamate (Glut or G; 5mM), oligomycin (Oligo, 0.02μM), FCCP (0.5-2μM), rotenone (Rot or R, 0.5μM), antimycin A (Ant A, 0.5μM), venetoclax (Vclax, 0.1nM-1μM), BAI1 (BAI1, 1μM-30μM), FCCP (5uM).

BAX knockdown in OCI-AML2 cells

OCI-AML2 cells were cultured in IMDM (Thermo Fisher Scientific, Waltham, MA) supplemented with glutamax, 10% FBS, and 1% penicillin/streptomycin and incubated at 37°C in 5% CO_2. Human shRNA lentiviral particles cloned into pLKO.1 vector (18mer *BAX*-specific shRNA 5' GACGAACTGGACAGTAACATG 3'), and one scramble control; 0.5mL each,>10^7 TU/ml) were purchased from Addgene (CAT#: 10878). To facilitate infection, cells and lentiviral particles were co-cultured at a seeding density of 5x10^5 cells per mL in a retronectin dish. Following 72 hours of infection, cultures were then subjected to puromycin selection by continuous exposure to 2 μg/mL puromycin in the culture media. Confirmation of *BAX* knockdown was performed via western blotting (standard protocol) and analyzed with densitometry using ImageJ software.

Sample prep for label-free proteomics

Cell pellets or isolated mitochondria pellets were lysed in urea lysis buffer (8M urea in 40mM Tris, 30mM NaCl, 1mM $CaCl_2$, 1 x cOmplete ULTRA mini EDTA-free protease inhibitor tablet; pH=8.0), as described previously. The samples were subjected to two freeze-thaw cycles, and sonicated with a probe sonicator in three 5s bursts (Q Sonica #CL-188; amplitude of 30). Samples were centrifuged at 10,000 x *g* for 10min at 4°C. Protein concentration was determined by BCA. Equal amounts of protein were reduced with 5mM DTT at 37°C for 30min, and then alkylated with 15mM iodoacetamide for 30min in the dark. Unreacted iodoacetamide was

quenched with DTT (15mm). Reduction and alkylation reaction were carried out at room temperature. Initial digestion was performed with Lys C (1:100 w:w) for 4hr at 32°C. Following dilution to 1.5M urea with 40mM Tris (pH=8.0), 30mM NaCl, 1mM $CaCl_2$, samples were digested overnight with sequencing grade trypsin (50:1 w/w) at 32°C. Samples were acidified to 0.5% TFA and then centrifuged at 4,000 x *g* for 10min at 4°C. Supernatant containing soluble peptides was desalted and then eluate was frozen and subjected to speedvac vacuum concentration.

nLC-MS/MS for label-free proteomics

Final peptides were resuspended in 0.1% formic acid, quantified (ThermoFisher Cat# 23275), and diluted to a final concentration of 0.25µg/µL. Samples were subjected to nanoLC-MS/MS analysis using an UltiMate 3000 RSLCnano system (ThermoFisher) coupled to a Q Exactive Plus Hybrid Quadrupole-Orbitrap mass spectrometer (ThermoFisher) via a nanoelectrospray ionization source. For each injection, 4µL (1µg) of sample was first trapped on an Acclaim PepMap 100 20mm x 0.075mm trapping column (ThermoFisher Cat# 164535; 5µL/min at 98/2 v/v water/acetonitrile with 0.1% formic acid). Analytical separation was performed over a 95min gradient (flow rate of 250nL/min) of 4-25% acetonitrile using a 2µm EASY-Spray PepMap RSLC C18 75µm x 250mm column (ThermoFisher Cat# ES802A) with a column temperature of 45ºC. MS1 was performed at 70,000 resolution, with an AGC target of $3x10^6$ ions and a maximum injection time (IT) of 100ms. MS2 spectra were collected by data-dependent acquisition (DDA) of the top 15 most abundant precursor ions with a charge greater than 1 per MS1 scan, with dynamic exclusion enabled for 20s. Precursor ions isolation window was 1.5m/z and normalized collision energy was 27. MS2 scans were performed at 17,500 resolution, maximum IT of 50ms, and AGC target of $1x10^5$ ions.

Data analysis for label-free proteomics

As described previously with some modification, Proteome Discoverer 2.2 (PDv2.2) was used for raw data analysis, with default search parameters including oxidation (15.995 Da on M) as a variable modification and carbamidomethyl (57.021 Da on C) as a fixed modification. Data

were searched against the Uniprot Homo Sapiens reference proteome (Proteome ID: UP000005640), as well as the Human Mito Carta 3.0 database. PSMs were filtered to a 1% FDR and grouped to unique peptides while maintaining a 1% FDR at the peptide level. Peptides were grouped to proteins using the rules of strict parsimony and proteins were filtered to 1% FDR. Peptide quantification was done using the MS1 precursor intensity. Imputation was performed via low abundance resampling. Using only high confidence master proteins, mitochondrial enrichment factor (MEF) was determined as previously described by comparing mitochondrial protein abundance (i.e., proteins identified to be mitochondrial by cross-reference with the MitoCarta 3.0 database) to total protein abundance.

Statistical evaluation of label-free proteomics

All proteomics samples were normalized to total protein abundance, and the protein tab in the PDv2.2 results was exported as a tab delimited .txt. file and analyzed. Protein abundance was converted to the Log2 space. For pairwise comparisons, tissue mean, standard deviation, p-value (p; two-tailed Student's t-test, assuming equal variance), and adjusted p-value (Benjamini Hochberg FDR correction) were calculated35. Mitochondrial functional assay results are expressed as the mean ± SEM (error bars). Data were normalized to viable cell counts and then corrected for the group mean MEF, with the final values expressed as pmol/s/million cells/MEF18. Throughout the paper, differences between groups were assessed by t-test, or one-way ANOVA, followed by Tukey's test where appropriate using GraphPad Prism 8 software (Version 8.4.2). Other statistical tests used are described in the figure legends. Statistical significance in the figures is indicated as follows: *$p < 0.05$; **$p < 0.01$; ***$p < 0.001$; ****$p < 0.0001$. Unless otherwise stated, figures were generated using GraphPad Prism 8 software (Version 8.4.2) or Biorender

Statistical analysis and software

Statistical analysis was performed using GraphPad Prism 8.4. All data are represented as mean ± SEM and analysis were conducted with a significance level set at $p<0.05$. Details of

statistical analysis are included within figure legends. Figures were generated using Biorender and GraphPad Prism 8.4.

Figure 9. BAI1 stabilizes uncoupled respiration of intact AML cells. All experiments were performed using intact cells. (A) Schematic depicting mitochondrial phenotyping of intact AML cells in the presence of BAI1. Intact cell respiratory capacity was measured in the presence of absence of 30uM BAI1 using (A) MV4;11, (B), OCI-AML2, or (C) HL60 cells. Data are presented as mean ±SEM and analyzed by two-way ANOVA (B-D). *p<0.05, **p<0.01, ***p<0.001, ****p<0.0001.

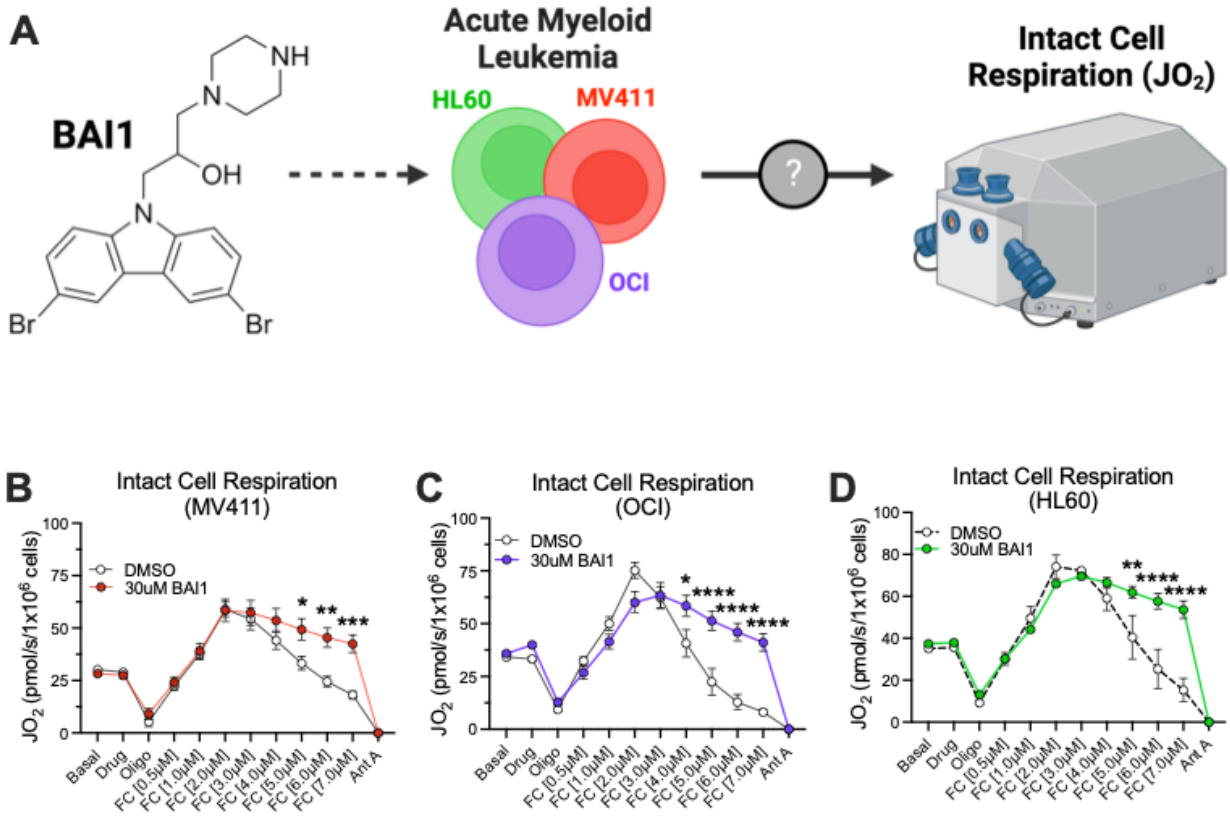

Figure 10. BAI1 reactivates OxPhos in AML. All experiments were performed using digitonin-permeabilized cells. (A) Schematic depicting mitochondrial phenotyping of permeabilized AML cells in the presence of BAI1. (B) Permeabilized cell respiratory capacity was measured in the presence of absence of 30uM BAI1 in AML cells. Permeabilized cell OxPhos respiratory kinetics were measured in the presence or absence of increasing doses of BAI1 in (C) MV4;11, (D) OCI-AML2, or (E) HL60 AML cells. (F) Comparison of permeabilized cell ADP-stimulated respiration in the presence or absence of 30uM BAI1 using MV411 cells. (G) Representative trace of permeabilized OCI-AML2 mitochondrial membrane potential during the OxPhos kinetics assay in the presence or absence of increasing doses of BAI1. (H) Oligomycin induced changes in polarization of the mitochondrial membrane potential was measured using either MV4;11, OCI-AML2 or HL60 cells in the presence or absence of increasing doses of BAI1. (I) Schematic depicting mechanism of BAI1 on AML cell mitochondrial membrane potential. Data are presented as mean ±SEM and analyzed by two-way ANOVA (C-F) or one-way ANOVA (B,H). *p<0.05, **p<0.01, ***p<0.001, ****p<0.0001.

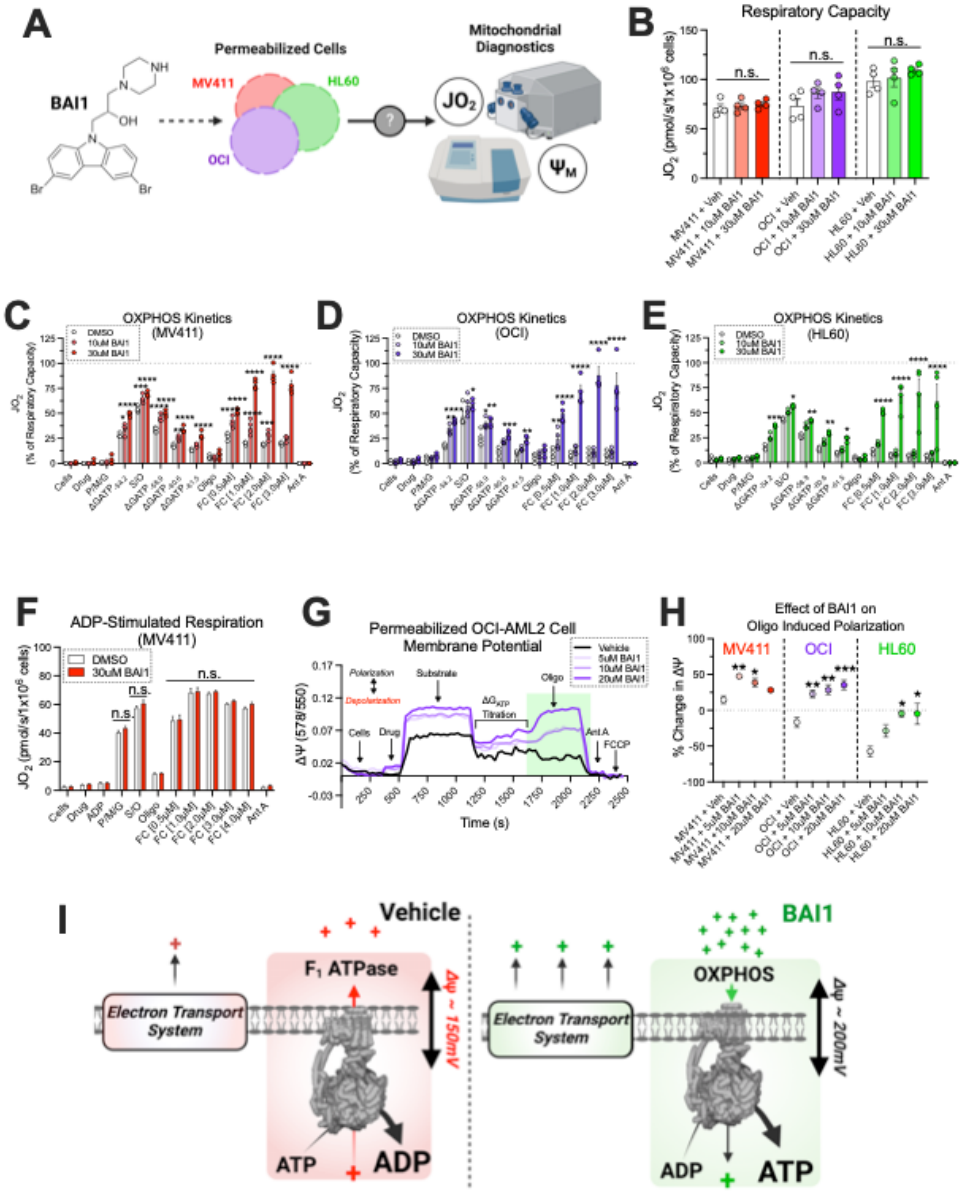

Figure 11. BAI1-mediated reactivation of AML OxPhos and the underlying cytotoxicity occur independently of BAX expression. All experiments were performed using whole intact cells or digitonin-permeabilized cells. (A) Viability of AML cells in the presence or absence of increasing doses of BAI1 was measured using propidium iodide after 48 hours. (B) Comparison of BAX expression in BAX knockdown cells using western blot. (C) Viability of BAX knockdown cells in the presence or absence of increasing doses of venetoclax was measured using propidium iodide after 48 hours. (D) Colony formation of BAX knockdown cells was measured in the presence or absence of increasing doses of venetoclax. (E) Comparison of intact cell respiration using BAX knockdown cells in the presence or absence of 30uM BAI1. (F) Comparison of permeabilized cell respiratory capacity using BAX knockdown cells. (G) Comparison of permeabilized cell OxPhos respiratory kinetics using BAX knockdown cells in the presence or absence of 30uM. BAI1. (H) Comparison of oligomycin induced changes in polarization of the mitochondrial membrane potential using BAX knockdown cells in the presence or absence of increasing doses of BAI1. (I) Comparison of viability of BAX knockdown cells in the presence or absence of increasing doses of BAI1 was measured using propidium iodide after 48 hours. (J) Schematic depicting BAX-independent reactivation of OxPhos by BAI1. Data are presented as mean ±SEM and analyzed by two-way ANOVA (A,C-E,G,I), one-way ANOVA (H), or unpaired t-test (B,F). *p<0.05, **p<0.01, ***p<0.001, ****p<0.0001.

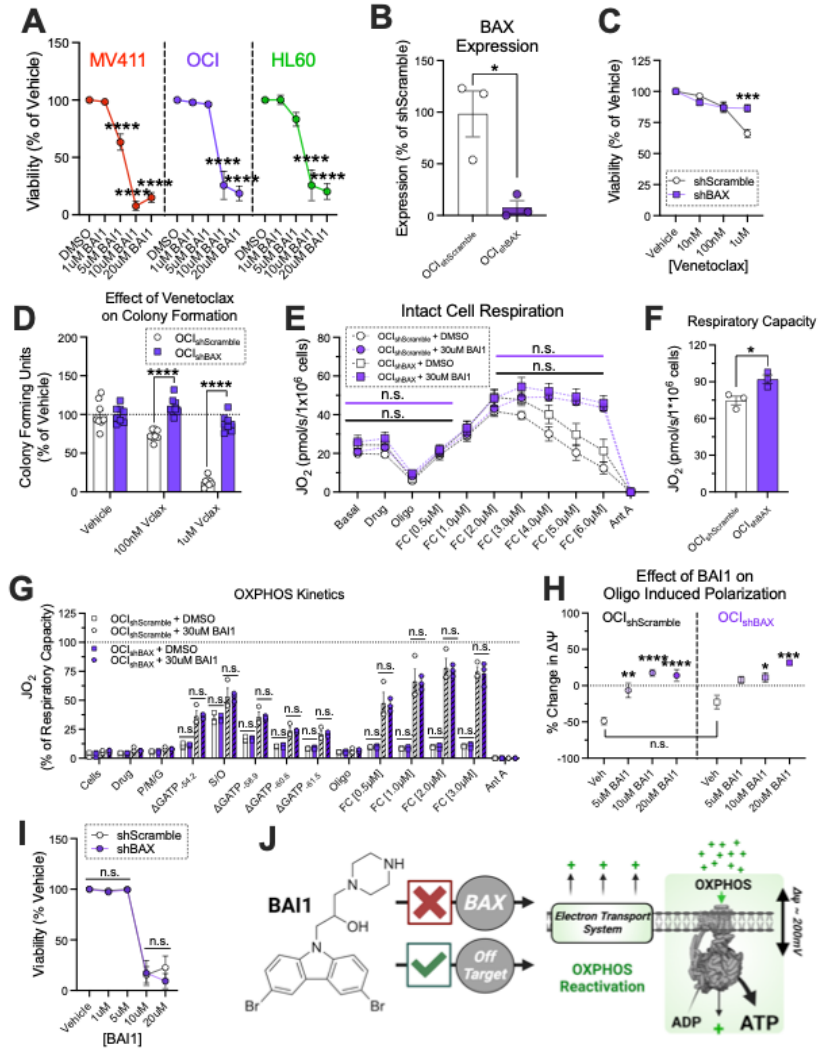

Figure 12. BAX inhibits AML respiration independently of cytochrome C release in response to venetoclax. All experiments were performed using digitonin-permeabilized cells. (A) Comparison of permeabilized cell OxPhos capacity using AML and PBMC cells in the presence of 1uM venetoclax. (B) Comparison of permeabilized cell OxPhos respiratory kinetics using MV411 cells in the presence or absence of 1uM CSA or 100nM venetoclax. (C) Comparison of permeabilized cell respiratory capacity using $OCI_{shScramble}$ cells in the presence or absence of cytochrome C or 1uM venetoclax. (D) Comparison of permeabilized cell respiratory capacity and OxPhos capacity using BAX knockdown cells in the presence or absence of increasing doses of BAI1. Data are presented as mean ±SEM and analyzed by two-way ANOVA (A-D). *p<0.05, **p<0.01, ***p<0.001, ****p<0.0001.

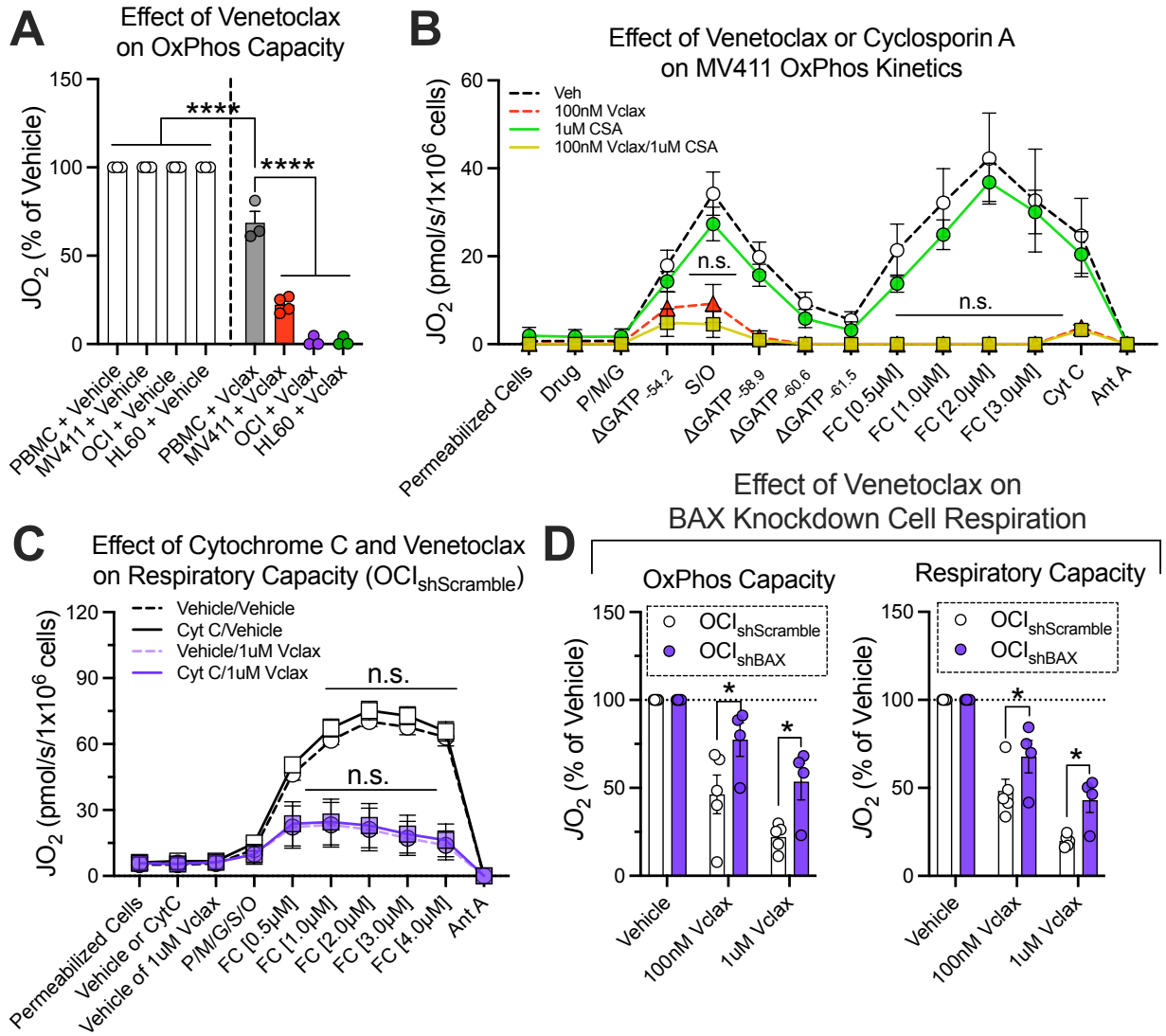

Supplemental Figure 6. AML present with elevations of BAX expression relative to mobilized PBMC cells (Related to Figure 9). (A) Comparison of BAX expression in AML and mobilized PBMC cells. Data are presented as mean ±SEM and analyzed by one-way ANOVA (A). *p<0.05, **p<0.01, ***p<0.001, ****p<0.0001.

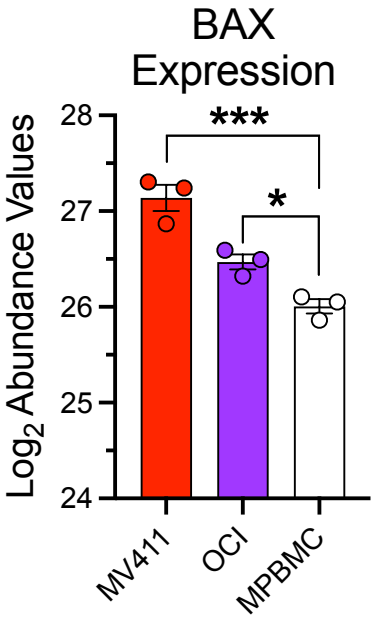

Supplemental Figure 7. OxPhos profiling of AML and PBMC cells in the presence or absence of BAI1 (Related to Figure 10). Permeabilized cell respiratory capacity was measured using (A) MV4;11, (B) OCI-AML2, or (C) HL60 cells in the presence or absence of increasing doses of BAI1. Permeabilized cell OxPhos respiratory kinetics were measured using (D) MV4;11, (E) OCI-AML2, (F) HL60, or (G) PBMC cells in the presence or absence of increasing doses of BAI1. Permeabilized cell membrane potential was measured using (H) MV4;11, (I) OCI-AML2, or (J) HL60 cells in the presence or absence of increasing doses of BAI1. Data are presented as mean ±SEM and analyzed by two-way ANOVA (A-J). *p<0.05, **p<0.01, ***p<0.001, ****p<0.0001.

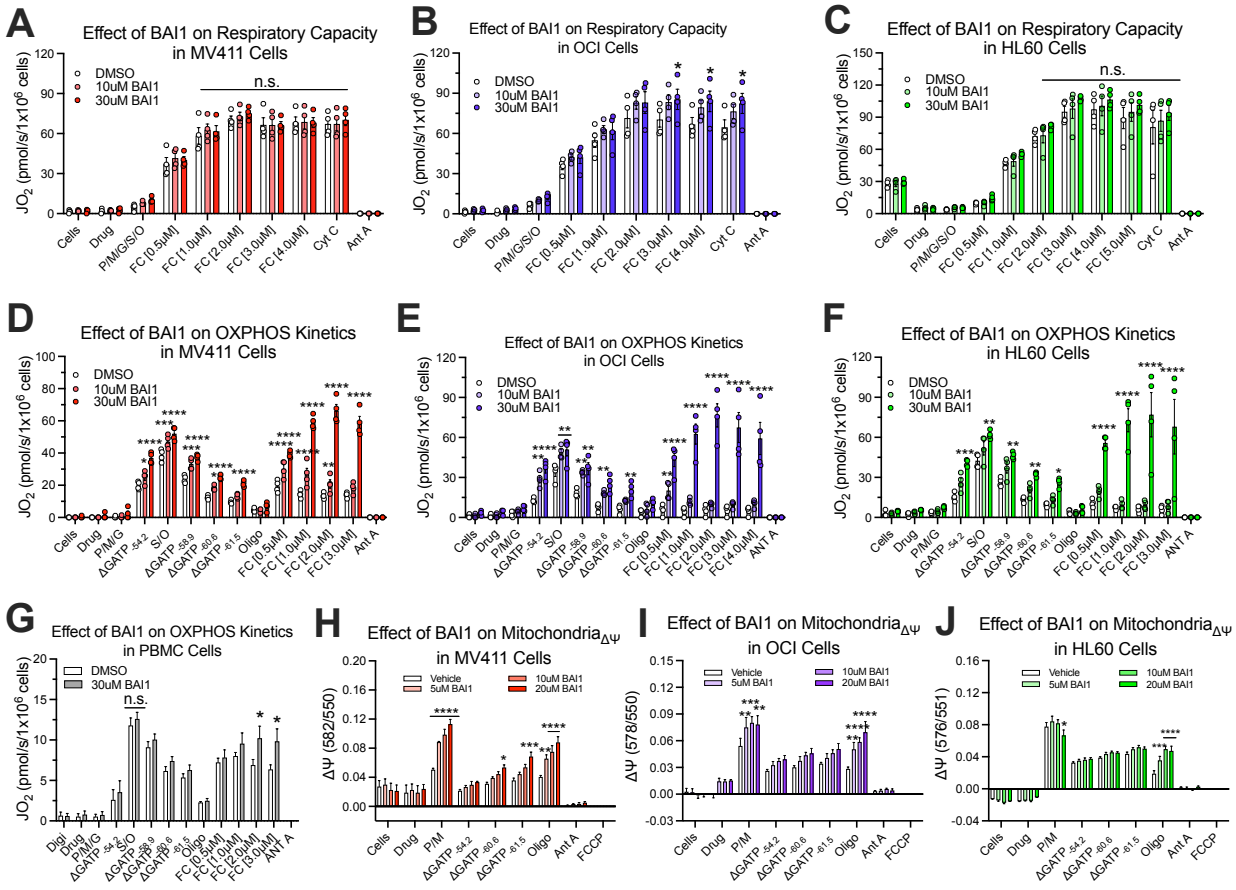

Supplemental Figure 8. OxPhos profiling of BAX knockdown cells in the presence or absence of BAI1 (Related to Figure 11)

(A) Representative western blot image of BAX expression in $OCI_{shScramble}$ or OCI_{shBAX} cells. (B) Comparison of permeabilized cell respiratory capacity using BAX knockdown cells. (C) Comparison of permeabilized cell OxPhos respiratory kinetics using BAX knockdown cells in the presence or absence of 30uM BAI1. Permeabilized cell membrane potential was measured using (D) $OCI_{shScramble}$ or (E) OCI_{shBAX} cells in the presence or absence of increasing doses of BAI1. Data are presented as mean ±SEM and analyzed by two-way ANOVA (B-E). *p<0.05, **p<0.01, ***p<0.001, ****p<0.0001.

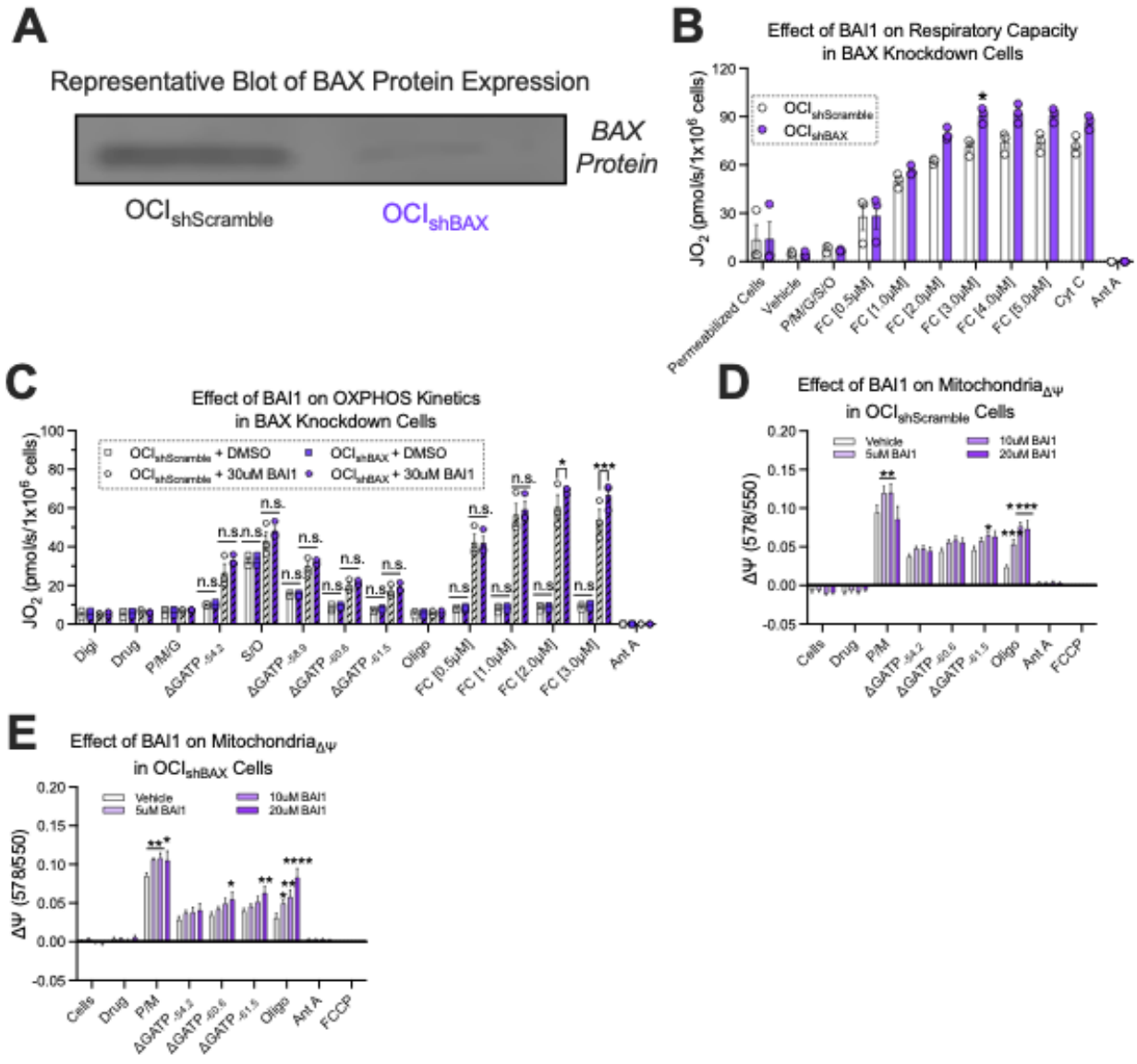

Supplemental Figure 9. OxPhos profiling of BAX knockdown cells in the presence or absence of venetoclax (Related to Figure 12). Permeabilized cell OxPhos respiratory kinetics was measured using (A) PBMC, (B) MV4;11, (C) OCI-AML2, or (D) HL60 cells in the presence or absence of 1uM venetoclax. Permeabilized cell OxPhos respiratory kinetics was measured using (E) $OCI_{shScramble}$ or (F) OCI_{shBAX} cells in the presence or absence of increasing doses of venetoclax. Permeabilized cell respiratory capacity was measured using (G) $OCI_{shScramble}$ or (H) OCI_{shBAX} cells in the presence or absence of increasing doses of venetoclax. Data are presented as mean ±SEM and analyzed by two-way ANOVA (A-H). *p<0.05, **p<0.01, ***p<0.001, ****p<0.0001.

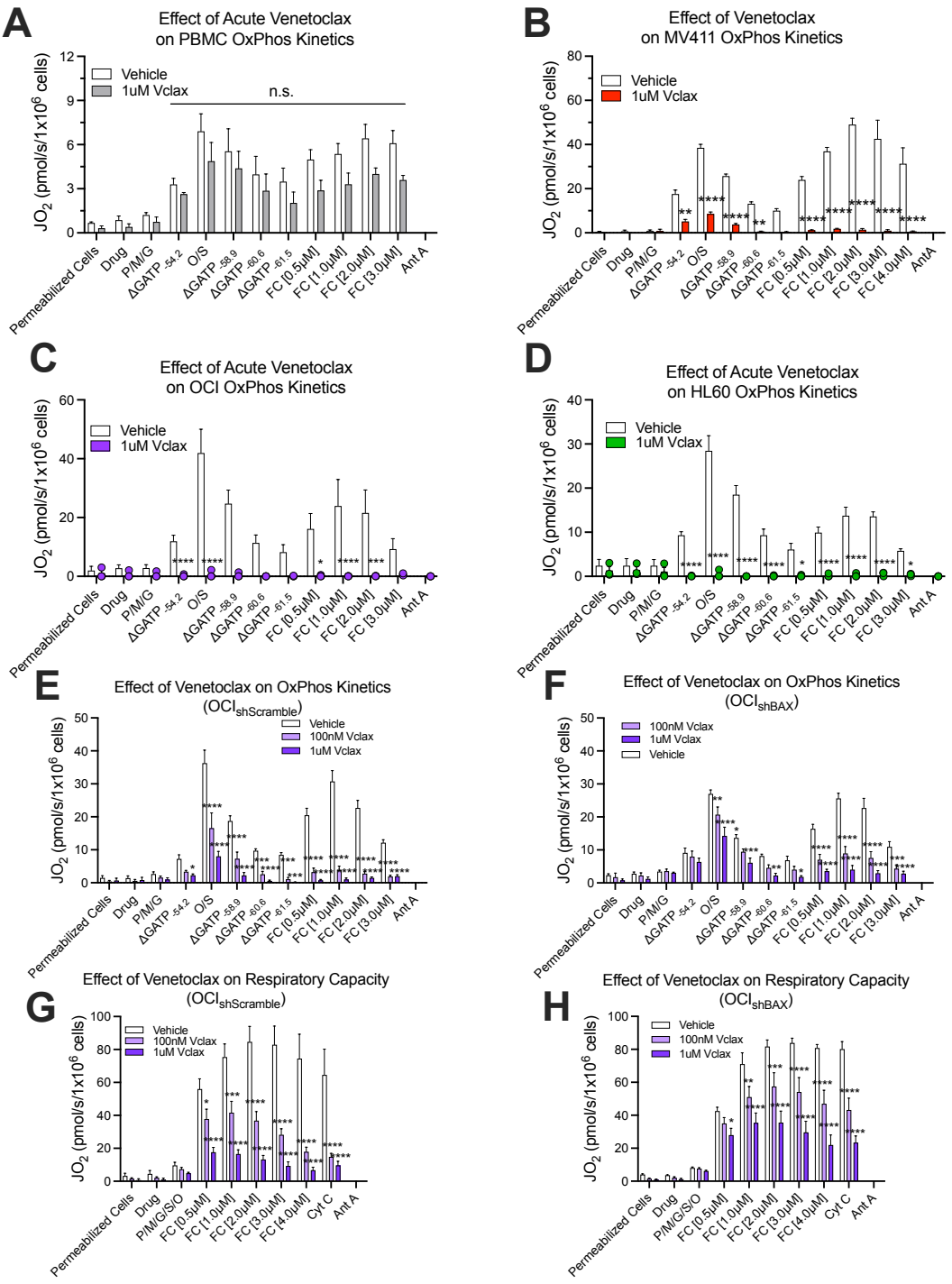

Chapter 4: Integrated Discussion

Major Findings

The AML mitochondrion presents with a unique model of mitochondrial bioenergetics relative to normal blood cells that we propose may be best described as “dephosphorylative oxidation” (i.e., DephOx), where the dephosphorylation of ATP supports the oxidation of carbon substrates. The reason DephOx occurs appears to be that AML cells are unable to polarize the $\Delta\Psi_m$ sufficiently to export ATP from the matrix space[92]. For ATP to exit the mitochondrial matrix, the free energy available in the AML $\Delta\Psi_m$ must be great enough to force ATP out of the mitochondrial matrix, via ANT (adenine nucleotide translocase), against the cytoplasmic ΔG_{ATP} (i.e., the ATP/ADP ratio in the cytoplasm). Instead, AML cells either recycle synthesized matrix ATP, or import cytosolic ATP into the matrix space where it is either 1) hydrolyzed by the F_1-ATPase, or 2) becomes inhibitory to AML respiratory flux. Respiratory flux was found to be much less important for AML survival when compared to polarization of the $\Delta\Psi_m$, which was found to be necessary for the survival of AML. Thus, AML, and even more so chemoresistant AML, appear to have acquired two particularly important cytoprotective mechanisms: 1) intrinsic lesions in the electron transport system that promote ATP consumption, and 2) a downregulation of *ATP5IF1*, the physiological inhibitor of the F_1-ATPase[47]. Together, these adaptations provide AML cells a survival advantage against respiratory insults while opposing depolarization of the $\Delta\Psi_m$, a hallmark of apoptosis, by consuming ATP.

The consumption of ATP by AML mitochondria appears to be important for AML survival for two distinct reasons: 1) F_1-ATPase activity sustains polarization of the $\Delta\Psi_m$, and 2) ATP-dependent inhibition of AML respiration from within the matrix limits the extent of $\Delta\Psi_m$ polarization (**Fig. 13A**). A low voltage potential may prevent cytotoxic ROS production[62], while appearing to keep AML respiratory flux uncoupled from the synthesis of ATP (**Fig. 13A**). Additionally, ATP hydrolysis by the F_1-ATPase 1) opposes a high matrix ΔG_{ATP} that would overtly inhibit respiratory flux, while 2) also sustaining a submaximal voltage potential (**Fig. 13A**). Nonetheless, AML

mitochondria bioenergetics are characterized by an ATP-dependent futile cycle that mimics an alternating current circuit model where the voltage potential is predominantly sustained at submaximal polarization. Although sustaining a voltage potential via the F_1-ATPase confers chemoresistance, this AML-specific mitochondrial bioenergetic pathway, termed "dephosphorylative oxidation", is actionable by compounds that either disrupt F_1-ATPase mediated $\Delta\Psi_m$, or reactivate OxPhos. Reactivation of OxPhos, as we suggest in Chapter III, appears to be cytotoxic due to a loss of ATP-dependent allosteric regulation of Complex IV that then results in cytotoxic ROS production of AML (**Fig. 13B**).

We suspect that AML are susceptible to cytotoxic ROS production due to increases in mitochondrial content[92], thereby amplifying ROS production upon reactivation of the entire respiratory network. For example, 17AAG (i.e., a reported inhibitor of TRAP1) was found to reactivate AML OxPhos in our previous work, and this was cytotoxic to AML cells[92]. As proof of concept in unpublished data, we measured maximal ROS production in isolated MV411 mitochondria energized with multiple substrates (i.e., pyruvate, malate, glutamate, octanoyl-carnitine, and succinate) and ΔG_{ATP} (i.e., a free energy of ATP hydrolysis value of -61.5 kJ/mol) in the presence or absence of 17-AAG. 17AAG was found to increase maximal ROS production of isolated MV411 mitochondria in the presence of ΔG_{ATP} (**Fig. 13C**). These data provide supporting evidence that reactivation of OxPhos induces cytotoxic ROS production in AML. Collectively, the research in this dissertation highlights a novel, AML-specific mitochondrial bioenergetic pathway, described as "dephosphorylative oxidation", that can be targeted by disrupting either F_1-ATPase mediated polarization of the $\Delta\Psi_m$, or reactivating AML OxPhos.

Future Directions

We proposed that AML can be selectively targeted by either reactivating OxPhos, or disrupting F_1-ATPase mediated polarization of the $\Delta\Psi_m$. Polarization by the F_1-ATPase can be disrupted using small molecule mitochondrial-targeted lipophilic compounds. However, other

compounds should be developed that target F_1-ATPase directly using a mechanism that mimics the conditionally-dependent mechanism[66] (i.e., selective inhibition of the F_1-ATPase, as opposed to the ATP synthase) of *ATP5IF1*, the physiological inhibitor of the F_1-ATPase. Inhibiting F_1-ATPase activity could be accomplished by the development of either small-molecule mimetics of *ATP5IF1*, or *ATP5IF1* peptide therapies. Alternatively, to develop novel therapies intended to specifically reactivate OxPhos, however, it would be beneficial to first determine the protein target of drugs that reactivate AML OxPhos (e.g., BAI1 and 17AAG). These OxPhos reactivating compounds may act by altering the conformation of VDAC (i.e., voltage dependent anion channel), the gatekeeper of the mitochondrion, as we suggest in our previous study[92]. However, VDAC has yet to be validated as the drug target of OxPhos reactivating compounds. As an alternative explanation, OxPhos reactivating compounds may act on a matrix effector (e.g., by inhibiting or activating an effector) that mediates ATP-dependent allostery of Complex IV, such as protein kinase A or protein phosphatase 1, based on a previous work[16]. Further investigations seeking to identify the precise drug target of AML OxPhos reactivators may be highly beneficial for developing a novel drug that can selectively target AML cells by reactivating OxPhos.

Figure 13. Proposed mechanism of death during reactivation of AML OxPhos. (A) Schematic depicting mechanism of ATP-dependent inhibition during AML dephosphorylative oxidation. (B) Schematic depicting mechanism of AML cell death when OxPhos is reactivated. (C) Comparison of maximal ROS production in the presence of ATP (a ΔG_{ATP} value of -61.5 kJ/mol) and in the presence or absence of 17AAG using isolated MV411 mitochondria. Data are presented as mean ±SEM and analyzed by an unpaired t-test (C). *p<0.05, **p<0.01, ***p<0.001, ****p<0.0001.

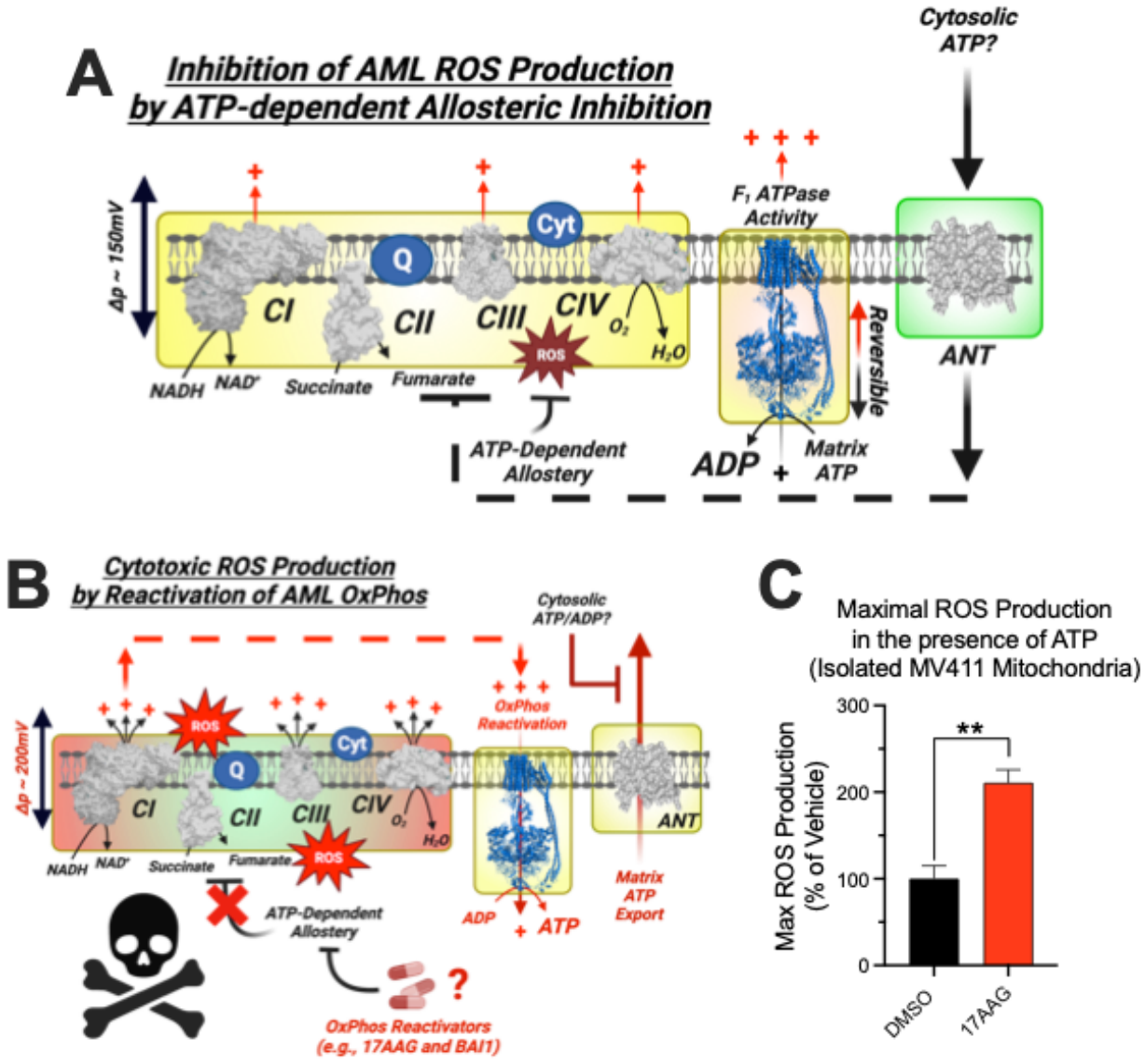

REFERENCES:

1. Abbas HA, Alfayez M, Kadia T, Ravandi-Kashani F, Daver N. Midostaurin In Acute Myeloid Leukemia: An Evidence-Based Review And Patient Selection. Cancer Manag Res. 2019 Oct 4;11:8817-8828. doi: 10.2147/CMAR.S177894. PMID: 31632141; PMCID: PMC6782026.
2. Adachi M, Higuchi H, Miura S, Azuma T, Inokuchi S, Saito H, Kato S, Ishii H. Bax interacts with the voltage-dependent anion channel and mediates ethanol-induced apoptosis in rat hepatocytes. Am J Physiol Gastrointest Liver Physiol. 2004 Sep;287(3):G695-705. doi: 10.1152/ajpgi.00415.2003. Epub 2004 Mar 25. PMID: 15044178.
3. Al Ageeli E. Alterations of Mitochondria and Related Metabolic Pathways in Leukemia: A Narrative Review. Saudi J Med Med Sci. 2020 Jan-Apr;8(1):3-11. doi: 10.4103/sjmms.sjmms_112_18. Epub 2019 Dec 23. PMID: 31929772; PMCID: PMC6945320.
4. Al-Aamri HM, Ku H, Irving HR, Tucci J, Meehan-Andrews T, Bradley C. Time dependent response of daunorubicin on cytotoxicity, cell cycle and DNA repair in acute lymphoblastic leukaemia. BMC Cancer. 2019 Feb 27;19(1):179. doi: 10.1186/s12885-019-5377-y. PMID: 30813936; PMCID: PMC6391779.
5. Almeida A, Almeida J, Bolaños JP, Moncada S. Different responses of astrocytes and neurons to nitric oxide: the role of glycolytically generated ATP in astrocyte protection. Proc Natl Acad Sci U S A. 2001 Dec 18;98(26):15294-9. doi: 10.1073/pnas.261560998. Epub 2001 Dec 11. PMID: 11742096; PMCID: PMC65023.
6. Amelio I, Cutruzzolá F, Antonov A, Agostini M, Melino G. Serine and glycine metabolism in cancer. Trends Biochem Sci. 2014 Apr;39(4):191-8. doi: 10.1016/j.tibs.2014.02.004. Epub 2014 Mar 20. PMID: 24657017; PMCID: PMC3989988.
7. Amgalan D, Garner TP, Pekson R, Jia XF, Yanamandala M, Paulino V, Liang FG, Corbalan JJ, Lee J, Chen Y, Karagiannis GS, Sanchez LR, Liang H, Narayanagari SR, Mitchell K, Lopez A, Margulets V, Scarlata M, Santulli G, Asnani A, Peterson RT, Hazan RB, Condeelis JS, Oktay MH, Steidl U, Kirshenbaum LA, Gavathiotis E, Kitsis RN. A small-molecule allosteric inhibitor of BAX protects against doxorubicin-induced cardiomyopathy. Nat Cancer. 2020 Mar;1(3):315-328. doi: 10.1038/s43018-020-0039-1. Epub 2020 Mar 2. PMID: 32776015; PMCID: PMC7413180.
8. Appaix F, Guerrero K, Rampal D, Izikki M, Kaambre T, Sikk P, Brdiczka D, Riva-Lavieille C, Olivares J, Longuet M, Antonsson B, Saks VA. Bax and heart mitochondria: uncoupling and inhibition of respiration without permeability transition. Biochim Biophys Acta. 2002 Dec 2;1556(2-3):155-67. doi: 10.1016/s0005-2728(02)00358-4. PMID: 12460673.
9. Appleby RD, Porteous WK, Hughes G, James AM, Shannon D, Wei YH, Murphy MP. Quantitation and origin of the mitochondrial membrane potential in human cells lacking mitochondrial DNA. Eur J Biochem. 1999 May;262(1):108-16. doi: 10.1046/j.1432-1327.1999.00350.x. PMID: 10231371.
10. Arnold S, Kadenbach B. Cell respiration is controlled by ATP, an allosteric inhibitor of cytochrome-c oxidase. Eur J Biochem. 1997 Oct 1;249(1):350-4. doi: 10.1111/j.1432-1033.1997.t01-1-00350.x. PMID: 9363790.
11. Arnold S, Kadenbach B. The intramitochondrial ATP/ADP-ratio controls cytochrome c oxidase activity allosterically. FEBS Lett. 1999 Jan 25;443(2):105-8. doi: 10.1016/s0014-5793(98)01694-9. PMID: 9989584.
12. Baker F, Polat IH, Abou-El-Ardat K, Alshamleh I, Thoelken M, Hymon D, Gubas A, Koschade SE, Vischedyk JB, Kaulich M, Schwalbe H, Shaid S, Brandts CH. Metabolic Rewiring Is Essential for AML Cell Survival to Overcome Autophagy Inhibition by Loss of

ATG3. Cancers (Basel). 2021 Dec 6;13(23):6142. doi: 10.3390/cancers13236142. PMID: 34885250; PMCID: PMC8657081.
13. Basak NP, Banerjee S. Mitochondrial dependency in progression of acute myeloid leukemia. Mitochondrion. 2015 Mar;21:41-8. doi: 10.1016/j.mito.2015.01.006. Epub 2015 Jan 29. PMID: 25640960.
14. Bason JV, Montgomery MG, Leslie AG, Walker JE. Pathway of binding of the intrinsically disordered mitochondrial inhibitor protein to F1-ATPase. Proc Natl Acad Sci U S A. 2014 Aug 5;111(31):11305-10. doi: 10.1073/pnas.1411560111. Epub 2014 Jul 21. PMID: 25049402; PMCID: PMC4128166.
15. Belzacq AS, Vieira HL, Verrier F, Vandecasteele G, Cohen I, Prévost MC, Larquet E, Pariselli F, Petit PX, Kahn A, Rizzuto R, Brenner C, Kroemer G. Bcl-2 and Bax modulate adenine nucleotide translocase activity. Cancer Res. 2003 Jan 15;63(2):541-6. PMID: 12543814.
16. Bender E, Kadenbach B. The allosteric ATP-inhibition of cytochrome c oxidase activity is reversibly switched on by cAMP-dependent phosphorylation. FEBS Lett. 2000 Jan 21;466(1):130-4. doi: 10.1016/s0014-5793(99)01773-1. PMID: 10648827.
17. Bernardi P, Gerle C, Halestrap AP, Jonas EA, Karch J, Mnatsakanyan N, Pavlov E, Sheu SS, Soukas AA. Identity, structure, and function of the mitochondrial permeability transition pore: controversies, consensus, recent advances, and future directions. Cell Death Differ. 2023 Aug;30(8):1869-1885. doi: 10.1038/s41418-023-01187-0. Epub 2023 Jul 17. PMID: 37460667; PMCID: PMC10406888.
18. Bollaert E, Claus M, Vandewalle V, Lenglez S, Essaghir A, Demoulin JB, Havelange V. MiR-15a-5p Confers Chemoresistance in Acute Myeloid Leukemia by Inhibiting Autophagy Induced by Daunorubicin. Int J Mol Sci. 2021 May 13;22(10):5153. doi: 10.3390/ijms22105153. PMID: 34068078; PMCID: PMC8152749.
19. Bosc C, Saland E, Bousard A, Gadaud N, Sabatier M, Cognet G, Farge T, Boet E, Gotanègre M, Aroua N, Mouchel PL, Polley N, Larrue C, Kaphan E, Picard M, Sahal A, Jarrou L, Tosolini M, Rambow F, Cabon F, Nicot N, Poillet-Perez L, Wang Y, Su X, Fovez Q, Kluza J, Argüello RJ, Mazzotti C, Avet-Loiseau H, Vergez F, Tamburini J, Fournié JJ, Tiong IS, Wei AH, Kaoma T, Marine JC, Récher C, Stuani L, Joffre C, Sarry JE. Mitochondrial inhibitors circumvent adaptive resistance to venetoclax and cytarabine combination therapy in acute myeloid leukemia. Nat Cancer. 2021 Nov;2(11):1204-1223. doi: 10.1038/s43018-021-00264-y. Epub 2021 Nov 11. PMID: 35122057.
20. Bouligny IM, Maher KR, Grant S. Augmenting Venetoclax Activity Through Signal Transduction in AML. J Cell Signal. 2023;4(1):1-12. doi: 10.33696/signaling.4.085. PMID: 36911757; PMCID: PMC9997087.
21. Boykov IN, Montgomery MM, Hagen JT, Aruleba RT, McLaughlin KL, Coalson HS, Nelson MA, Pereyra AS, Ellis JM, Zeczycki TN, Vohra NA, Tan SF, Cabot MC, Fisher-Wellman KH. Pan-tissue mitochondrial phenotyping reveals lower OXPHOS expression and function across cancer types. Sci Rep. 2023 Oct 5;13(1):16742. doi: 10.1038/s41598-023-43963-5. PMID: 37798427; PMCID: PMC10556099.
22. Buchet K, Godinot C. Functional F1-ATPase essential in maintaining growth and membrane potential of human mitochondrial DNA-depleted rho degrees cells. J Biol Chem. 1998 Sep 4;273(36):22983-9. doi: 10.1074/jbc.273.36.22983. PMID: 9722521.
23. Buettner R, Nguyen LXT, Morales C, Chen MH, Wu X, Chen LS, Hoang DH, Hernandez Vargas S, Pullarkat V, Gandhi V, Marcucci G, Rosen ST. Targeting the metabolic vulnerability of acute myeloid leukemia blasts with a combination of venetoclax and 8-chloro-adenosine. J Hematol Oncol. 2021 Apr 26;14(1):70. doi: 10.1186/s13045-021-01076-4. PMID: 33902674; PMCID: PMC8074444.

24. Bui D, Ravasz D, Chinopoulos C. The Effect of 2-Ketobutyrate on Mitochondrial Substrate-Level Phosphorylation. Neurochem Res. 2019 Oct;44(10):2301-2306. doi: 10.1007/s11064-019-02759-8. Epub 2019 Feb 27. PMID: 30810978; PMCID: PMC6776489.
25. Capeloa T, Krzystyniak J, d'Hose D, Canas Rodriguez A, Payen VL, Zampieri LX, Van de Velde JA, Benyahia Z, Pranzini E, Vazeille T, Fransolet M, Bouzin C, Brusa D, Michiels C, Gallez B, Murphy MP, Porporato PE, Sonveaux P. MitoQ Inhibits Human Breast Cancer Cell Migration, Invasion and Clonogenicity. Cancers (Basel). 2022 Mar 16;14(6):1516. doi: 10.3390/cancers14061516. PMID: 35326667; PMCID: PMC8946220.
26. Castro I, Sampaio-Marques B, Ludovico P. Targeting Metabolic Reprogramming in Acute Myeloid Leukemia. Cells. 2019 Aug 24;8(9):967. doi: 10.3390/cells8090967. PMID: 31450562; PMCID: PMC6770240.
27. Chen Q, Kirk K, Shurubor YI, Zhao D, Arreguin AJ, Shahi I, Valsecchi F, Primiano G, Calder EL, Carelli V, Denton TT, Beal MF, Gross SS, Manfredi G, D'Aurelio M. Rewiring of Glutamine Metabolism Is a Bioenergetic Adaptation of Human Cells with Mitochondrial DNA Mutations. Cell Metab. 2018 May 1;27(5):1007-1025.e5. doi: 10.1016/j.cmet.2018.03.002. Epub 2018 Apr 12. PMID: 29657030; PMCID: PMC5932217.
28. Chen WW, Birsoy K, Mihaylova MM, Snitkin H, Stasinski I, Yucel B, Bayraktar EC, Carette JE, Clish CB, Brummelkamp TR, Sabatini DD, Sabatini DM. Inhibition of ATPIF1 ameliorates severe mitochondrial respiratory chain dysfunction in mammalian cells. Cell Rep. 2014 Apr 10;7(1):27-34. doi: 10.1016/j.celrep.2014.02.046. Epub 2014 Mar 27. PMID: 24685140; PMCID: PMC4040975.
29. Chen ZX, Pervaiz S. Bcl-2 induces pro-oxidant state by engaging mitochondrial respiration in tumor cells. Cell Death Differ. 2007 Sep;14(9):1617-27. doi: 10.1038/sj.cdd.4402165. Epub 2007 May 18. Erratum in: Cell Death Differ. 2012 Mar;19(3):551. PMID: 17510660.
30. Chinopoulos C, Gerencser AA, Mandi M, Mathe K, Töröcsik B, Doczi J, Turiak L, Kiss G, Konràd C, Vajda S, Vereczki V, Oh RJ, Adam-Vizi V. Forward operation of adenine nucleotide translocase during F0F1-ATPase reversal: critical role of matrix substrate-level phosphorylation. FASEB J. 2010 Jul;24(7):2405-16. doi: 10.1096/fj.09-149898. Epub 2010 Mar 5. PMID: 20207940; PMCID: PMC2887268.
31. Cho ES, Cha YH, Kim HS, Kim NH, Yook JI. The Pentose Phosphate Pathway as a Potential Target for Cancer Therapy. Biomol Ther (Seoul). 2018 Jan 1;26(1):29-38. doi: 10.4062/biomolther.2017.179. PMID: 29212304; PMCID: PMC5746035.
32. Chong SJF, Iskandar K, Lai JXH, Qu J, Raman D, Valentin R, Herbaux C, Collins M, Low ICC, Loh T, Davids M, Pervaiz S. Serine-70 phosphorylated Bcl-2 prevents oxidative stress-induced DNA damage by modulating the mitochondrial redox metabolism. Nucleic Acids Res. 2020 Dec 16;48(22):12727-12745. doi: 10.1093/nar/gkaa1110. PMID: 33245769; PMCID: PMC7736805.
33. de Beauchamp L, Himonas E, Helgason GV. Mitochondrial metabolism as a potential therapeutic target in myeloid leukaemia. Leukemia. 2022 Jan;36(1):1-12. doi: 10.1038/s41375-021-01416-w. Epub 2021 Sep 24. PMID: 34561557; PMCID: PMC8727299.
34. de Queiroz RM, Oliveira IA, Piva B, Bouchuid Catão F, da Costa Rodrigues B, da Costa Pascoal A, Diaz BL, Todeschini AR, Caarls MB, Dias WB. Hexosamine Biosynthetic Pathway and Glycosylation Regulate Cell Migration in Melanoma Cells. Front Oncol. 2019 Mar 5;9:116. doi: 10.3389/fonc.2019.00116. PMID: 30891426; PMCID: PMC6411693.
35. Derissen EJ, Beijnen JH, Schellens JH. Concise drug review: azacitidine and decitabine. Oncologist. 2013;18(5):619-24. doi: 10.1634/theoncologist.2012-0465. Epub 2013 May 13. PMID: 23671007; PMCID: PMC3662854.
36. DiNardo CD, Tiong IS, Quaglieri A, MacRaild S, Loghavi S, Brown FC, Thijssen R, Pomilio G, Ivey A, Salmon JM, Glytsou C, Fleming SA, Zhang Q, Ma H, Patel KP, Kornblau SM, Xu Z, Chua CC, Chen X, Blombery P, Flensburg C, Cummings N, Aifantis I, Kantarjian H,

Huang DCS, Roberts AW, Majewski IJ, Konopleva M, Wei AH. Molecular patterns of response and treatment failure after frontline venetoclax combinations in older patients with AML. Blood. 2020 Mar 12;135(11):791-803. doi: 10.1182/blood.2019003988. PMID: 31932844; PMCID: PMC7068032.
37. Döhner, H. et al. Diagnosis and management of AML in adults: 2017 ELN recommendations from an international expert panel. Blood 129, 424–447 (2017).
38. Döhner, H. et al. Diagnosis and management of AML in adults: 2022 recommendations from an international expert panel on behalf of the ELN. Blood 140, 1345–1377 (2022).
39. Dong Y, Zhao X, Feng X, Zhou Y, Yan X, Zhang Y, Bu J, Zhan D, Hayashi Y, Zhang Y, Xu Z, Huang R, Wang J, Zhao T, Xiao Z, Ju Z, Andreassen PR, Wang QF, Chen W, Huang G. SETD2 mutations confer chemoresistance in acute myeloid leukemia partly through altered cell cycle checkpoints. Leukemia. 2019 Nov;33(11):2585-2598. doi: 10.1038/s41375-019-0456-2. Epub 2019 Apr 9. PMID: 30967619; PMCID: PMC6785365.
40. Dugan J, Pollyea D. Enasidenib for the treatment of acute myeloid leukemia. Expert Rev Clin Pharmacol. 2018 Aug;11(8):755-760. doi: 10.1080/17512433.2018.1477585. Epub 2018 Jul 24. PMID: 29770715.
41. Farge T, Saland E, de Toni F, Aroua N, Hosseini M, Perry R, Bosc C, Sugita M, Stuani L, Fraisse M, Scotland S, Larrue C, Boutzen H, Féliu V, Nicolau-Travers ML, Cassant-Sourdy S, Broin N, David M, Serhan N, Sarry A, Tavitian S, Kaoma T, Vallar L, Iacovoni J, Linares LK, Montersino C, Castellano R, Griessinger E, Collette Y, Duchamp O, Barreira Y, Hirsch P, Palama T, Gales L, Delhommeau F, Garmy-Susini BH, Portais JC, Vergez F, Selak M, Danet-Desnoyers G, Carroll M, Récher C, Sarry JE. Chemotherapy-Resistant Human Acute Myeloid Leukemia Cells Are Not Enriched for Leukemic Stem Cells but Require Oxidative Metabolism. Cancer Discov. 2017 Jul;7(7):716-735. doi: 10.1158/2159-8290.CD-16-0441. Epub 2017 Apr 17. PMID: 28416471; PMCID: PMC5501738.
42. Fendt SM, Bell EL, Keibler MA, Olenchock BA, Mayers JR, Wasylenko TM, Vokes NI, Guarente L, Vander Heiden MG, Stephanopoulos G. Reductive glutamine metabolism is a function of the α-ketoglutarate to citrate ratio in cells. Nat Commun. 2013;4:2236. doi: 10.1038/ncomms3236. PMID: 23900562; PMCID: PMC3934748.
43. Feng L, Zhang PY, Gao W, Yu J, Robson SC. Targeting chemoresistance and mitochondria-dependent metabolic reprogramming in acute myeloid leukemia. Front Oncol. 2023 Sep 7;13:1244280. doi: 10.3389/fonc.2023.1244280. PMID: 37746249; PMCID: PMC10513429.
44. Fisher-Wellman KH, Davidson MT, Narowski TM, Lin CT, Koves TR, Muoio DM. Mitochondrial Diagnostics: A Multiplexed Assay Platform for Comprehensive Assessment of Mitochondrial Energy Fluxes. Cell Rep. 2018 Sep 25;24(13):3593-3606.e10. doi: 10.1016/j.celrep.2018.08.091. PMID: 30257218; PMCID: PMC6237617.
45. Fisher-Wellman KH, Hagen JT, Kassai M, Kao LP, Nelson MAM, McLaughlin KL, Coalson HS, Fox TE, Tan SF, Feith DJ, Kester M, Loughran TP Jr, Claxton DF, Cabot MC. Alterations in sphingolipid composition and mitochondrial bioenergetics represent synergistic therapeutic vulnerabilities linked to multidrug resistance in leukemia. FASEB J. 2022 Jan;36(1):e22094. doi: 10.1096/fj.202101194RRR. PMID: 34888943; PMCID: PMC9058980.
46. Gallipoli P, Giotopoulos G, Tzelepis K, Costa ASH, Vohra S, Medina-Perez P, Basheer F, Marando L, Di Lisio L, Dias JML, Yun H, Sasca D, Horton SJ, Vassiliou G, Frezza C, Huntly BJP. Glutaminolysis is a metabolic dependency in FLT3ITD acute myeloid leukemia unmasked by FLT3 tyrosine kinase inhibition. Blood. 2018 Apr 12;131(15):1639-1653. doi: 10.1182/blood-2017-12-820035. Epub 2018 Feb 20. PMID: 29463564; PMCID: PMC6061932.
47. García-Aguilar A, Cuezva JM. A Review of the Inhibition of the Mitochondrial ATP Synthase by IF1 *in vivo*: Reprogramming Energy Metabolism and Inducing Mitohormesis. Front

Physiol. 2018 Sep 19;9:1322. doi: 10.3389/fphys.2018.01322. PMID: 30283362; PMCID: PMC6156145.
48. Gottlieb E, Armour SM, Harris MH, Thompson CB. Mitochondrial membrane potential regulates matrix configuration and cytochrome c release during apoptosis. Cell Death Differ. 2003 Jun;10(6):709-17. doi: 10.1038/sj.cdd.4401231. PMID: 12761579.
49. Gregory MA, Nemkov T, Park HJ, Zaberezhnyy V, Gehrke S, Adane B, Jordan CT, Hansen KC, D'Alessandro A, DeGregori J. Targeting Glutamine Metabolism and Redox State for Leukemia Therapy. Clin Cancer Res. 2019 Jul 1;25(13):4079-4090. doi: 10.1158/1078-0432.CCR-18-3223. Epub 2019 Apr 2. PMID: 30940653; PMCID: PMC6642698.
50. Grove CS, Vassiliou GS. Acute myeloid leukaemia: a paradigm for the clonal evolution of cancer? Dis Model Mech. 2014 Aug;7(8):941-51. doi: 10.1242/dmm.015974. PMID: 25056697; PMCID: PMC4107323.
51. Harris MH, Vander Heiden MG, Kron SJ, Thompson CB. Role of oxidative phosphorylation in Bax toxicity. Mol Cell Biol. 2000 May;20(10):3590-6. doi: 10.1128/MCB.20.10.3590-3596.2000. PMID: 10779348; PMCID: PMC85651.
52. Hashiguchi K, Zhang-Akiyama QM. Establishment of human cell lines lacking mitochondrial DNA. Methods Mol Biol. 2009;554:383-91. doi: 10.1007/978-1-59745-521-3_23. PMID: 19513686.
53. Heimlich G, McKinnon AD, Bernardo K, Brdiczka D, Reed JC, Kain R, Krönke M, Jürgensmeier JM. Bax-induced cytochrome c release from mitochondria depends on alpha-helices-5 and -6. Biochem J. 2004 Feb 15;378(Pt 1):247-55. doi: 10.1042/BJ20031152. PMID: 14614769; PMCID: PMC1223939.
54. Henkenius K, Greene BH, Barckhausen C, Hartmann R, Märken M, Kaiser T, Rehberger M, Metzelder SK, Parak WJ, Neubauer A, Brendel C, Mack E. Maintenance of cellular respiration indicates drug resistance in acute myeloid leukemia. Leuk Res. 2017 Nov;62:56-63. doi: 10.1016/j.leukres.2017.09.021. Epub 2017 Sep 28. PMID: 28985623.
55. Herst PM, Howman RA, Neeson PJ, Berridge MV, Ritchie DS. The level of glycolytic metabolism in acute myeloid leukemia blasts at diagnosis is prognostic for clinical outcome. J Leukoc Biol. 2011 Jan;89(1):51-5. doi: 10.1189/jlb.0710417. Epub 2010 Oct 19. PMID: 20959411.
56. Iacobini M, Menichelli A, Palumbo G, Multari G, Werner B, Del Principe D. Involvement of oxygen radicals in cytarabine-induced apoptosis in human polymorphonuclear cells. Biochem Pharmacol. 2001 Apr 15;61(8):1033-40. doi: 10.1016/s0006-2952(01)00548-2. PMID: 11286995.
57. Israelsen WJ, Vander Heiden MG. Pyruvate kinase: Function, regulation and role in cancer. Semin Cell Dev Biol. 2015 Jul;43:43-51. doi: 10.1016/j.semcdb.2015.08.004. Epub 2015 Aug 13. PMID: 26277545; PMCID: PMC4662905.
58. Jacque N, Ronchetti AM, Larrue C, Meunier G, Birsen R, Willems L, Saland E, Decroocq J, Maciel TT, Lambert M, Poulain L, Hospital MA, Sujobert P, Joseph L, Chapuis N, Lacombe C, Moura IC, Demo S, Sarry JE, Recher C, Mayeux P, Tamburini J, Bouscary D. Targeting glutaminolysis has antileukemic activity in acute myeloid leukemia and synergizes with BCL-2 inhibition. Blood. 2015 Sep 10;126(11):1346-56. doi: 10.1182/blood-2015-01-621870. Epub 2015 Jul 17. PMID: 26186940; PMCID: PMC4608389.
59. Jangaard NO, Unkeless J, Atkinson DE. The inhibition of citrate synthase by adenosine triphosphate. Biochim Biophys Acta. 1968 Jan 8;151(1):225-35. doi: 10.1016/0005-2744(68)90177-0. PMID: 4867623.
60. Jennings RB, Reimer KA, Steenbergen C. Effect of inhibition of the mitochondrial ATPase on net myocardial ATP in total ischemia. J Mol Cell Cardiol. 1991 Dec;23(12):1383-95. doi: 10.1016/0022-2828(91)90185-o. PMID: 1839801.

61. Jonckheere AI, Smeitink JA, Rodenburg RJ. Mitochondrial ATP synthase: architecture, function and pathology. J Inherit Metab Dis. 2012 Mar;35(2):211-25. doi: 10.1007/s10545-011-9382-9. Epub 2011 Aug 27. PMID: 21874297; PMCID: PMC3278611.
62. Kadenbach B. Complex IV - The regulatory center of mitochondrial oxidative phosphorylation. Mitochondrion. 2021 May;58:296-302. doi: 10.1016/j.mito.2020.10.004. Epub 2020 Oct 15. PMID: 33069909.
63. Kapoor I, Bodo J, Hill BT, Hsi ED, Almasan A. Targeting BCL-2 in B-cell malignancies and overcoming therapeutic resistance. Cell Death Dis. 2020 Nov 2;11(11):941. doi: 10.1038/s41419-020-03144-y. PMID: 33139702; PMCID: PMC7608616.
64. Karch J, Kwong JQ, Burr AR, Sargent MA, Elrod JW, Peixoto PM, Martinez-Caballero S, Osinska H, Cheng EH, Robbins J, Kinnally KW, Molkentin JD. Bax and Bak function as the outer membrane component of the mitochondrial permeability pore in regulating necrotic cell death in mice. Elife. 2013 Aug 27;2:e00772. doi: 10.7554/eLife.00772. PMID: 23991283; PMCID: PMC3755340.
65. Khan AUH, Rathore MG, Allende-Vega N, Vo DN, Belkhala S, Orecchioni S, Talarico G, Bertolini F, Cartron G, Lecellier CH, Villalba M. Human Leukemic Cells performing Oxidative Phosphorylation (OXPHOS) Generate an Antioxidant Response Independently of Reactive Oxygen species (ROS) Production. EBioMedicine. 2015 Nov 26;3:43-53. doi: 10.1016/j.ebiom.2015.11.045. PMID: 26870816; PMCID: PMC4739420.
66. Kobayashi R, Ueno H, Okazaki KI, Noji H. Molecular mechanism on forcible ejection of ATPase inhibitory factor 1 from mitochondrial ATP synthase. Nat Commun. 2023 Mar 31;14(1):1682. doi: 10.1038/s41467-023-37182-9. PMID: 37002198; PMCID: PMC10066207.
67. Kreitz J, Schönfeld C, Seibert M, Stolp V, Alshamleh I, Oellerich T, Steffen B, Schwalbe H, Schnütgen F, Kurrle N, Serve H. Metabolic Plasticity of Acute Myeloid Leukemia. Cells. 2019 Jul 31;8(8):805. doi: 10.3390/cells8080805. PMID: 31370337; PMCID: PMC6721808.
68. Kroemer G, Reed JC. Mitochondrial control of cell death. Nat Med. 2000 May;6(5):513-9. doi: 10.1038/74994. PMID: 10802706.
69. Lagadinou ED, Sach A, Callahan K, Rossi RM, Neering SJ, Minhajuddin M, Ashton JM, Pei S, Grose V, O'Dwyer KM, Liesveld JL, Brookes PS, Becker MW, Jordan CT. BCL-2 inhibition targets oxidative phosphorylation and selectively eradicates quiescent human leukemia stem cells. Cell Stem Cell. 2013 Mar 7;12(3):329-41. doi: 10.1016/j.stem.2012.12.013. Epub 2013 Jan 17. PMID: 23333149; PMCID: PMC3595363.
70. Lapa B, Gonçalves AC, Jorge J, Alves R, Pires AS, Abrantes AM, Coucelo M, Abrunhosa A, Botelho MF, Nascimento-Costa JM, Sarmento-Ribeiro AB. Acute myeloid leukemia sensitivity to metabolic inhibitors: glycolysis showed to be a better therapeutic target. Med Oncol. 2020 Jul 28;37(8):72. doi: 10.1007/s12032-020-01394-6. PMID: 32725458.
71. Larrue C, Saland E, Vergez F, Serhan N, Delabesse E, Mansat-De Mas V, Hospital MA, Tamburini J, Manenti S, Sarry JE, Récher C. Antileukemic Activity of 2-Deoxy-d-Glucose through Inhibition of N-Linked Glycosylation in Acute Myeloid Leukemia with FLT3-ITD or c-KIT Mutations. Mol Cancer Ther. 2015 Oct;14(10):2364-73. doi: 10.1158/1535-7163.MCT-15-0163. Epub 2015 Jul 23. PMID: 26206337.
72. Lemasters JJ. Metabolic implications of non-electrogenic ATP/ADP exchange in cancer cells: A mechanistic basis for the Warburg effect. Biochim Biophys Acta Bioenerg. 2021 Jul 1;1862(7):148410. doi: 10.1016/j.bbabio.2021.148410. Epub 2021 Mar 13. PMID: 33722515; PMCID: PMC8096716.
73. Leytin V, Allen DJ, Mutlu A, Gyulkhandanyan AV, Mykhaylov S, Freedman J. Mitochondrial control of platelet apoptosis: effect of cyclosporin A, an inhibitor of the mitochondrial permeability transition pore. Lab Invest. 2009 Apr;89(4):374-84. doi: 10.1038/labinvest.2009.13. Epub 2009 Feb 23. PMID: 19238135.

74. Liu F, Kalpage HA, Wang D, Edwards H, Hüttemann M, Ma J, Su Y, Carter J, Li X, Polin L, Kushner J, Dzinic SH, White K, Wang G, Taub JW, Ge Y. Cotargeting of Mitochondrial Complex I and Bcl-2 Shows Antileukemic Activity against Acute Myeloid Leukemia Cells Reliant on Oxidative Phosphorylation. Cancers (Basel). 2020 Aug 24;12(9):2400. doi: 10.3390/cancers12092400. PMID: 32847115; PMCID: PMC7564145.
75. Liu J, Chen Y, Yu L, Yang L. Mechanisms of venetoclax resistance and solutions. Front Oncol. 2022 Oct 12;12:1005659. doi: 10.3389/fonc.2022.1005659. PMID: 36313732; PMCID: PMC9597307.
76. Liu L, Patnana PK, Xie X, Frank D, Nimmagadda SC, Rosemann A, Liebmann M, Klotz L, Opalka B, Khandanpour C. High Metabolic Dependence on Oxidative Phosphorylation Drives Sensitivity to Metformin Treatment in *MLL/AF9* Acute Myeloid Leukemia. Cancers (Basel). 2022 Jan 19;14(3):486. doi: 10.3390/cancers14030486. PMID: 35158754; PMCID: PMC8833593.
77. Ma J, Liu B, Yu D, Zuo Y, Cai R, Yang J, Cheng J. SIRT3 deacetylase activity confers chemoresistance in AML via regulation of mitochondrial oxidative phosphorylation. Br J Haematol. 2019 Oct;187(1):49-64. doi: 10.1111/bjh.16044. Epub 2019 Jun 24. Erratum in: Br J Haematol. 2020 Feb;188(4):586. PMID: 31236919; PMCID: PMC6790595.
78. Ma Z, Ye W, Wang J, Huang X, Huang J, Li X, Hu C, Li C, Zhou Y, Lin X, Wei W, Qian Y, Zhou Y, Mao S, Yin X, Zhu B, Jin J. Glutamate dehydrogenase 1: A novel metabolic target in inhibiting acute myeloid leukaemia progression. Br J Haematol. 2023 Aug;202(3):566-577. doi: 10.1111/bjh.18884. Epub 2023 May 25. PMID: 37231991.
79. Maldonado EN, Lemasters JJ. ATP/ADP ratio, the missed connection between mitochondria and the Warburg effect. Mitochondrion. 2014 Nov;19 Pt A:78-84. doi: 10.1016/j.mito.2014.09.002. Epub 2014 Sep 16. PMID: 25229666; PMCID: PMC4254332.
80. Marchetti P, Castedo M, Susin SA, Zamzami N, Hirsch T, Macho A, Haeffner A, Hirsch F, Geuskens M, Kroemer G. Mitochondrial permeability transition is a central coordinating event of apoptosis. J Exp Med. 1996 Sep 1;184(3):1155-60. doi: 10.1084/jem.184.3.1155. PMID: 9064332; PMCID: PMC2192776.
81. Matre P, Velez J, Jacamo R, Qi Y, Su X, Cai T, Chan SM, Lodi A, Sweeney SR, Ma H, Davis RE, Baran N, Haferlach T, Su X, Flores ER, Gonzalez D, Konoplev S, Samudio I, DiNardo C, Majeti R, Schimmer AD, Li W, Wang T, Tiziani S, Konopleva M. Inhibiting glutaminase in acute myeloid leukemia: metabolic dependency of selected AML subtypes. Oncotarget. 2016 Nov 29;7(48):79722-79735. doi: 10.18632/oncotarget.12944. PMID: 27806325; PMCID: PMC5340236.
82. Memme JM, Erlich AT, Phukan G, Hood DA. Exercise and mitochondrial health. J Physiol. 2021 Feb;599(3):803-817. doi: 10.1113/JP278853. Epub 2019 Dec 9. PMID: 31674658.
83. Merchant SL, Culos K, Wyatt H. Ivosidenib: IDH1 Inhibitor for the Treatment of Acute Myeloid Leukemia. J Adv Pract Oncol. 2019 Jul;10(5):494-500. doi: 10.6004/jadpro.2019.10.5.7. Epub 2019 Jul 1. PMID: 33457062; PMCID: PMC7779565.
84. Mesbahi Y, Trahair TN, Lock RB, Connerty P. Exploring the Metabolic Landscape of AML: From Haematopoietic Stem Cells to Myeloblasts and Leukaemic Stem Cells. Front Oncol. 2022 Feb 10;12:807266. doi: 10.3389/fonc.2022.807266. PMID: 35223487; PMCID: PMC8867093.
85. Metelkin E, Goryanin I, Demin O. Mathematical modeling of mitochondrial adenine nucleotide translocase. Biophys J. 2006 Jan 15;90(2):423-32. doi: 10.1529/biophysj.105.061986. Epub 2005 Oct 20. PMID: 16239329; PMCID: PMC1367049.
86. Mishra SK, Millman SE, Zhang L. Metabolism in acute myeloid leukemia: mechanistic insights and therapeutic targets. Blood. 2023 Mar 9;141(10):1119-1135. doi: 10.1182/blood.2022018092. PMID: 36548959; PMCID: PMC10375271.

87. MITCHELL P. Coupling of phosphorylation to electron and hydrogen transfer by a chemi-osmotic type of mechanism. Nature. 1961 Jul 8;191:144-8. doi: 10.1038/191144a0. PMID: 13771349.
88. Mootha VK, Wei MC, Buttle KF, Scorrano L, Panoutsakopoulou V, Mannella CA, Korsmeyer SJ. A reversible component of mitochondrial respiratory dysfunction in apoptosis can be rescued by exogenous cytochrome c. EMBO J. 2001 Feb 15;20(4):661-71. doi: 10.1093/emboj/20.4.661. PMID: 11179211; PMCID: PMC145422.
89. Morgenstern M, Peikert CD, Lübbert P, Suppanz I, Klemm C, Alka O, Steiert C, Naumenko N, Schendzielorz A, Melchionda L, Mühlhäuser WWD, Knapp B, Busch JD, Stiller SB, Dannenmaier S, Lindau C, Licheva M, Eickhorst C, Galbusera R, Zerbes RM, Ryan MT, Kraft C, Kozjak-Pavlovic V, Drepper F, Dennerlein S, Oeljeklaus S, Pfanner N, Wiedemann N, Warscheid B. Quantitative high-confidence human mitochondrial proteome and its dynamics in cellular context. Cell Metab. 2021 Dec 7;33(12):2464-2483.e18. doi: 10.1016/j.cmet.2021.11.001. Epub 2021 Nov 19. PMID: 34800366; PMCID: PMC8664129.
90. Moujalled DM, Brown FC, Chua CC, Dengler MA, Pomilio G, Anstee NS, Litalien V, Thompson E, Morley T, MacRaild S, Tiong IS, Morris R, Dun K, Zordan A, Shah J, Banquet S, Halilovic E, Morris E, Herold MJ, Lessene G, Adams JM, Huang DCS, Roberts AW, Blombery P, Wei AH. Acquired mutations in BAX confer resistance to BH3-mimetic therapy in acute myeloid leukemia. Blood. 2023 Feb 9;141(6):634-644. doi: 10.1182/blood.2022016090. Erratum in: Blood. 2023 Aug 3;142(5):494. PMID: 36219880.
91. Mullen AR, Wheaton WW, Jin ES, Chen PH, Sullivan LB, Cheng T, Yang Y, Linehan WM, Chandel NS, DeBerardinis RJ. Reductive carboxylation supports growth in tumour cells with defective mitochondria. Nature. 2011 Nov 20;481(7381):385-8. doi: 10.1038/nature10642. PMID: 22101431; PMCID: PMC3262117.
92. Nelson MA, McLaughlin KL, Hagen JT, Coalson HS, Schmidt C, Kassai M, Kew KA, McClung JM, Neufer PD, Brophy P, Vohra NA, Liles D, Cabot MC, Fisher-Wellman KH. Intrinsic OXPHOS limitations underlie cellular bioenergetics in leukemia. Elife. 2021 Jun 16;10:e63104. doi: 10.7554/eLife.63104. PMID: 34132194; PMCID: PMC8221809.
93. Okuno D, Iino R, Noji H. Rotation and structure of FoF1-ATP synthase. J Biochem. 2011 Jun;149(6):655-64. doi: 10.1093/jb/mvr049. Epub 2011 Apr 26. PMID: 21524994.
94. Ong YL, McMullin MF, Bailie KE, Lappin TR, Jones FG, Irvine AE. High bax expression is a good prognostic indicator in acute myeloid leukaemia. Br J Haematol. 2000 Oct;111(1):182-9. doi: 10.1046/j.1365-2141.2000.02315.x. PMID: 11091199.
95. Ostergaard E. Disorders caused by deficiency of succinate-CoA ligase. J Inherit Metab Dis. 2008 Apr;31(2):226-9. doi: 10.1007/s10545-008-0828-7. Epub 2008 Apr 4. PMID: 18392745.
96. Panina SB, Baran N, Brasil da Costa FH, Konopleva M, Kirienko NV. A mechanism for increased sensitivity of acute myeloid leukemia to mitotoxic drugs. Cell Death Dis. 2019 Aug 13;10(8):617. doi: 10.1038/s41419-019-1851-3. PMID: 31409768; PMCID: PMC6692368.
97. Pavlova NN, Thompson CB. The Emerging Hallmarks of Cancer Metabolism. Cell Metab. 2016 Jan 12;23(1):27-47. doi: 10.1016/j.cmet.2015.12.006. PMID: 26771115; PMCID: PMC4715268.
98. Peña-Blanco A, García-Sáez AJ. Bax, Bak and beyond - mitochondrial performance in apoptosis. FEBS J. 2018 Feb;285(3):416-431. doi: 10.1111/febs.14186. Epub 2017 Sep 4. PMID: 28755482.
99. Penner PE, Cohen LH. Effects of adenosine triphosphate and magnesium ions on the fumarase reaction. J Biol Chem. 1969 Feb 10;244(3):1070-5. PMID: 4976787.
100. Poulain L, Sujobert P, Zylbersztejn F, Barreau S, Stuani L, Lambert M, Palama TL, Chesnais V, Birsen R, Vergez F, Farge T, Chenevier-Gobeaux C, Fraisse M, Bouillaud F, Debeissat C, Herault O, Récher C, Lacombe C, Fontenay M, Mayeux P, Maciel TT, Portais JC, Sarry JE, Tamburini J, Bouscary D, Chapuis N. High mTORC1 activity drives glycolysis

addiction and sensitivity to G6PD inhibition in acute myeloid leukemia cells. Leukemia. 2017 Nov;31(11):2326-2335. doi: 10.1038/leu.2017.81. Epub 2017 Mar 10. PMID: 28280275.
101. Rahmani M, Nkwocha J, Hawkins E, Pei X, Parker RE, Kmieciak M, Leverson JD, Sampath D, Ferreira-Gonzalez A, Grant S. Cotargeting BCL-2 and PI3K Induces BAX-Dependent Mitochondrial Apoptosis in AML Cells. Cancer Res. 2018 Jun 1;78(11):3075-3086. doi: 10.1158/0008-5472.CAN-17-3024. Epub 2018 Mar 20. PMID: 29559471; PMCID: PMC5984704.
102. Ramzan R, Vogt S, Kadenbach B. Stress-mediated generation of deleterious ROS in healthy individuals - role of cytochrome c oxidase. J Mol Med (Berl). 2020 May;98(5):651-657. doi: 10.1007/s00109-020-01905-y. Epub 2020 Apr 20. PMID: 32313986; PMCID: PMC7220878.
103. Rego AC, Vesce S, Nicholls DG. The mechanism of mitochondrial membrane potential retention following release of cytochrome c in apoptotic GT1-7 neural cells. Cell Death Differ. 2001 Oct;8(10):995-1003. doi: 10.1038/sj.cdd.4400916. PMID: 11598797.
104. Robak T, Wierzbowska A. Current and emerging therapies for acute myeloid leukemia. Clin Ther. 2009;31 Pt 2:2349-70. doi: 10.1016/j.clinthera.2009.11.017. PMID: 20110045.
105. Roberts AW. Therapeutic development and current uses of BCL-2 inhibition. Hematology Am Soc Hematol Educ Program. 2020 Dec 4;2020(1):1-9. doi: 10.1182/hematology.2020000154. PMID: 33275682; PMCID: PMC7727569.
106. Rojas-Pirela M, Andrade-Alviárez D, Rojas V, Kemmerling U, Cáceres AJ, Michels PA, Concepción JL, Quiñones W. Phosphoglycerate kinase: structural aspects and functions, with special emphasis on the enzyme from Kinetoplastea. Open Biol. 2020 Nov;10(11):200302. doi: 10.1098/rsob.200302. Epub 2020 Nov 25. PMID: 33234025; PMCID: PMC7729029.
107. Sasaki K, Ravandi F, Kadia TM, DiNardo CD, Short NJ, Borthakur G, Jabbour E, Kantarjian HM. De novo acute myeloid leukemia: A population-based study of outcome in the United States based on the Surveillance, Epidemiology, and End Results (SEER) database, 1980 to 2017. Cancer. 2021 Jun 15;127(12):2049-2061. doi: 10.1002/cncr.33458. Epub 2021 Apr 5. PMID: 33818756.
108. Schimmer AD. Novel Mitochondrial Mechanisms of Cytarabine Resistance in Primary AML Cells. Cancer Discov. 2017 Jul;7(7):670-672. doi: 10.1158/2159-8290.CD-17-0476. PMID: 28684410.
109. Shallis RM, Wang R, Davidoff A, Ma X, Zeidan AM. Epidemiology of acute myeloid leukemia: Recent progress and enduring challenges. Blood Rev. 2019 Jul;36:70-87. doi: 10.1016/j.blre.2019.04.005. Epub 2019 Apr 29. PMID: 31101526.
110. Sharon D, Cathelin S, Mirali S, Di Trani JM, Yanofsky DJ, Keon KA, Rubinstein JL, Schimmer AD, Ketela T, Chan SM. Inhibition of mitochondrial translation overcomes venetoclax resistance in AML through activation of the integrated stress response. Sci Transl Med. 2019 Oct 30;11(516):eaax2863. doi: 10.1126/scitranslmed.aax2863. PMID: 31666400.
111. Shimizu S, Konishi A, Kodama T, Tsujimoto Y. BH4 domain of antiapoptotic Bcl-2 family members closes voltage-dependent anion channel and inhibits apoptotic mitochondrial changes and cell death. Proc Natl Acad Sci U S A. 2000 Mar 28;97(7):3100-5. doi: 10.1073/pnas.97.7.3100. Erratum in: Proc Natl Acad Sci U S A 2000 Aug 1;97(16):9347. PMID: 10737788; PMCID: PMC16199.
112. Shimizu S, Narita M, Tsujimoto Y. Bcl-2 family proteins regulate the release of apoptogenic cytochrome c by the mitochondrial channel VDAC. Nature. 1999 Jun 3;399(6735):483-7. doi: 10.1038/20959. Erratum in: Nature 2000 Oct 12;407(6805):767. PMID: 10365962.
113. Shimizu S, Tsujimoto Y. Proapoptotic BH3-only Bcl-2 family members induce cytochrome c release, but not mitochondrial membrane potential loss, and do not directly

modulate voltage-dependent anion channel activity. Proc Natl Acad Sci U S A. 2000 Jan 18;97(2):577-82. doi: 10.1073/pnas.97.2.577. PMID: 10639121; PMCID: PMC15372.
114. Smith RJ. Glutamine metabolism and its physiologic importance. JPEN J Parenter Enteral Nutr. 1990 Jul-Aug;14(4 Suppl):40S-44S. doi: 10.1177/014860719001400402. PMID: 2205730.
115. Song A, Altabbakh O, Sallman DA, Padron E, Talati C, Hussaini MO. Acquisition of IDH2 mutations in relapsed/refractory AML is associated with worse patient outcomes. Eur J Haematol. 2021 Dec;107(6):609-616. doi: 10.1111/ejh.13698. Epub 2021 Aug 30. PMID: 34407254.
116. Song K, Li M, Xu X, Xuan LI, Huang G, Liu Q. Resistance to chemotherapy is associated with altered glucose metabolism in acute myeloid leukemia. Oncol Lett. 2016 Jul;12(1):334-342. doi: 10.3892/ol.2016.4600. Epub 2016 May 17. PMID: 27347147; PMCID: PMC4906727.
117. Song K, Li M, Xu XJ, Xuan L, Huang GN, Song XL, Liu QF. HIF-1α and GLUT1 gene expression is associated with chemoresistance of acute myeloid leukemia. Asian Pac J Cancer Prev. 2014;15(4):1823-9. doi: 10.7314/apjcp.2014.15.4.1823. PMID: 24641416.
118. Sriskanthadevan S, Jeyaraju DV, Chung TE, Prabha S, Xu W, Skrtic M, Jhas B, Hurren R, Gronda M, Wang X, Jitkova Y, Sukhai MA, Lin FH, Maclean N, Laister R, Goard CA, Mullen PJ, Xie S, Penn LZ, Rogers IM, Dick JE, Minden MD, Schimmer AD. AML cells have low spare reserve capacity in their respiratory chain that renders them susceptible to oxidative metabolic stress. Blood. 2015 Mar 26;125(13):2120-30. doi: 10.1182/blood-2014-08-594408. Epub 2015 Jan 28. PMID: 25631767; PMCID: PMC4375109.
119. Stief SM, Hanneforth AL, Weser S, Mattes R, Carlet M, Liu WH, Bartoschek MD, Domínguez Moreno H, Oettle M, Kempf J, Vick B, Ksienzyk B, Tizazu B, Rothenberg-Thurley M, Quentmeier H, Hiddemann W, Vosberg S, Greif PA, Metzeler KH, Schotta G, Bultmann S, Jeremias I, Leonhardt H, Spiekermann K. Loss of KDM6A confers drug resistance in acute myeloid leukemia. Leukemia. 2020 Jan;34(1):50-62. doi: 10.1038/s41375-019-0497-6. Epub 2019 Jun 14. PMID: 31201358; PMCID: PMC7214274.
120. Stuani L, Sabatier M, Saland E, Cognet G, Poupin N, Bosc C, Castelli FA, Gales L, Turtoi E, Montersino C, Farge T, Boet E, Broin N, Larrue C, Baran N, Cissé MY, Conti M, Loric S, Kaoma T, Hucteau A, Zavoriti A, Sahal A, Mouchel PL, Gotanègre M, Cassan C, Fernando L, Wang F, Hosseini M, Chu-Van E, Le Cam L, Carroll M, Selak MA, Vey N, Castellano R, Fenaille F, Turtoi A, Cazals G, Bories P, Gibon Y, Nicolay B, Ronseaux S, Marszalek JR, Takahashi K, DiNardo CD, Konopleva M, Pancaldi V, Collette Y, Bellvert F, Jourdan F, Linares LK, Récher C, Portais JC, Sarry JE. Mitochondrial metabolism supports resistance to IDH mutant inhibitors in acute myeloid leukemia. J Exp Med. 2021 May 3;218(5):e20200924. doi: 10.1084/jem.20200924. PMID: 33760042; PMCID: PMC7995203.
121. Sullivan LB, Gui DY, Hosios AM, Bush LN, Freinkman E, Vander Heiden MG. Supporting Aspartate Biosynthesis Is an Essential Function of Respiration in Proliferating Cells. Cell. 2015 Jul 30;162(3):552-63. doi: 10.1016/j.cell.2015.07.017. PMID: 26232225; PMCID: PMC4522278.
122. Sun P, Bai T, Ma T, Ding J. Molecular mechanism of the dual regulatory roles of ATP on the αγ heterodimer of human NAD-dependent isocitrate dehydrogenase. Sci Rep. 2020 Apr 10;10(1):6225. doi: 10.1038/s41598-020-63425-6. PMID: 32277159; PMCID: PMC7148312.
123. Tan TW, Tsai HR, Lu HF, Lin HL, Tsou MF, Lin YT, Tsai HY, Chen YF, Chung JG. Curcumin-induced cell cycle arrest and apoptosis in human acute promyelocytic leukemia HL-60 cells via MMP changes and caspase-3 activation. Anticancer Res. 2006 Nov-Dec;26(6B):4361-71. PMID: 17201156.
124. Thol F, Ganser A. Treatment of Relapsed Acute Myeloid Leukemia. Curr Treat Options Oncol. 2020 Jun 29;21(8):66. doi: 10.1007/s11864-020-00765-5. PMID: 32601974; PMCID: PMC7324428.

125. Thol F, Heuser M. Treatment for Relapsed/Refractory Acute Myeloid Leukemia. Hemasphere. 2021 Jun 1;5(6):e572. doi: 10.1097/HS9.0000000000000572. PMID: 34095756; PMCID: PMC8171365.
126. Toda C, Diano S. Mitochondrial UCP2 in the central regulation of metabolism. Best Pract Res Clin Endocrinol Metab. 2014 Oct;28(5):757-64. doi: 10.1016/j.beem.2014.02.006. Epub 2014 Mar 7. PMID: 25256770.
127. Toleikis A, Trumbeckaite S, Majiene D. Cytochrome C effect on respiration of heart mitochondria: influence of various factors. Biosci Rep. 2005 Oct-Dec;25(5-6):387-97. doi: 10.1007/s10540-005-2897-2. PMID: 16307383.
128. Tong X, Zhou F. Integrated bioinformatic analysis of mitochondrial metabolism-related genes in acute myeloid leukemia. Front Immunol. 2023 Apr 17;14:1120670. doi: 10.3389/fimmu.2023.1120670. PMID: 37138869; PMCID: PMC10149950.
129. Ueno H, Suzuki T, Kinosita K Jr, Yoshida M. ATP-driven stepwise rotation of FoF1-ATP synthase. Proc Natl Acad Sci U S A. 2005 Feb 1;102(5):1333-8. doi: 10.1073/pnas.0407857102. Epub 2005 Jan 24. PMID: 15668386; PMCID: PMC545493.
130. van Gastel N, Spinelli JB, Sharda A, Schajnovitz A, Baryawno N, Rhee C, Oki T, Grace E, Soled HJ, Milosevic J, Sykes DB, Hsu PP, Vander Heiden MG, Vidoudez C, Trauger SA, Haigis MC, Scadden DT. Induction of a Timed Metabolic Collapse to Overcome Cancer Chemoresistance. Cell Metab. 2020 Sep 1;32(3):391-403.e6. doi: 10.1016/j.cmet.2020.07.009. Epub 2020 Aug 6. PMID: 32763164; PMCID: PMC8397232.
131. Varghese S, Pramanik S, Williams LJ, Hodges HR, Hudgens CW, Fischer GM, Luo CK, Knighton B, Tan L, Lorenzi PL, Mackinnon AL, McQuade JL, Hailemichael Y, Roszik J, Peng W, Vashisht Gopal YN. The Glutaminase Inhibitor CB-839 (Telaglenastat) Enhances the Antimelanoma Activity of T-Cell-Mediated Immunotherapies. Mol Cancer Ther. 2021 Mar;20(3):500-511. doi: 10.1158/1535-7163.MCT-20-0430. Epub 2020 Dec 23. PMID: 33361272; PMCID: PMC7933078.
132. Veech RL, Todd King M, Pawlosky R, Kashiwaya Y, Bradshaw PC, Curtis W. The "great" controlling nucleotide coenzymes. IUBMB Life. 2019 May;71(5):565-579. doi: 10.1002/iub.1997. Epub 2019 Jan 9. PMID: 30624851; PMCID: PMC6850382.
133. Wang ES, Frankfurt O, Orford KW, Bennett M, Flinn IW, Maris M, et al.. Phase 1 study of Cb-839, a first-in-Class, orally administered small molecule inhibitor of glutaminase in patients with Relapsed/Refractory leukemia. *Blood* (2015) 126(23):2566–. doi: 10.1182/blood.V126.23.2566.2566
134. Wang HW, Zeng H. [Newest Reaserch Advance on Targeting Glycolysis Pathways in Acute Myeloid Leukemia --Review]. Zhongguo Shi Yan Xue Ye Xue Za Zhi. 2020 Apr;28(2):690-694. Chinese. doi: 10.19746/j.cnki.issn.1009-2137.2020.02.056. PMID: 32319418.
135. Williams MS, Amaral FM, Simeoni F, Somervaille TC. A stress-responsive enhancer induces dynamic drug resistance in acute myeloid leukemia. J Clin Invest. 2020 Mar 2;130(3):1217-1232. doi: 10.1172/JCI130809. PMID: 31770110; PMCID: PMC7269587.
136. Williams MS, Basma NJ, Amaral FMR, Wiseman DH, Somervaille TCP. Blast cells surviving acute myeloid leukemia induction therapy are in cycle with a signature of FOXM1 activity. BMC Cancer. 2021 Oct 28;21(1):1153. doi: 10.1186/s12885-021-08839-9. PMID: 34711181; PMCID: PMC8554867.
137. Yang L, Venneti S, Nagrath D. Glutaminolysis: A Hallmark of Cancer Metabolism. Annu Rev Biomed Eng. 2017 Jun 21;19:163-194. doi: 10.1146/annurev-bioeng-071516-044546. Epub 2017 Mar 8. PMID: 28301735.
138. Yap TA, Daver N, Mahendra M, Zhang J, Kamiya-Matsuoka C, Meric-Bernstam F, Kantarjian HM, Ravandi F, Collins ME, Francesco MED, Dumbrava EE, Fu S, Gao S, Gay JP, Gera S, Han J, Hong DS, Jabbour EJ, Ju Z, Karp DD, Lodi A, Molina JR, Baran N, Naing A, Ohanian M, Pant S, Pemmaraju N, Bose P, Piha-Paul SA, Rodon J, Salguero C,

Sasaki K, Singh AK, Subbiah V, Tsimberidou AM, Xu QA, Yilmaz M, Zhang Q, Li Y, Bristow CA, Bhattacharjee MB, Tiziani S, Heffernan TP, Vellano CP, Jones P, Heijnen CJ, Kavelaars A, Marszalek JR, Konopleva M. Complex I inhibitor of oxidative phosphorylation in advanced solid tumors and acute myeloid leukemia: phase I trials. Nat Med. 2023 Jan;29(1):115-126. doi: 10.1038/s41591-022-02103-8. Epub 2023 Jan 19. PMID: 36658425.

139. Zanotti F, Guerrieri F, Che YW, Scarfò R, Papa S. Proton translocation by the H+-ATPase of mitochondria. Effect of modification by monofunctional reagents of thiol residues in F0 polypeptides. Eur J Biochem. 1987 May 4;164(3):517-23. doi: 10.1111/j.1432-1033.1987.tb11157.x. PMID: 2883005.

140. Zeng P, Lu W, Tian J, Qiao S, Li J, Glorieux C, Wen S, Zhang H, Li Y, Huang P. Reductive TCA cycle catalyzed by wild-type IDH2 promotes acute myeloid leukemia and is a metabolic vulnerability for potential targeted therapy. J Hematol Oncol. 2022 Mar 21;15(1):30. doi: 10.1186/s13045-022-01245-z. PMID: 35313945; PMCID: PMC8935709.

141. Zhang J, Lei W, Chen X, Wang S, Qian W. Oxidative stress response induced by chemotherapy in leukemia treatment. Mol Clin Oncol. 2018 Mar;8(3):391-399. doi: 10.3892/mco.2018.1549. Epub 2018 Jan 10. PMID: 29599981; PMCID: PMC5867396.

142. Zheng J. Energy metabolism of cancer: Glycolysis versus oxidative phosphorylation (Review). Oncol Lett. 2012 Dec;4(6):1151-1157. doi: 10.3892/ol.2012.928. Epub 2012 Sep 20. PMID: 23226794; PMCID: PMC3506713.

Appendix A: Institutional Review Board Approval Letter A

EAST CAROLINA UNIVERSITY
University & Medical Center Institutional Review Board
Willis Building · Mail Stop 682
600 Moye Boulevard · Greenville, NC 27834
Office **252-744-2914** · Fax **252-744-2284** ·
rede.ecu.edu/umcirb/

Notification of Amendment Approval

From: Biomedical IRB
To: Kelsey Fisher-Wellman
CC:
Kelsey Fisher-Wellman
Patricia Brophy
Date: 11/1/2023
Re: Ame13_UMCIRB 18-001328
UMCIRB 18-001328
Bioenergetic characterization of peripheral blood cells.

Your Amendment has been reviewed and approved using expedited review for the period of 10/31/2023 to 1/4/2024. It was the determination of the UMCIRB Chairperson (or designee) that this revision does not impact the overall risk/benefit ratio of the study and is appropriate for the population and procedures proposed.

Please note that any further changes to this approved research may not be initiated without UMCIRB review except when necessary to eliminate an apparent immediate hazard to the participant. All unanticipated problems involving risks to participants and others must be promptly reported to the UMCIRB. A continuing or final review must be submitted to the UMCIRB prior to the date of study expiration.The investigator must adhere to all reporting requirements for this study.

Approved consent documents with the IRB approval date stamped on the document should be used to consent participants (consent documents with the IRB approval date stamp are found under the Documents tab in the study workspace).

The approval includes the following items:

Document	Description
Consent Form_KFW_10.5.23 clean.doc(0.10)	Consent Forms

For research studies where a waiver or alteration of HIPAA Authorization has been approved, the IRB states that each of the waiver criteria in 45 CFR 164.512(i)(1)(i)(A) and (2)(i) through (v) have been met. Additionally, the elements of PHI to be collected as described in items 1 and 2 of the Application for Waiver of Authorization have been determined to be the minimal necessary for the specified research.

The Chairperson (or designee) does not have a potential for conflict of interest on this study.

Appendix B: Institutional Review Board Approval Letter B

EAST CAROLINA UNIVERSITY
University & Medical Center Institutional Review Board
4N-64 Brody Medical Sciences Building· Mail Stop 682
600 Moye Boulevard · Greenville, NC 27834
Office **252-744-2914** · Fax **252-744-2284** ·
rede.ecu.edu/umcirb/

Notification of Amendment Approval

From: Biomedical IRB
To: Kelsey Fisher-Wellman
CC:
Sue Joyner
Date: 10/21/2022
Re: Ame4 UMCIRB 19-002331
UMCIRB 19-002331
Bioenergetic characterization of solid tumors and primary leukemias.

Your Amendment has been reviewed and approved using expedited review on 10/21/2022. It was the determination of the UMCIRB Chairperson (or designee) that this revision does not impact the overall risk/benefit ratio of the study and is appropriate for the population and procedures proposed.

Please note that any further changes to this approved research may not be initiated without UMCIRB review except when necessary to eliminate an apparent immediate hazard to the participant. All unanticipated problems involving risks to participants and others must be promptly reported to the UMCIRB. The investigator must submit a Final Report application to the UMCIRB prior to the Expected End Date provided in the IRB application. If the study is not completed by this date, an Amendment will need to be submitted to extend the Expected End Date. The investigator must adhere to all reporting requirements for this study.

Approved consent documents with the IRB approval date stamped on the document should be used to consent participants (consent documents with the IRB approval date stamp are found under the Documents tab in the study workspace).

The approval includes the following items:

Document	Description
Matthew DeAntonio, Daniel Makoko, Rachel Darden, Derrick Almond, Kaleigh Nunley, Toria Wilson, Alison Colao, Brandi Mills, Kelly Martin, Shahana Patel, and Henry Charvat are being added to the study team.	
Susan Eubanks, Rita Bowden, Nelson Moore, Tiffanie Moore, Ramatu Pham, Kelsey Belk, Elizabeth Waddell, Haley Lopez, and Kelsey McLaughlin are being removed from the study team.	

For research studies where a waiver or alteration of HIPAA Authorization has been approved, the IRB states that each of the waiver criteria in 45 CFR 164.512(i)(1)(i)(A) and (2)(i) through (v) have been met. Additionally, the elements of PHI to be collected as described in items 1 and 2 of the Application for Waiver of Authorization have been determined to be the minimal necessary for the specified research.

The Chairperson (or designee) does not have a potential for conflict of interest on this study.